

Investigating Whether the FGF Pathways Are Involved
In Scleral Ossicle Development

By

Shruti Kumar

A Thesis Submitted to Saint Mary's University, Halifax, Nova Scotia
in Partial Fulfilment of the Requirements for
the Degree of Master of Science in Applied Science

August, 2017, Halifax, Nova Scotia

© Shruti Kumar, 2017

Approved: Dr. Tamara Franz-Odendaal
Supervisor

Approved: Dr. Anne Dalziel
External Examiner

Approved: Dr. Sophia Stone
Supervisory Committee Member

Approved: Dr. Samuel Veres
Supervisory Committee Member

Date: August 9th 2017

Table of Contents:

Table of Contents.....	ii
List of Tables	v
List of Figures	vi
Abstract.....	viii
List of Abbreviations	ix
Acknowledgements.....	xi
1.0 Introduction	1
1.1 Early Stages of Intramembranous Bone Development.....	2
1.2 Chick Scleral Ossicles.....	3
1.3 Fibroblast Growth Factor Signalling.....	10
1.3.1 Fibroblast growth factors.....	10
1.3.2 Fibroblast Growth Factor Receptors.....	13
1.3.3 Downstream FGF-FGFR Signalling Pathways	15
1.3.4 Inhibitors of FGF Pathway.....	17
1.4 FGFR Expression in Placodal Interactions	17
1.5 FGFRs in Bone Development.....	20
1.6 Objectives and Hypothesis.....	22
1.7 Significance of this Research.....	23
2.0 Materials and Methods.....	24
2.1 Chicken Embryo	24
2.2 Ex-Ovo Culturing	24
2.3 Probe Preparation and Whole Mount In Situ Hybridization (WMISH)	26
2.3.1 Cloning	26
2.3.2 Isolation of Plasmid.....	27
2.3.3 Linearization of Plasmid	28
2.3.4 Polymerase Chain Reaction	30
2.3.5 Gel Electrophoresis	31
2.3.6 DNA Sequencing.....	31
2.3.7 RNA probe synthesis	32

2.3.8 Whole Mount In Situ Hybridization (WHIMS).....	34
2.4 Cryosectioning	36
2.5 Imaging and Analysis.....	37
2.6 Manipulation tools.....	38
2.6.1 Tungsten needle.....	38
2.6.2 Microinjections needle	39
2.7 Inhibition by SU5402.....	39
2.7.1 Preparation of SU5402.....	39
2.7.2 Preparation of Beads	40
2.7.3 Limb Bead Implantation.....	41
2.7.4 Eye Bead Implantation.....	41
2.7.5 Microinjections	42
2.8 Alkaline-Phosphatase (AP) Staining	43
2.9 Alcian Blue Cartilage Staining	43
2.10 Statistical Analysis.....	44
3.1 FGFR In Situ Hybridization	45
3.1.1 Probe Validation	45
3.1.2 FGFR1b Expression.....	50
3.1.3 FGFR1c Expression	56
3.1.4 FGFR2b Expression.....	61
3.1.5 FGFR2c Expression	66
3.1.6 FGFR3b Expression.....	72
3.1.7 FGFR3c Expression	77
3.2 Bead Implantation	82
3.2.1 Effect of SU5402 Treatment on Limb Development.....	82
3.2.2 Effect of SU5402 on Scleral Ossicle Development.....	85
3.3 Microinjections	88
3.3.1 Control Microinjections	90
3.3.2 SU5402 Microinjections.....	92
3.3.3 Comparison of Defects in DMSO and SU5402	93
3.3.4 Comparison of Number of Ossicles in DMSO and SU5402 Microinjections.....	93
4.0 Discussion.....	97

4.1 In Situ Hybridization of FGFRs.....	97
4.1.1 FGFR Expression at Early Stage	97
4.1.2 FGFR Expression at Mid Stage.....	101
4.1.3 FGFR Expression at Late Stage	107
4.1.4 Summary of FGFR Expression	113
4.1.5 FGFR Expression in the Interpapillary Regions	114
4.1.6 Spatial Expression of FGFR Isoforms.....	115
4.1.7 Possible FGFRs involved in the scleral ossicle system.....	116
4.2 Inhibition of the FGF Pathway	120
5.0 Summary and Conclusion	123
Literature Cited	125
Appendix A: Protocols.....	145
Appendix A1: Chick Alkaline Phosphatase Staining Protocol	145
Appendix A2: Alcian Blue Cartilage Staining.....	149
Appendix A3: Preparing LB Broth and Agar Plates	151
Appendix A4: Removing Plasmids from Filter Paper	152
Appendix A5: Cloning.....	153
Appendix A6: Restriction Digestion and Clean-up of Plasmid	157
Appendix A7: Polymerase Chain Reaction.....	159
Appendix A8: RNA Probe Synthesis	161
Appendix A9: DIG-High Prime Labelling and Detection Protocol (Dot Blot).....	162
Appendix A10: Whole Mount In Situ Hybridization Protocol	166
Appendix B: Blast Outcomes for Sequencing Data Using NCBI Blast	179
Appendix C: Supplementary Figures.....	188
Appendix D: Supplementary Tables.....	199
Appendix E: Statistical Calculations	204
Appendix E1: Calculations for Dixon’s Q-test for outliers.....	204
Appendix E2: Fisher’s Exact test SPSS outputs	206
Appendix E3: Independent Two-tailed T-tests MiniTab outputs.....	208
Appendix E4: Calculations for one way ANOVA.....	211

List of Tables

Table 1.1. FGFs in vertebrates are divided into seven subfamilies	11
Table 3.1. Measurements of wing cartilages at HH29/30 after AG1X2 bead implantation at HH20/21.....	84
Table 3.2. Number of scleral condensations at HH37 in the left and right eyes of embryos that were implanted with AG1X2 beads soaked in either DMSO, 3mg/ml SU5402 or in 6mg/ml SU5402.....	88
Table 3.3. Frequency of the different categories of defects observed in eyes microinjected with DMSO and 6mg/ml SU5402.....	91
Table 3.4. Number of ossicles at HH37 in left and right microinjected eye of DMSO control group and 6mg/ml SU5402 group.....	94
Table 4.1. Intensity of expression of each FGFR isoform in papilla #12 and its CR from HH30 to 37	115
Table D1. Measurements of wing cartilages at HH29/30 after affigel bead implantation at HH20/21.....	199
Table D2. Number of papillae in left and right eye of control non-injected embryos ...	200
Table D3. Raw ImageJ data for quantitative analysis of expression intensity of papilla #12 and its contiguous region.....	201
Table D4. Raw ImageJ data for field of FGFR expression in papilla #12 and its contiguous region	203

List of Figures

Figure 1.1. Process of intramembranous ossification	4
Figure 1.2. The development of scleral ossicles	6
Figure 1.3. Schematic of a chicken embryonic eye.....	7
Figure 1.4. The FGFR pathway	14
Figure 2.1. Ex-ovo culturing set up.	25
Figure 2.2. Representative gel images of probe preparation.....	29
Figure 2.3. Representation of a dot-blot	33
Figure 3.1. In situ hybridisation of control embryo eyes at HH35 showing no gene expression	48
Figure 3.2. Cryosections through conjunctival papillae of control embryo eyes at HH35	49
Figure 3.3. A schematic representation of a section through a papilla at HH32/33.....	49
Figure 3.4. FGFR1b in situ hybridization from HH30 to HH37 in the chick eye	54
Figure 3.5. Cryosections of FGFR1b in situ hybridization	55
Figure 3.6. FGFR1c in situ hybridization from HH30 to HH37 in the chick eye	59
Figure 3.7. Cryosections of FGFR1c in situ hybridization.....	60
Figure 3.8. FGFR2b in situ hybridization from HH30 to HH37 in the chick eye	64
Figure 3.9. Cryosections of FGFR2b in situ hybridization	65
Figure 3.10. FGFR2c in situ hybridization from HH30 to HH37 in the chick eye	70
Figure 3.11. Cryosections of FGFR2c in situ hybridization.....	71
Figure 3.12. FGFR3b in situ hybridization from HH30 to HH37 in the chick eye	75
Figure 3.13. Cryosections of FGFR3b in situ hybridization	76
Figure 3.14. FGFR3c in situ hybridization from HH30 to HH37 in the chick eye	80
Figure 3.15. Cryosections of FGFR3c in situ hybridization.....	81
Figure 3.16. Alcian blue cartilage staining of wing limbs.....	85
Figure 3.17. Representative right eyes implanted with AG1X2 beads at HH34 and stained for AP at HH37	87
Figure 3.18.Examples of the classification of defects observed in scleral condensations after microinjection with 6mg/ml SU5402 at HH34 and stained for AP at HH37	89
Figure 3.19. Percentage of eyes with each defect (mild, moderate and severe) observed in scleral condensations at HH37 in each group of microinjected eyes.....	91
Figure 3.20. Average number of ossicles in left and right eyes for each group of microinjections.....	96
Figure 4.1. Schematic showing comparative expression of FGFR isoforms at early stage (HH30-31) of scleral ossicle developmental system	98

Figure 4.2. Schematic showing comparative expression of FGFR isoforms at mid stage (HH32-34) of scleral ossicle developmental system	102
Figure 4.3. Schematic diagram showing the field of expression for FGFRs surrounding papilla #12 at HH33.....	105
Figure 4.4. Schematic showing comparative expression of FGFR isoforms at late stage (HH35-37) of scleral ossicle developmental system.....	109
Figure C1. Methodology for ImageJ analysis of expression intensity at papilla #12.....	188
Figure C2. Methodology for ImageJ analysis of field of expression at papilla #12.....	189
Figure C3. The whole mount in situ hybridization of BMP2 at HH35.....	190
Figure C4. Cryosection of FGFR2c in situ hybridization in nasal group papilla.....	191
Figure C5. Key for the schematics of FGFR ISH expressions in Figure 4.1, 4.2 and 4.4 as well as Figure C6 to C11.....	192
Figure C6. Schematic of FGFR1b ISH.....	193
Figure C7. Schematic of FGFR1c ISH	194
Figure C8. Schematic of FGFR2b ISH.....	195
Figure C9. Schematic of FGFR2c ISH	196
Figure C10. Schematic of FGFR3b ISH.....	197
Figure C11. Schematic of FGFR3c ISH	198

Abstract:

Investigating Whether the FGF Pathways
Are Involved In Scleral Ossicle Development

By Shruti Kumar

During animal development, fibroblast growth factors (FGF) play several important roles. Both 'b' and 'c' isoforms of *fibroblast growth factor receptors* 1-3 were expressed in the conjunctival papillae, a ring of small epithelial thickenings in the corneal-scleral limbus that induce scleral ossicles, a ring of neural crest derived intramembranous bones in the chick sclera. Whereas, downregulation of the *FGFR* isoforms was observed during the later stages of scleral ossicle induction. All *FGFR* isoforms were expressed in the epithelium, however, only *FGFR1c*, *2c*, *3b*, and *3c* were expressed in the mesenchyme. I also examined the potential role of the FGF pathway during scleral ossicle induction, however, these results were inconclusive. This research provides insight into the expression of another major developmental gene family that could play an important role in the scleral ossicle system and helps to further conceptualize the basic signalling networks involved during scleral ossicle formation.

August 9th, 2017

List of Abbreviations:

Ab - Antibody

AP – Alkaline phosphatase

BCIP – 5-bromo-4-chloro-3-indoyle phosphate

BMP – Bone morphogenetic protein

CNI – Control no injection

CR – Contiguous region

DepC – Diethyl pyrocarbonate

df – Degrees of freedom

dH₂O – Distilled water

DIG - Digoxigenin

DMSO – Dimethyl sulfoxide

E – Embryonic day

EDTA – Ethylenediaminetetraacetic acid

FGF – Fibroblast growth factor

FGFR – Fibroblast growth factor receptor

HH – Hamburger and Hamilton stage

HSPG – Heparin sulfate proteoglycan

IHH – Indian Hedgehog

ISH – *in situ* hybridization

LB – Luria Bertani

NBT – nitro blue tetrazolium

PCR – Polymerase chain reaction

SHH – Sonic hedgehog

TGF- β – Transforming growth factor beta

VEGF – Vascular endothelial growth factor

WMISH – whole mount *in situ* hybridization

Wnt - wingless

Acknowledgements:

First and foremost, I would like to thank my supervisor, Dr. Tamara Franz-Odendaal, for giving me the opportunity to work in this interesting field of developmental biology. I had waited so long for this opportunity, thank you! Thank you also for your constant guidance and support and especially for teaching me time management skills. I would also like to thank my supervisory committee, Dr. Sophia Stone and Dr. Samuel Veres. Thank you for your invaluable guidance and feedback.

Thank you to Dr. Bryan Crawford, without whom this amazing opportunity might not have come my way. Thank you for believing in me. Thank you Dr. Gary Schoenwolf for providing me with the probes I needed for my research. I would next like to thank all the members of the Franz-Odendaal lab, past and present. I would especially like to thank Dr. Sewvandani Atukorallaya and Christine Hammer for making me feel like I've always been part of the lab. You were always available to help and I appreciate everything you've done for me.

Most of all, I would like to thank my parents for all their support and encouragement. Thank you for your patience and putting up with all my panic calls. You both are my rock!

1.0 Introduction

Continuous basic cell processes such as cell proliferation, cell differentiation and cell migration are the key to embryonic development and morphogenesis, and patterning lies at the center of these processes. During tissue morphogenesis, transforming growth factor- β (*TGF- β*)/bone morphogenetic protein (*BMP*), hedgehog (*HH*), fibroblast growth factor (*FGF*) and wingless (*Wnt*) families are key signalling pathways that play several important roles during development (Gilbert, 2000). Similarly, these factors are also involved in regulating bone development. Bone formation or osteogenesis commonly occurs by two different processes: endochondral ossification, a process which requires formation of a cartilage scaffold prior to matrix deposition, or intramembranous ossification in which there is direct deposition of bone and no cartilage involvement. Unfortunately, much of the research on bone development focuses on limb development in mammals or birds which occurs via typical endochondral ossification (Franz-Odenaal, 2010). Craniofacial bones and other flat bones such as the clavicle form through intramembranous ossification, for which very little is known about the role of *TGF- β* /*BMP*, *HH*, *FGF* and *Wnt*. Of these, *FGF* is one of the most important factors in skull roof development and mutations in their receptors are involved in craniosynostosis, a birth defect characterised by premature closure of sutures (Kimonis *et al.*, 2007).

The cells involved in intramembranous bone formation can be derived from either the mesoderm (paraxial or lateral plate) or from the neural crest cells (Hall, 2005).

During neural tube formation, the dorsal most region of the neural ectoderm undergoes an epithelial to mesenchymal transition and gives rise to the neural crest cells (Hall, 1975; Zhang *et al.*, 2014). These neural crest cells then migrate to other regions of the embryo and differentiate into specific cell types (Gilbert, 2000; Santagati and Rijli, 2003; Cordero *et al.*, 2011; Zhang *et al.*, 2014). Neural crest cells that migrate to the craniofacial region and form the craniofacial mesenchyme are called cranial neural crest cells. Cells in the craniofacial mesenchyme differentiate to form cartilage, connective tissue, cranial neurons and bones of the face and skull (Gilbert, 2000; Santagati and Rijli, 2003; Cordero *et al.*, 2011; Zhang *et al.*, 2014). The most popular bones for studying intramembranous ossification are the calvariae, or the skull roof bones which are also derived from neural crest cells. Fate maps of the chick skull indicate that some of the neural crest derived intramembranous bones include, the squamosal, dentary, maxilla and premaxilla, nasal as well as the anterior part of the frontal bone (Santagati and Rijli, 2003; Evans and Noden, 2006; Gross and Hanken, 2008). Scleral ossicles are thus similar to the calvariae in that they are also intramembranous bones formed from the cranial neural crest cells (Couly *et al.*, 1993).

1.1 Early Stages of Intramembranous Bone Development

The process of bone development is similar amongst vertebrates such as mouse and chicken and involves same cell types such as osteoblasts and chondrocytes (Franz-Odenaal, 2010). An important step in the development of bone is the formation of

skeletogenic condensations in the mesenchyme (Figure 1.1). The formation of these condensations often requires inducing factors from the epithelium that, through epithelial to mesenchymal interactions, cause aggregation of cells in the mesenchyme (Hall and Miyake, 1992, 1995, 2000). The condensations must reach a critical size before cellular differentiation can occur. The size of the condensation is important since too small a size may lead to no skeletal formation and too large a size can lead to an abnormally large bone (Hall and Miyake, 1992, 1995). During intramembranous ossification, the cells within these mesenchymal condensations differentiate into osteoblasts (Franz-Odenaal *et al.*, 2006). Polarized osteoblasts secrete osteoid matrix which later becomes calcified (Franz-Odenaal, 2010). The osteoblasts that get trapped within this matrix differentiate into osteocytes (Figure 1.1). An important aspect of bone development is the continuous remodelling of the bone by osteoclasts. A continuous balance between osteoclasts, which resorb bone matrix, and osteoblasts, which deposit bone, is required to maintain growth and repair of bone both during development and in adults (Väänänen *et al.*, 2000).

1.2 Chick Scleral Ossicles

The cornea and sclera of the eye is made up of fibrous connective tissue. In most vertebrates, excluding placental mammals, snakes and some amphibians, the eye consists of intraocular skeletal elements (Franz-Odenaal and Vickaryous, 2006). In

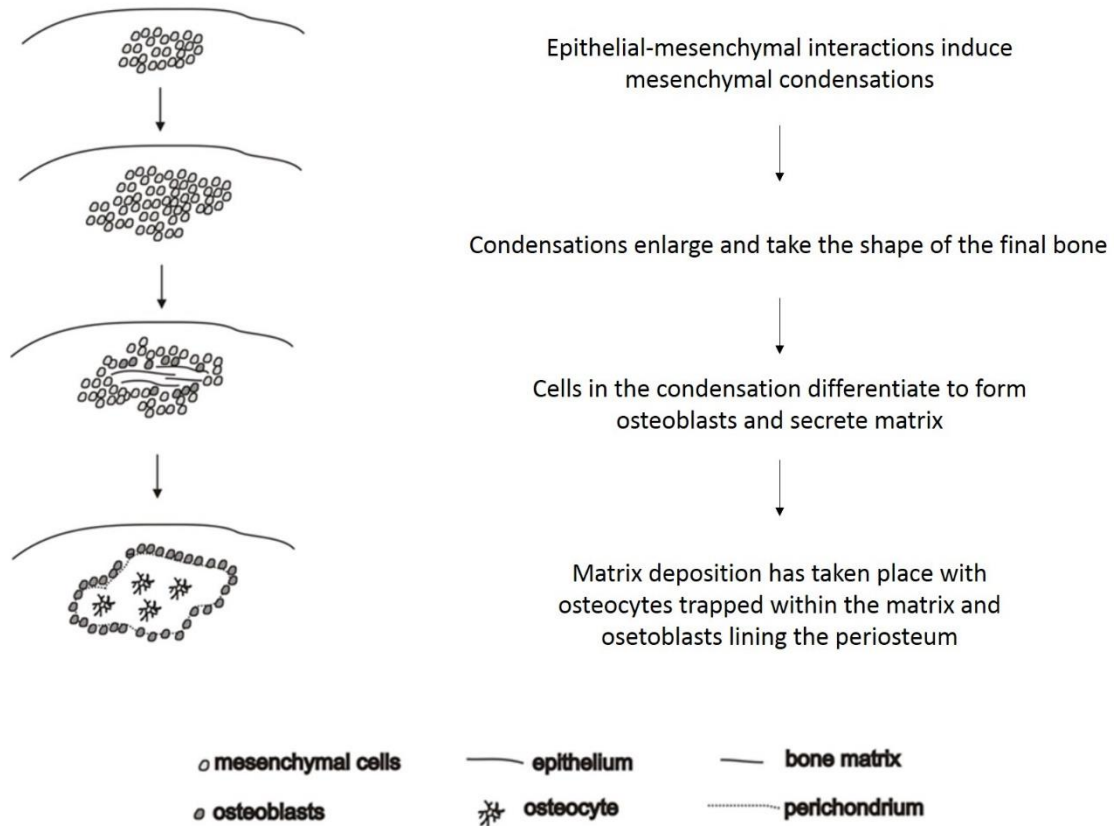
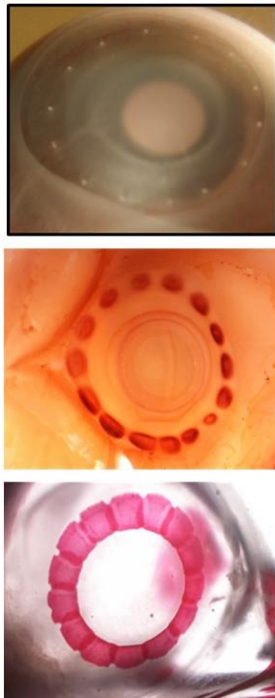


Figure 1.1. Process of intramembranous ossification. Mesenchymal cells condense and increase in number prior to their differentiation into osteoblasts. Cells at the center of the condensation differentiate into osteoblasts and secrete matrix. Some osteoblasts become trapped in the matrix and become osteocytes while other osteoblasts continue to secrete matrix. Adapted from Franz-Odenaal (2011).

reptiles, including birds (but not snakes) and fishes, the sclera is further supported by scleral cartilage and scleral ossicles. The number and morphology of the scleral ossicles can differ greatly between the different taxa (Franz-Odendaal and Vickaryous, 2006). In the adult chicken, scleral ossicles are overlapping, trapezoid shaped bones (Coulombre and Coulombre, 1973; Franz-Odendaal and Vickaryous, 2006). Similar to all bone formation, scleral ossicles also require epithelial-mesenchymal interactions (Pinto and Hall, 1991; Franz-Odendaal, 2008). The process begins when epithelial structures called conjunctival papillae form at the corneal-scleral limbus (Murray, 1943; Coulombre and Coulombre, 1962; Figure 1.2). The developmental stages of conjunctival papillae in the chick have been described extensively by Murray (1943). These papillae then induce cell condensations in the neural crest derived mesenchyme (ectomesenchyme, Figure 1.2) leading to bone formation (Fyfe and Hall, 1983). The formation of scleral ossicles in the mesenchyme is dependent upon the presence of conjunctival papillae in the epithelium as the ossicles fail to form in their absence (Coulombre and Coulombre, 1962). The papillae induce ossicle formation in a 1:1 ratio such that each papillae induces the formation of a single ossicle directly beneath it (Coulombre and Coulombre, 1962).

The domestic chicken *Gallus gallus* has 14-16 conjunctival papillae per eye (Franz-Odendaal, 2008; Figure 1.3). The first papilla forms at approximately 6.5 days of embryonic development at Hamburger and Hamilton stage 30 (HH30) over the ciliary



Induction of conjunctival papillae



Epithelial-mesenchymal interactions



Mesenchymal condensations and induction of scleral ossicles



Scleral ossicle formation

Figure 1.2. The development of scleral ossicles. Conjunctival papillae form at the corneal-scleral limbus and through epithelial-mesenchymal interactions induce condensations in the mesenchyme which can be observed using alkaline phosphatase staining. These mesenchymal condensations ultimately form the scleral ossicles. Images are taken from the Franz-Ondendaal Bone Development Lab.

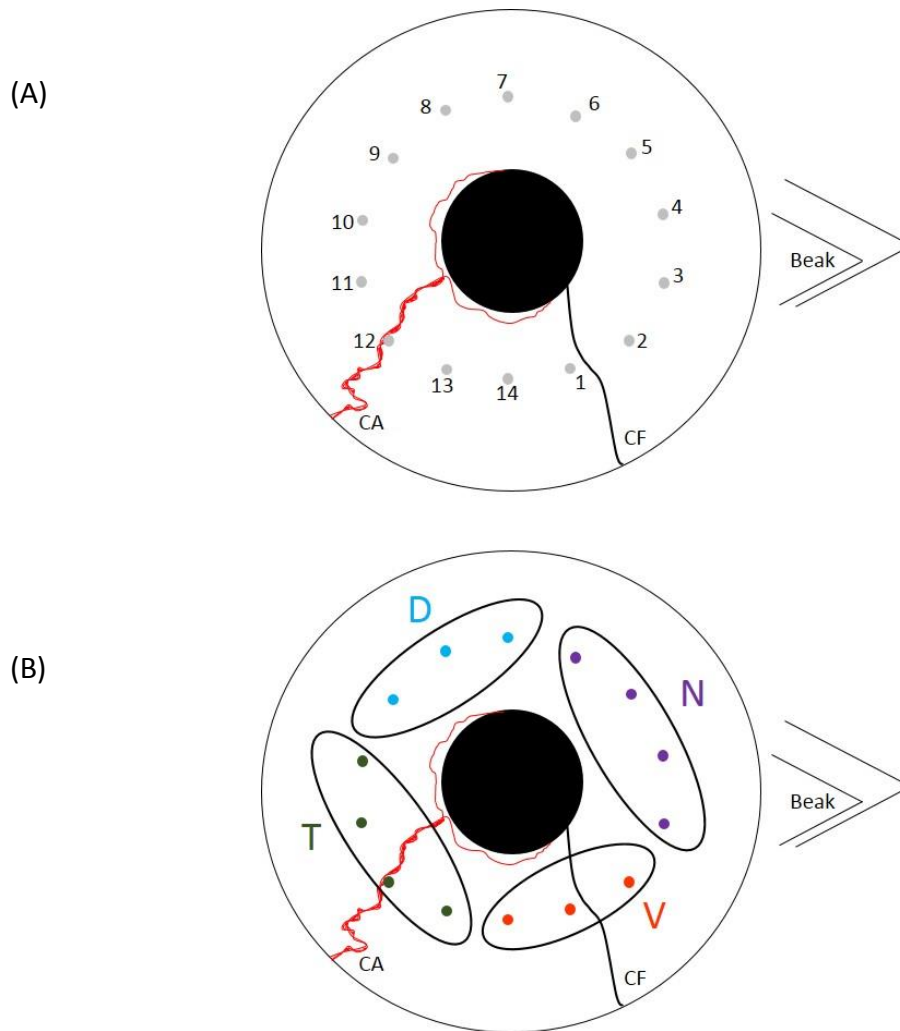


Figure 1.3. Schematic of a chicken embryonic eye. (A) The papillae are numbered from 1-14 starting from the papillae that develops over the choroid fissure and going counter clockwise. The first papilla (#12) develops over the ciliary artery at HH30. (B) This is followed by the temporal, nasal, dorsal and ventral groups, respectively. The last papilla forms over the choroid fissure and a complete papillae ring can be seen by HH34. CA: Ciliary artery, CF: Choroid fissure, D: Dorsal group, N: Nasal group, T: Temporal group, V: Ventral group.

artery (Hamburger and Hamilton, 1951) and is assigned the number 12 (Coulombre and Coulombre, 1962; Franz-Odenaal, 2008). Next, papillae appear neighbouring the first papilla in the temporal region (papillae #10-#13) followed by the nasal (papillae #2-#6), dorsal (papillae #7-#9) and ventral groups (papillae #14 and #1). The last papilla (papilla #1) can be observed at HH34, embryonic day (E) 8 over the choroid fissure (Hamburger and Hamilton, 1951; Coulombre and Coulombre, 1962; Figure 1.3). After inducing the underlying scleral ossicles to form, the papillae then begin to degenerate. The first skeletogenic condensations can be observed at HH36 (E10). Ossicle condensations increase in size via cell migration until the beginning of mineralization (Jabalee *et al.*, 2013) and by HH38 (E12), all papillae have disappeared and a thin boney ring of scleral ossicles can be observed (Franz-Odenaal, 2008). To form the complete sclerotic ring, the scleral ossicles begin to overlap each other at approximately HH39 and are held together by dense connective tissue (Franz-Odenaal, 2008). The order in which the skeletogenic condensations form follows that of the conjunctival papillae.

Induction of scleral ossicles requires diffusible signals from the epithelium to the mesenchyme (Pinto and Hall, 1991). Studies in our lab have identified key signalling molecules involved in scleral ossicle induction. *Sonic Hedgehog (SHH)* and *Indian hedgehog (IHH)* are expressed at HH35 and HH36 coinciding with the time when ossicle condensations form (Duench and Franz-Odenaal, 2012). Inhibition of the *HH* pathway by a cyclopamine soaked bead (a *HH* inhibitor) at HH35 resulted in absence of the ossicle beneath the implanted papilla. Duench and Franz-Odenaal (2012) hypothesized

that *SHH* is required for the maintenance of the papillae while *IHH* is important for the induction of skeletogenic condensations in the mesenchyme. *Bone morphogenetic protein (BMP)* was also found to play key roles in ossicle induction (Duench and Franz-Odendaal, 2012). *BMP2* was expressed from HH34.5 to HH36 in the conjunctival papillae. Inhibition of *BMP2* through a Noggin soaked bead (a *BMP* inhibitor) resulted in missing ossicles underneath the bead site. Inhibition of *BMP2* also resulted in decreased expression of *IHH* indicating that these two developmental pathways interact with each other during scleral ossicle development (Duench and Franz-Odendaal, 2012).

Jourdeuil and Franz-Odendaal (2016) identified other genes that are possibly involved in the development of the conjunctival papillae and perhaps in the induction of scleral condensations. β -*catenin* was expressed in the epithelium prior to papillae formation and is likely required for pre-patterning the epithelium in order to make the epithelium competent to receive inducing signals from the mesenchyme. Indeed, Pinto and Hall (1991) showed that the conjunctival epithelium receives signals from the mesenchyme. Jourdeuil and Franz-Odendaal (2017) thus proposed that the epithelium undergoes a placode stage (similar to that in feather, hair and teeth) prior to papillae formation and that the placode receives inductive signals from the mesenchyme resulting in formation of papillae. Other genes expressed in the conjunctival papillae include *Prox 1*, and *Ednrb* and *Inhba* (Jourdeuil and Franz-Odendaal, 2016). These genes were observed for a short duration during papillae development from HH31 to HH34, although their role in conjunctival papillae development has not yet been elucidated.

1.3 Fibroblast Growth Factor Signalling:

1.3.1 Fibroblast growth factors

Fibroblast growth factors (FGFs) are a family of growth factor proteins that are found in both vertebrates and invertebrates. In vertebrates, FGFs and their receptors [fibroblast growth factor receptors, FGFRs] play essential roles in development. They are extensively expressed in all types of cells and tissues and are involved in various cellular functions. During embryonic development they are required for cell proliferation, differentiation and migration as well as angiogenesis (Itoh and Ornitz, 2004). In adults, they play important roles in tissue repair and in the control of the nervous system (Eswarakumar *et al.*, 2005). In humans, FGFs are proteins of 150-250 amino acids containing a conserved 120 amino acid core with 30-60% amino acid identity between each other (Itoh and Ornitz, 2004).

In vertebrates, four FGFRs (*FGFR1-4*) have been identified, along with ten FGFs in zebrafish *Danio rerio* (FGF2–4, 6, 8, 10, 17a, 17b, 18, 24), six in *Xenopus* (FGF2–4, 8–10), 22 in mice *Mus musculus* (FGF1–18, 20–23) and human *Homo sapiens* (FGF1–14, 16–23) and 13 in chicken *Gallus* (FGF1–4, 8–10, 12, 13, 16, 18–20) (Thisse and Thisse, 2005). Through phylogenetic alignment, FGFs can be categorized into seven subfamilies and each subfamily has a high affinity to one of the four FGFRs (Table 1.1; Zhang *et al.*, 2006). FGFs in the extracellular matrix are found bound to the co-factors heparin or heparan sulfate proteoglycans (HSPG) (Mohammadi *et al.*, 2005). HSPGs are macromolecules that have heparan sulfate (HS) at their core and are required to

Table 1.1. FGFs in vertebrates are divided into seven subfamilies. Each FGF subfamily is specific to a particular receptor. The FGF19 subfamily are endocrine ligands with weak activation of FGFRs whereas the FGF11 subfamily does not activate FGFRs. FGF ligands in bold are found in chicken. (Adapted from Eswarakumar et al., 2005).

FGF Subfamily	Ligands	Receptor specificity
FGF1	FGF1 FGF2	All FGFRs and their isoforms FGFR1b, 1c, 2c, 3c and FGFR4
FGF4	FGF4 FGF5 FGF6	FGFR1c, 2c, 3c and FGFR4 FGFR1c FGFR1c and 2c
FGF7	FGF3 FGF7 FGF10 FGF22	FGFR1b and 2b FGFR2b FGFR1b and 2b FGFR2b
FGF8	FGF8 FGF17 FGF18	FGFR1c, 3c and FGFR4 FGFR1c, 2c, 3c and FGFR4 FGFR1c, 2c, 3c and FGFR4
FGF9	FGF9 FGF16 FGF20	FGFR2c, 3b, 3c and FGFR4 FGFR4 FGFR1c and 2c
FGF19	FGF19 FGF21 FGF23	FGFR1c, 2c, 3c and FGFR4 FGFR1c and 3c FGFR1c, 3c and FGFR4
FGF11 (iFGFs)	FGF11 FGF12 FGF13 FGF14	No activation of FGFRs

facilitate binding of FGFs to their receptors. HS stabilizes FGFs by preventing thermal denaturation and proteolysis and forms a bridge connecting FGFs to FGFRs (Itoh and Ornitz, 2004; Ornitz and Itoh, 2015). Unique HS binding patterns result in variation in downstream FGF signalling during development (Thisse and Thisse, 2005). The FGF signalling pathway works across the epithelium-mesenchyme boundaries such that an FGF in the epithelium will activate another FGF in the mesenchyme; this prevents autocrine signalling within compartments (Ornitz and Itoh, 2015).

Most FGFs have N-terminal cleavable signal peptides and are readily secreted from the cell, however, exceptions include FGF1, 2 and the FGF9 subfamily. FGF1 and 2 lack cleavable signal peptides and are displayed on the cell surface as well as within the extracellular matrix. When they are released from the cell, it is by an exocytotic pathway that is not associated with the endoplasmic reticulum-Golgi pathway (Ornitz and Itoh, 2001). The FGF4, 7 and 8 subfamilies contain an N-terminal cleavable signal peptide and are readily cleaved and released into the extracellular matrix and bind to HS. The N-terminal signal peptide is absent in the FGF9 subfamily but these FGFs are readily secreted from the cell due to the presence of an internal hydrophobic sequence that allows their secretion out of the cell through the endoplasmic reticulum (Revest *et al.*, 2000; Ornitz and Itoh, 2015).

The FGF11 subfamily, also called intracellular FGFs (iFGFs), acts intracellularly and does not bind to FGFRs (Pownall and Isaacs, 2010). The FGF19 subfamily are endocrine FGFs. They do not bind to HS in the extracellular matrix which allows them to

act as endocrine factors. Instead, their activation of FGFRs require the klotho family proteins (Goetz *et al.*, 2007; Ornitz and Itoh, 2015).

1.3.2 Fibroblast Growth Factor Receptors

FGFRs are tyrosine kinase receptors that contain an extracellular ligand binding domain, a transmembrane domain and an intracellular tyrosine kinase domain (Figure 1.4). The extracellular domain is composed of three immunoglobulin-like domains (I, II and III). There are seven to eight acidic residues (termed the acid box) in the linker region between domain I and II and a heparin binding site in domain II (Eswarakumar *et al.*, 2005). Furthermore, *FGFRs*1-3 can undergo alternative splicing at its carboxy-terminal in the immunoglobulin-like domain III, forming either IIIb or IIIc isoforms (Miki *et al.*, 1992; Eswarakumar *et al.*, 2005). Generally, alternative splicing occurs in exons 7-10 of the *FGFRs*. *FGFR1* contains 18 exons and alternative splicing takes place between exons 7 and 8 to give isoform *FGFR1b* and *FGFR1c* (Huret, 2009). *FGFR2* contains 21 exons and alternative splicing occurs between exons 9 and 10 to give isoforms *FGFR2b* and *FGFR2c* respectively (Kato, 2009). *FGFR3* contains 19 exons, and alternative splicing occurs between exon 7 and 8 to give isoform *FGFR3b* and *FGFR3c* (Bonaventure, 1998). These isoforms are also often described to be specific to either the epithelium (IIIb) or the mesenchyme (IIIc; reviewed in Ornitz and Itoh, 2001). However, during early developmental stages, no such specification exists and the receptors only become more tissue specific as development proceeds (Nishita *et al.*, 2011). *FGFR4* does not

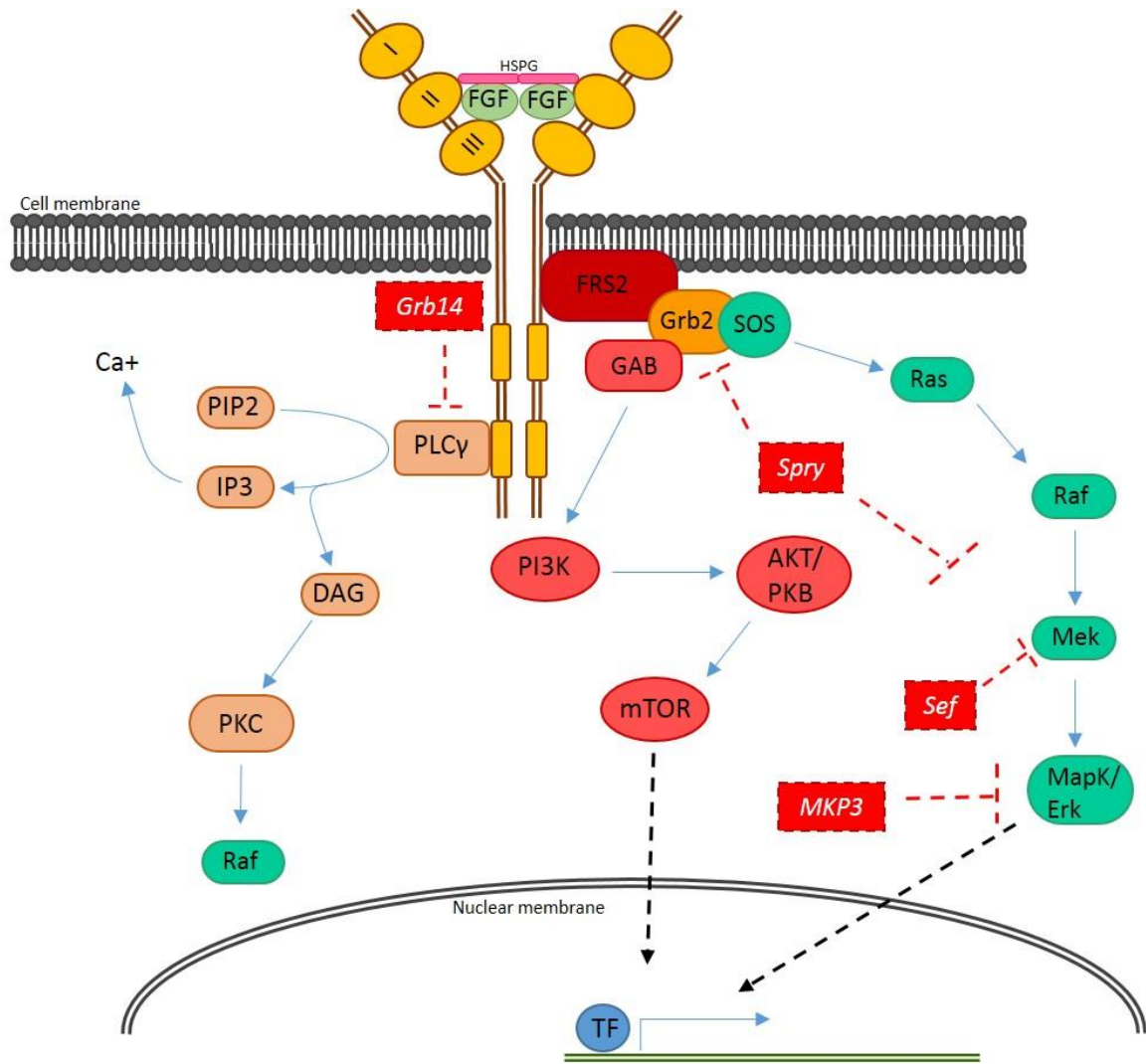


Figure 1.4. The FGFR pathway. Activation requires a 2:2:2 complex of FGF-FGFR-HSPG. FGF related changes in the cell are carried out through the activation of Ras/MAP kinase (in green), PI3K/AKT (in pink) and PLC γ intracellular signalling pathways (in brown). Inhibitors (in red) of the pathway include Spry, Sef, MKP3 and Grb14. Blue arrows indicate activation and red dashed lines show inhibition. Modified from Pownall and Isaacs (2010) and Ornitz and Itoh (2015).

undergo alternative splicing. Moreover, binding experiments show that ligand binding takes place between immunoglobulin-like domains II and III whereas the immunoglobulin-like domain I and acid box have an autoinhibitory function (reviewed in Eswarakumar *et al.*, 2005). Therefore, Oslen *et al.* (2004) proposed that the FGFR exists in two forms; an autoinhibited closed form and an active open form that will result in dimerization and activation of the receptor. This hypothesis was further supported by Sarabipour and Hristova (2016). Both forms exist in equilibrium and the binding of FGF along with their cofactors shifts this equilibrium towards the active form resulting in dimerization and autotransphosphorylation of the receptor and activating further downstream intracellular signalling pathways.

1.3.3 Downstream FGF-FGFR Signalling Pathways

The activation of FGFR takes place through its homodimerization when FGF molecules with HSPG attach to either the extracellular IgII or to the IgIII domain in a 2:2:2 configuration (Schlessinger *et al.*, 2000; Zhang *et al.*, 2006). Homodimerization causes phosphorylation of several tyrosine residues in the intracellular domain of the receptor. Other intracellular proteins attached to these phosphorylated tyrosine residues, become activated and lead to activation of downstream signalling pathways (Itoh and Ortiz, 2004). The intracellular downstream pathways that can be activated through FGF-FGFR signalling are; the Ras/MAP kinase pathway, the phosphoinositide-3 kinase (PI3K)/AKT pathway and the phospholipase C γ (PLC γ) pathway (Figure 1.4).

However, integrins, cadherins and neural cell adhesion molecules are also recognized to activate the FGF pathway through non-canonical activation of the FGFR (reviewed in Polanska *et al.*, 2009).

The Ras/MAP kinase pathway, which is required for cell proliferation and differentiation, is activated by the phosphorylation of FGFR substrate 2 (FRS2; reviewed in Eswarakumar *et al.*, 2005). FRS2 is a membrane bound protein, which when activated, leads to the binding of Grb2 and SOS complex. This results in activation of Ras which activates Raf followed by activation of MEK and MAP kinases. The MAP kinases enter the nucleus and phosphorylate appropriate transcription factors (Thisse and Thisse, 2005). Grb2, through the binding and phosphorylation of the Gab scaffolding protein is also involved in the activation of PI3K which in turn activates AKT/protein kinase B. AKT/protein kinase B are important for regulating cell survival and growth not only in malignant cells but also in normal development (Nicholson and Anderson, 2002). Autophosphorylation of tyrosine residues in the intracellular domain of the FGFRs also activates the PLC γ pathway. PLC γ hydrolyzes phosphatidylinositol-4,5-diphosphate (PIP₂) to inositol-1,4,5-triphosphate (IP₃) and diacylglycerol (DAG; Ueda *et al.*, 1996). IP₃ induces the release of calcium and DAG activates protein kinase C (PKC). This PKC then activates Raf thereby activating the downstream MAP kinase pathway without activating Ras. The PLC γ pathway is involved in cell migration (Ueda *et al.*, 1996).

1.3.4 Inhibitors of *FGF* Pathway

Apart from HSPG specificity, the *FGFR* pathway is also regulated by inhibitors (Figure 1.4). The Sprouty (SPRY) proteins are generally involved in the inhibition of receptor tyrosine kinases and downstream MAPK pathway. In the FGF signalling pathway, SPRY acts upstream of Ras and binds to the Grb/SOS complex (Hanafusa *et al.*, 2002; Pownall and Isaacs, 2010). In some cases, SPRY can also bind directly to Raf inhibiting the activation of Raf by PKC (Sasaki *et al.*, 2003; Thisse and Thisse, 2005; Pownall and Isaacs, 2010). Another protein, *sef*, has similar expression to FGF and functions by binding to MEK and inhibiting the dissociation of MEK-ERK thereby inhibiting the transportation of MAPK to the nucleus (Torii *et al.*, 2004; Thisse and Thisse, 2005; Ornitz and Itoh, 2015). Other inhibitors include MAP kinase phosphatase 3 (MKP3) which dephosphorylates the active MAPK protein (Camps *et al.*, 2000; Zhao and Zhang, 2001; Thisse and Thisse, 2005) and GRB14, an adaptor protein which by binding to *FGFR* tyrosine residues inhibits activation of the PLC γ pathway (Browaeys-Poly *et al.*, 2010; Ornitz and Itoh, 2015).

1.4 *FGFR* Expression in Placodal Interactions:

Since this thesis focuses on *FGFR* expression, a discussion of FGFRs during placodal development follows. Similar to the process of conjunctival papillae development, both feather and tooth development require epithelial-mesenchymal

interactions and form through epithelial thickenings called placodes (reviewed in Jourdeuil and Franz-Odenaal, 2016).

The development of feathers begins by formation of a dense dermis and establishment of a dermis feather tract (reviewed in Chen *et al.*, 2015). Upon the formation of feather tracts, the morphogens involved distribute themselves in the tissue to form the bud and inter-bud regions. This is followed by the formation of epithelial placodes in the bud region and condensations in the dermis below the placodes. The feather buds then undergo morphogenesis to eventually form the feather (reviewed in Chen *et al.*, 2015). *FGFR1* is first expressed in the feather tracts prior to bud formation and is later observed in the dermis during condensation formation (Noji *et al.*, 1992; Song *et al.*, 1996). The expression of *FGFR1* increases in the feather buds after its formation and decreases in the inter-bud region. In contrast, *FGFR2* is expressed in the anterior of the feather buds and between the buds (Noji *et al.*, 1992). *FGFR3* on the other hand is observed throughout the mesenchyme. A mutant chicken, called *scaleless*, with significantly reduced feathers and scales, has only a few conjunctival papillae and develops only a few large scleral ossicles (Palmoski and Goetinck, 1970). *Scaleless* chickens have a mutation in *FGF20* (Wells *et al.*, 2012) and do not express *FGFR1* (Song *et al.*, 1996). It is unknown whether they express *FGFR2c*, the other receptor that binds *FGF20* (Table 1).

There are four stages in tooth development, the first signals are observed in the presumptive epithelium in the initiation-stage prior to epithelial thickening

(Porntaveetus *et al.*, 2011). This is followed by placode formation and the invagination of the epithelium to form the bud. The inner and outer enamels as well as the dental follicle are formed at the cap-stage and terminal differentiation into odontoblasts occurs at the bell-stage (Porntaveetus *et al.*, 2011). The initiation and early bud-stage are similar to the papillae formation stage during scleral ossicle development. In the initiation stage, before epithelial thickening, *FGF17*, 8 and 9 was observed in the epithelium (Kettunen *et al.*, 1998; Porntaveetus *et al.*, 2011) and the receptor that they activate, *FGFR1c*, was observed in the mesenchyme (Kettunen *et al.*, 1998). In addition, *FGF10* was detected in the epithelium as well as the mesenchyme (Kettunen *et al.*, 2000) and it most likely associates with the *FGFR2b* receptor found in the epithelium (Kettunen *et al.*, 1998). During the epithelial thickening, in the mesenchyme, *FGF10* was weakly expressed (Kettunen *et al.*, 2000) and most likely activates *FGFR2b* in the epithelium. In the epithelium, *FGF15* was weakly expressed on the buccal side of the tooth germ, and *FGF20* was strongly expressed at the tip, these act on *FGFR1c* found in the mesenchyme (Kettunen *et al.*, 1998). At the bud stage, *FGF20* was expressed at the posterior part of the tooth germ epithelium (Porntaveetus *et al.*, 2011) along with *FGF4*, 8 and 9 (Kettunen *et al.*, 1998). *FGF18* was expressed in the mesenchyme in both the buccal and lingual part but not beneath the epithelial bud (Porntaveetus *et al.*, 2011). *FGF10* was also expressed at these sites (Kettunen *et al.*, 2000). In the late bud stage, *FGF3* was weakly expressed at the tip of the epithelium as well as in the adjacent condensed mesenchyme (Kettunen *et al.*, 2000). Here, *FGFs* were most likely activated by

association with *FGFR2b* in the epithelium and *FGFR1c* and *2c* in the mesenchyme (Kettunen *et al.*, 1998).

Since the early stages of feather and tooth formation are similar to that of the early stages of conjunctival papillae development, they can be used to hypothesize signalling patterns during conjunctival papillae development (Jourdeuil and Franz-Odendaal, 2016).

1.5 *FGFRs* in Bone Development:

The role of FGF in bone development is often studied through mouse and chick models of limb development as well as calvariae development. The majority of these studies however, have been conducted on the development of limbs and the role of *FGFs* in endochondral development (Peters *et al.*, 1992; Ohuchi *et al.*, 1997; Sekine *et al.*, 1999; Lewandoski *et al.*, 2000 are just a few). In contrast, not as much is known about the role of *FGFs* in intramembranous ossification and calvarial bone development. Mutations in *FGFRs1-3* are known to cause craniosynostosis which is often characterized by premature closure of sutures in the skull, for example Apert's Syndrome (Ornitz and Marie, 2002). *FGFR3* mutations have also been attributed to various dwarfing chondrodysplasias, such as achondroplasia and hypochondroplasia (Superti-Furga *et al.*, 1995; Hecht and Francomano, 1995; Ornitz and Marie, 2002). In calvarial bones, *FGFRs1-3* are involved from the pre-osteoblast differentiation to the mature osteoblast. *FGFR1* and *2* are expressed in the mesenchyme before ossification. During early

development, *FGFR1* promotes osteoblast differentiation, however, it inhibits mineralization by mature osteoblasts (Jacob *et al.*, 2006; Long, 2012). *FGFR2* promotes preosteoblast proliferation during early stages and is later involved in the differentiation of osteoblasts (Eswarakumar *et al.*, 2002; Yu *et al.*, 2003; Long, 2012). After ossification, they are found along with *FGFR3c* in proliferating pre-osteoblasts and osteoblasts (Delezoide *et al.*, 1998). *FGFR2* is involved in osteoblast differentiation (Haÿ *et al.*, 2002; Ornitz and Marie, 2002). Whereas *FGFR3* might be involved in osteoid mineralization (Jacob *et al.*, 2006; Long, 2012). In this way, *FGFRs* may be involved in the maintenance of osteoblast numbers, essential for proper bone growth and development.

During endochondral bone development, such as in long bone development, *FGFR1* is expressed in the mesenchyme and *FGFR2b* in the epithelium at the limb bud initiation stage (Delezoide *et al.*, 1998). *FGF10* from the mesenchyme is the initial signal required for induction of *FGF8* in the ectoderm. Here, *FGF10* binds to *FGFR2b* and induces expression of *FGF8* which in turn binds to *FGFR1* and helps to maintain the required levels of *FGF10* in the underlying mesenchyme (Peters *et al.*, 1992). When mesenchymal condensations begin to occur (to form the limb cartilage), *FGFR2c* can be detected in the condensation, whereas *FGFR1* can be observed in the periphery of the condensation. At the same time, *FGFR2b* is expressed in the apical ectodermal ridge (Ohuchi *et al.*, 1997). Later, *FGFRs1* and 2 are expressed in the periosteum and the perichondrium (Delezoide *et al.*, 1998) indicating a role in osteoblast proliferation and differentiation. *FGFR3* is only observed at the mesenchymal condensations in areas

where chondrogenesis has begun and it is therefore suggested that *FGFR3c* could be involved in chondrocyte proliferation and differentiation (Peters *et al*, 1992; Delezoide *et al*, 1998; Ornitz and Marie, 2002).

1.6 Objectives and Hypothesis:

The goal of this thesis was to investigate whether the *FGF* pathway is involved in the scleral ossicle system. The study had two main objectives:

- 1) To determine the expression patterns of the *FGFR1-3* isoforms at different stages of conjunctival papillae and scleral ossicle development.
- 2) To determine whether the *FGF* pathway is involved in ossicle development.

The spatio-temporal expression pattern of *FGFRs1-3* at the different stages of the scleral ossicle development system (HH30-37) was determined using whole mount *in situ* hybridization (WMISH). Based on the expression of *FGFRs* observed during feather, tooth and bone development, I hypothesize that prior to papillae development, *FGFR2b* will be observed in the epithelium and *FGFRs 1c* and *3c* will be expressed in the mesenchyme. In contrast, *FGFRs 1b*, *2c* and *3b* will be expressed after the papillae have formed. During scleral ossicle induction, *FGFR1c* and *3c* will be expressed in the mesenchyme due to their role in pre-osteoblast proliferation. Whereas later during ossicle development, all *FGFRs* will be expressed due to their role in osteoblast differentiation.

To determine whether the *FGF* pathway is involved in scleral ossicle development, an *FGFR* inhibitor, SU5402, was applied at HH34 (at the time when all conjunctival papillae have formed) and the effect on scleral ossicle development was observed. SU5402 is a tyrosine kinase inhibitor, commonly used to inhibit FGFRs by preventing binding of FGFs to their receptors (Toledo *et al.*, 1999). Due to the importance of *FGFR* in osteoblast lineage as well as their importance in placode formation in other systems, I hypothesize that inhibition of the *FGF* pathway will result in missing ossicles and therefore a reduction in ossicle number.

1.7 Significance of this Research

This research aims to identify whether FGFRs are involved in intramembranous ossification by using the chick scleral ossicle system as a model. The research thus has the potential to identify additional FGFs that could be involved in the development of other intramembranous bones. It will also pave the path for further investigation into possible protein signalling pathways that may influence or be influenced by the expression of FGFRs during abnormal intramembranous bone formation (e.g. in disorders such as craniosynostosis). Furthermore, the identification of FGFRs during conjunctival papillae development will provide important knowledge on the development of non-neurogenic placodes. Additionally, due to the absence of scleral ossicles in mammals, unravelling the molecular signals underlying scleral ossicle development will provide insights into the evolutionary changes of the mammalian eye.

2.0 Materials and Methods

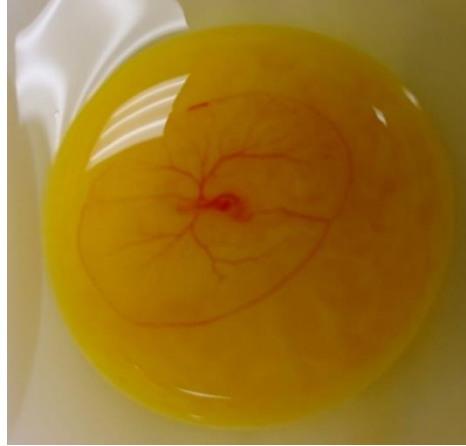
2.1 Chicken Embryo:

Fertilized chicken eggs were obtained from Nova Scotia Agricultural College (Truro, NS) and kept at 4°C until incubation. The eggs were incubated at $37 \pm 1^\circ\text{C}$ in 40% humidity and turned 180° once daily. Chicken embryos were staged according to Hamburger and Hamilton (1951) staging criteria.

2.2 Ex-Ovo Culturing:

At approximately 3 days post fertilization (HH20/21), eggs were removed from the incubator for *ex-ovo* culturing, also known as shell-less culturing (Figure 2.1A; Cloney and Franz-Odendaal, 2015). The eggs were wiped with 70% ethanol, cracked and the embryo (Figure 2.1A) was carefully placed in a new weigh boat (Fisherbrand, 08732113, 89 x 89 x 25mm; Figure 2.1B). Eggs were discarded if they were infertile (where no visible heartbeat or developing vasculature was observed) or damaged (those embryos whose yolk sac had broken). To the *ex-ovo* embryo, 40 μL of penicillin-streptomycin (containing 5000U penicillin and 5mg/ml streptomycin: Sigma, P4458) was pipetted onto the albumin to prevent infection. A Tupperware box (12 x 12 x 6cm), its cover and the cover of a square petri plate (90 x 15mm) were wiped with 70% ethanol and allowed to dry. The Tupperware box was lined with a thick layer of Kimwipes which were then soaked in autoclaved distilled water. The weigh boat containing the embryo was placed inside the container and covered with the square petri-plate cover (90 x 15mm). The

(A)



(B)



(C)



Figure 2.1. *Ex-ovo* culturing set up. (A) 3-day old embryo, HH20; (B) the embryo is grown outside the shell in a weigh boat placed inside a Tupperware container; (C) same embryo in a closed container to maintain humidity.

Tupperware box cover was then placed on top leaving all sides open to allow good air flow. The box was placed inside an incubator at 37°C until next required (Figure 2.1C). Autoclaved distilled water was added to the Kimwipes using a plastic Pasteur pipette every 2-3 days to prevent the embryo from drying up and to maintain humidity inside the container. Additionally, a tray of water was placed inside the incubator. Embryos were cultured until E6.5, 7, 7.5, 8, 9, 10 and 11 (HH30-37) for WMISH and until E8 (HH34) for bead implantation.

2.3 Probe Preparation and Whole Mount In Situ Hybridization (WMISH):

2.3.1 Cloning

Plasmids containing *FGFRs* 1b, 1c, 2b, 2c, 3b and 3c were a kind gift from Dr. Gary Schoenwolf (Department of Neurology and Anatomy, University of Utah School of Medicine, USA). pCRII-Topo plasmids were removed from the filter paper by placing the filter paper in a sterile Eppendorf tube with TE buffer (pH 8.0) for 5 minutes. The tube was then vortexed at 3000 rpm for 1 minute and incubated at room temperature for 30 minutes. The filter paper was carefully removed from the tube and placed in a new sterile Eppendorf tube. Both tubes were stored at -20°C (Appendix A4).

Competent *E. coli* cells (HB101 competent cells, Promega L1011) were removed from storage at -80°C, allowed to thaw on ice and 100µL of cells were pipetted into chilled 2mL Eppendorf tubes. Plasmids were transformed into competent *E. coli* cells (see Appendix A5 for more details) by adding 10µL of the plasmids to the experimental

tubes. 10 μ L of TE buffer (pH 8.0) was added to the control tubes. Tubes were placed on ice for 15-20 minutes, heat shocked for 45 seconds in a 42°C water bath and placed back on ice for 2 minutes. To each of the tubes, 900 μ L of cold LB broth was added and the tubes were incubated for one hour at 37°C with shaking. From each tube, 100 μ L was pipetted onto agar plates and streaked using sterile loops. The plates were turned upside down and incubated at 37°C.

The next day, the edges of autoclaved glass test tubes were flamed and a small amount of LB broth (\pm 1 inch of solution) was poured into the tubes. A small sterile pipette tip was used to pick up a single colony from the agar plate and this was placed inside the tube containing the LB broth. The tubes were incubated overnight at 37°C with shaking (NewBrunswick Scientific, Excella E24 Incubator Shaker Series) to increase the number of clones.

2.3.2 Isolation of Plasmid

Plasmids containing *FGFR* cDNA were isolated using a mini preparation protocol (Appendix A5 for details). From the overnight culture containing the transformed cells, 2mL of the culture was transferred into a sterile Eppendorf tube and centrifuged at 13000 rpm for 1 minute to give a small bacterial pellet. The supernatant was discarded and 250 μ L of cold buffer with 0.82 μ L of RNase A (Sigma, R-4642) was added and the pellet was homogenized into the solution by vigorous pipetting. To the mix, 250 μ L of cold lysis solution was added and the tube was placed on ice for 5 minutes. The tubes were placed back on ice for 5 minutes after adding 250 μ L of cold potassium acetate

and then centrifuged at 13000 rpm for 5 minutes. The supernatant was transferred into a new sterile Eppendorf tube, 200µL of phenol from phenol-chloroform was added to the tube and shaken vigorously for 30 seconds. The tube was centrifuged for 5 minutes at 13000 rpm and the top layer was transferred into a new tube while the bottom layer was discarded. Equal amounts of 100% isopropanol was added and the tube was incubated for 5 minutes, then centrifuged at 13000 rpm for 5 minutes to form a pellet. The supernatant was discarded, 200µL of 95% ethanol was added and the pellet was washed by inversion. The tube was centrifuged at 13000 rpm for 5 minutes to resettle the pellet, the supernatant was discarded and the tube was bench dried upside down. Once dry, the pellet was re-suspended in 50µL of SuperQ H₂O. Half a microliter of this purified plasmid was run on a 0.8% agarose gel to confirm desired results (Section 2.3.5; Figure 2.2A).

2.3.3 Linearization of Plasmid

All *FGFR* cDNA had been inserted into the pCRII-Topo plasmid, a 4kb plasmid. Restriction sites flanking the area of insert were unknown, therefore an NcoI restriction enzyme site far from the area of insert was selected. The plasmids were linearized (Appendix A6) by mixing 5µL of the plasmid obtained from mini preparation with 1.5µL of NcoI restriction endonuclease (Sigma, R8761) and 10x endonuclease buffer SH (Sigma, B3657). A final reaction volume of 50µL was made by adding 38.5µL of DEPC H₂O. The reaction mix was incubated at 37°C overnight to allow linearization and then heat inactivated the next day by incubating at 65°C for 15 minutes. The digest was

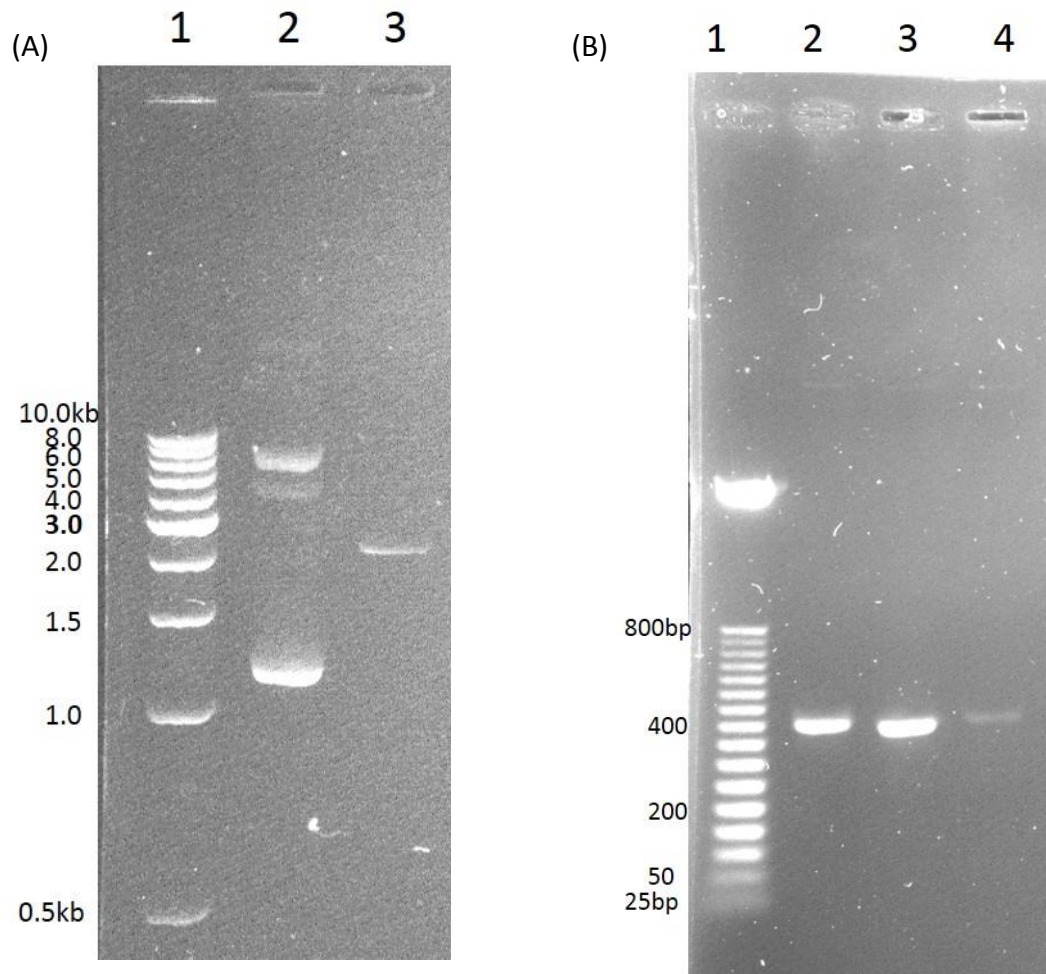


Figure 2.2. Representative gel images of probe preparation. (A) miniprep and restriction digest of FGFR3b; lane 1: 1kb ladder, 2: miniprep; 3: restriction digest. (B) PCR of FGFR3b; lane 1: 50bp ladder; 2: PCR 3: clean-up PCR elution 1; 4: clean-up PCR elution 2

cleaned using the High-Pure PCR product purification kit (Roche-11 732) according to the manufacturer's instructions. Half a microliter of the digest was run on a 0.8% agarose gel [0.8g agarose (Sigma, A9539), 100ml 1x TBE] to confirm linearization (Figure 2.2A).

2.3.4 Polymerase Chain Reaction

Once linearized, the plasmid DNA and insert were amplified via polymerase chain reaction (PCR) to obtain the gene of interest (Appendix A7). The area of gene of interest was flanked by M13 primer binding sites. A 50 μ L master mix was made containing 10 μ L of 5x reaction buffer (Biolabs, #B0324S), 1 μ L of dNTP mix (Biolabs, #N0447L), 2.81 μ L each of M13 forward (Promega, Q5391) and reverse primers (Promega, Q5401), 0.25 μ L of Taq polymerase (Biolabs, #M0324S) and 32.63 μ L of DepC H₂O to give a final volume of 49.5 μ L. To the master mix, 0.5 μ L of template DNA (linearized plasmid DNA) was added, the tube was briefly spun to mix all the reagents and placed into the Mastercycler PCR machine. The PCR reaction was 35 cycles (Appendix A7). The PCR product was cleaned using the High-Pure PCR product purification kit (Roche-11 732) according to the manufacturer's instructions and two elutions were made where elution 1 had a higher concentration of DNA. All *FGFR* cDNA was approximately 170bp long, however, the PCR product contains the region between the two M13 sites, not just the insert, and therefore a product of approximately 440bp was expected. One microliter of the PCR product was run

alongside a 50bp ladder (Promega, G452A) on a 0.8% agarose gel to confirm the desired product size (Figure 2.2B).

2.3.5 Gel Electrophoresis

A 100ml 0.8% agarose gel was made in 1x TBE (89mM Tris-Cl, 89mM boric acid, 2mM EDTA, pH 8.0) with 6 μ L of 3X GelRed nucleic acid stain (Biotium 41003) and was set with a 13 well wide-toothed comb. A sample of 0.5 μ L was mixed with 2 μ L of 6x loading dye (Promega, G190A) and DepC H₂O. A total of 6 μ L, was loaded onto the gel. Plasmids and restriction digests were run alongside a 1kb ladder (Promega, G694A) and PCR products were run with a 50bp ladder (Promega, G4521). Electrophoresis was done at 100V for 1 hour and 30 minutes. The brightest band on each ladder corresponds to approximately 1 μ g/ μ L of DNA (Figure 2.2). Therefore, the gel was used to estimate both the size and concentrations of the samples. Gel images were taken using the Bio Doc-It™ 220 Imaging System.

2.3.6 DNA Sequencing

To ensure that the PCR product was specific to the gene of interest, cleaned PCR samples were sent for sequencing to the DNA sequencing facility at The Hospital for Sick Kids in Toronto, Canada (<http://www.tcag.ca/>). The samples were processed and sent to the facility according to the sample submission guidelines. Cleaned PCR products were diluted in DepC H₂O such that 1 μ L of the sample would contain approximately 10ng of DNA. Upon receiving the results, the sequence was blasted using the NCBI Blast tool against the database of *Gallus gallus*. Blast results showed 98%-100% identity for *Gallus*

gallus FGFR specific to each isoform (Appendix B). The sequence of each gene was identified and the sequences were also blasted against each other to ensure that any expression observed from whole mount *in situ* hybridization would not be due to the probe of one *FGFR* isoform binding to sites of another isoform. Each Blast resulted in 0% sequence similarity.

2.3.7 RNA probe synthesis

Digoxigenin-labelled RNA probes were made using a DIG-RNA labelling kit (Roche-11 175 029 10; see Appendix A8). In a final volume of 20 μ L, 1 μ g of template DNA (from elution one of cleaned PCR product) was mixed with 2 μ L of 10x DIG labelling, 2 μ L of 10x transcription buffer, 1 μ L of protector RNase inhibitor, 2 μ L of either RNA polymerase T7 (for *FGFR* 1c, 2b, 2c, 3b and 3c) or Sp6 (for *FGFR*1b) and DepC H₂O. The mix was incubated in the thermocycler at 37°C for 2 hours. To degrade the template DNA, 2 μ L of DNaseI recombinant RNase free (Roche, 04 716 728 001) was added and to the sample and the tube was incubated in the thermocycler for a further 15 minutes. The reaction was stopped by adding 2 μ L of 0.2M EDTA (pH 8.0). One microliter of this product was used to perform a dot blot and the rest was stored at -20°C.

A dot blot was performed to confirm labelling of the RNA probe (Figure 2.3; Appendix A9 for details). One microliter of each of the RNA probes and a control labelled RNA (provided in the DIG-RNA labelling kit) was used to create a dilution series of five different concentrations of probe (10ng/ μ L, 1ng/ μ L, 10pg/ μ L, 3pg/ μ L and

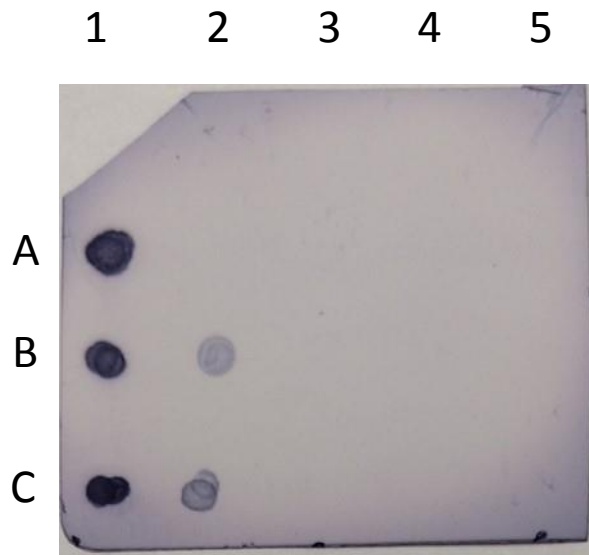


Figure 2.3. Representation of a dot-blot. Row A shows controlled labelled RNA and row B and C are FGFR3b and 3c probes respectively. Column 1-5 are dilutions with final RNA concentrations of 10ng/ μ L, 1 ng/ μ L, 10pg/ μ L, 3pg/ μ L and 1pg/ μ L respectively.

1pg/ μ L). A microliter of each of the dilutions was placed onto a nitrocellulose membrane (Roche, 11 209 299 001). The membrane was baked at 120°C for 30 minutes to fix the nucleic acids onto the membrane and then washed for 2 minutes in maleic acid buffer (0.1M maleic acid, 0.15M NaCl). The membrane was then placed in blocking solution (2% sheep serum, 3% skim milk powder in 1x TBST) for 20 minutes, washed in 1x TBST for 5 minutes and incubated in digoxigenin-antibody solution [1:5000 anti-DIG-AP antibody (Roche, 11 093 274 910) in 1x TBST] for 30 minutes with shaking at room temperature. After washing twice for 15 minutes in washing buffer (0.1 M maleic acid, 0.15 M NaCl, 0.3% Tween 20) and then in detection buffer (0.1 M Tris-Cl, 0.1 M NaCl, pH 8.0) for 15 minutes at room temperature with shaking, the membrane was incubated in the dark in 10ml of fresh colour solution (0.15 mg/mL BCIP, 0.30 mg/mL NBT in distilled water). The reaction was observed every 30 seconds until the development of the first dot and then periodically for 30 minutes. The probe was considered successfully labelled if the first dot developed colour in the same time frame to that of the control RNA dot. The reaction was stopped by washing the membrane in TE buffer (pH8.0) for 5 minutes at room temperature with shaking.

2.3.8 Whole Mount *In Situ* Hybridization (WHIMS)

A Whole mount *in situ* hybridization protocol was adapted from Nieto *et al.* (1996) and Franz-Odenaal (2008) (Appendix A10 for detailed protocol). Embryos were grown *ex-ovo* and staged according to the Hamburger and Hamilton (1951) staging criteria. Embryo heads were fixed overnight in 4°C from HH30 through to HH37 in 4%

DepC treated paraformaldehyde (PFA). The next day, embryos were serially dehydrated through cold methanol and stored at -20°C in 100% methanol for at least four weeks before processing further.

The heads were bisected and the eye lids and nictitating membrane were removed along with the vitreous humor and the lens. The half heads were rehydrated through the graded methanol series and bleached overnight in 10% hydrogen peroxide to remove eye pigment. The next day, the half heads were permeabilized in 10µg/mL proteinase K, post fixed in 4% PFA/1x PBST/0.25% glutaraldehyde and preconditioned in prehybridization solution. They were then incubated overnight at 60°C in 5mL of prehybridization solution with 2µL of probe (for *FGFRs* 1c, 2b, 2c, 3b and 3c). 3µL of probe was used for *FGFR* 1b as colour development during the dot-blot was slightly slower than that of the control RNA dot and other *FGFR* probes. The following day, the half heads were washed to remove unbound probe, placed in blocking solution, and then incubated overnight at 4°C in anti-DIG antibody solution. Embryo heads were washed several times in 1x TBST to remove excess antibody and then incubated in 1x TBST with 2mM levamisole. The solution was replaced with fresh 2mM levamisole in 1x TBST once every day for a period of three days to reduce background. The heads were then incubated for 12 hours in colour detection solution. Once complete, the reaction was stopped by washing the half heads several times in 5mM EDTA in 1x PBST. They were then post-fixed in 4% PFA and washed in 1x PBS. Post WMISH, the anterior of the eye was dissected from the rest of the eye. The retinal pigmented epithelium as well as

the neural retina was removed using fine blunt forceps. If required, the background staining was leached by further incubating the samples in 90% methanol for several hours. The tissues were then stored in 50% glycerol/distilled water at 4°C.

For each gene, two controls were also processed, a no probe control as well as a no antibody control, to ensure that the expression pattern observed was due to the binding of the probe alone. All probes were made from previously validated genes that showed no sense expression (Nishita *et al.*, 2011) therefore no sense probe controls were carried out. The protocol was carried out on six half heads from six different embryos for each stage for each gene (i.e., n=6 for HH30 for FGFR1b, n=6 for HH31 for FGFR1b, n=6 for HH30 for FGFR1c and so on).

2.4 Cryosectioning:

To determine the localization of the *FGFR* expression, cryosectioning was performed on eye tissues that had undergone WMISH. Due to time constraints, only two stages were selected for sectioning for each gene. The first was the time point at which expression in the first group of papillae is distinct and the second selected time point was when a significant change in expression was observed. HH32 and 33 were selected for *FGFR1b* while HH32 and 34 were selected for *FGFRs1c, 2b, 2c, 3b* and *3c*. A small section was cut from each of these eye tissues such that it contained papilla #12 as well as two neighbouring papillae of the temporal group, papillae #11 and #13. A 1% agar [1g agar (Sigma, A7002), 100ml dH₂O] solution was made and allowed to cool for 1

minute before being poured into a small petri plate. In the petri plate, the agar was allowed to cool for another minute. The eye tissue was washed in distilled water for 15 minutes to remove the glycerol, blotted using Kimwipes and placed in the solidifying agar. Once the agar had completely solidified, it was cut into a rectangle with the eye tissue embedded in the middle. The block of agar containing the tissue was then soaked in 30% sucrose until it sunk to the bottom of the tube (2-3 days). To section, the block was glued onto a chuck using Jung tissue freezing medium (Lecia Microsystems, 020108926). Sections were cut at -20°C at a thickness of 14µm and collected on a glass slide.

2.5 Imaging and Analysis:

Whole mount in situ hybridisation stained tissue was observed using the dissecting microscope (Nikon SMZ1000) and slides containing cryosections were observed using the Nikon Eclipse 50i compound microscope. Photographs were taken using a Nikon camera and NIS Elements software. The software was also used to add scale bars to the images. Intensity analysis of expression in WMISH tissues at papillae #12, was done using ImageJ (Appendix C, Figure C1). To do this analysis, images were inverted and converted to greyscale. The area, mean grey value as well as the integrated density of papilla #12 and a small area of their contiguous region (Appendix C, Figure C1) was measured and recorded. An average of three measurements were taken. Similarly, an average of three measurements was also recorded for areas beside the papillae

where no expression was observed (background) and this was used to calculate the corrected intensity (McCloy *et al.*, 2014; Appendix D, Table D4). The following formula was used to calculate the corrected intensity: corrected intensity = integrated density – (area x mean grey value of background). ImageJ was also used to measure the field of expression surrounding the temporal group of papillae. Two maximum diameter measurements were taken at a 90° angle to one another to estimate the field of expression as accurately as possible (Appendix C, Figure C2). Again an average of three measurements was taken and recorded in millimeter (Appendix D, Table D5). To draw a schematic diagram of the field of expression, the diameter measurements in Appendix D, Table D5 were increased by a factor of 100.

2.6 Manipulation tools:

2.6.1 Tungsten needle:

To make needles for bead implantation, the small end of a glass Pasteur pipette was placed under the flame of a Bunsen burner and pulled. The pulled end was then carefully broken with a diamond tip cutter to create an opening. A fine tungsten wire (0.1mm) was carefully placed into the opening and held in place using forceps. The pipette was then once more placed under the flame of a Bunsen burner for the glass to melt around the tungsten needle and seal it in place. To sharpen the needles, an electric charge was set up in a plastic beaker containing 1N NaOH. Wire clamps were connected to a transformer with a paperclip attached to one of the clamps. The paperclip and

clamp were inserted into the beaker containing NaOH to create an electric charge. The needle was submerged into the beaker until the desired sharpness was achieved. Needles were observed under the microscope to ensure required sharpness.

2.6.2 Microinjections needle:

To make needles for microinjections, small capillary tubes (0.5mm inner diameter; Sutter Instrument Co., BF100-50-10) were pulled using a Flaming/Brown micropipette puller (Sutter Instrument Co., Model P-97). The program was set at heat 500, pull 60 and velocity 75. The tips of the needles were etched under the microscope by placing it on top of a glass slide covered in parafilm and using a fresh razor.

Prior to use, the needle was tested and the droplet size was measured. To do this, the needle was filled with 1% DMSO in 0.1% fast green and the needle was connected to a microinjection instrument (Eppendorf, FemtoJet, express). A droplet was injected onto some glycerol on a slide and the size of the droplet was measured. An injection pressure (P_i) of 150-300 was used to give a droplet volume of approximately 2.5nL.

2.7 Inhibition by SU5402:

2.7.1 Preparation of SU5402:

SU5402 (Sigma, SML0443) is a tyrosine kinase inhibitor, commonly used to inhibit FGF-FGFR signalling pathway by preventing binding of FGFs to their (FGFR)

receptors (Toledo *et al.*, 1999). A stock concentration of 50mg/ml SU5402 was made in 100% DMSO according to manufacturer's instructions. From this stock, a working concentration of 3mg/mL and 6mg/mL SU5402 was made by diluting the stock in 50% DMSO (made in distilled water). The working concentration of SU5402 had approximately 56% DMSO and therefore a working concentration of 56% DMSO was used as control.

2.7.2 Preparation of Beads:

Affi-gel blue agarose beads (Bio-Rad, 153-7302) of 60-80 μ m size or charged AG1X2 beads (BioRad 140-1241) of 100-150 μ m size were selected and treated with 1 μ L of SU5402. In control samples, these beads were treated with DMSO. Beads were placed in a cap of an Eppendorf tube; the beads of appropriate size were selected and transferred into an Eppendorf tube containing autoclaved 1x PBS. The beads were washed several times in autoclaved 1x PBS and then the tube was briefly spun down at 13000 rpm. The required number of beads were then placed into a new Eppendorf cap and allowed to air dry and shrink for an hour prior to incubation with the desired solution. The rest of the beads were stored in 1x PBS at 4°C. 1 μ L SU5402 (of 3mg/mL or 6mg/mL) or DMSO was added to each bead in the Eppendorf cap and the beads were allowed to soak in the inhibitor for an hour prior to implantation.

2.7.3 Limb Bead Implantation

Shell-less cultured embryos at HH20/21 (\approx E3) were removed from the incubator and placed under a dissection microscope. The Tupperware box lid and the square petri cover were wiped with 70% ethanol. The wing bud was accessed by tearing open the chorioallantoic membrane and the amniotic membrane. Affi-gel blue beads (n=3 for 3mg/mL SU5402) or AG1X2 beads pre-soaked in SU5402 (n= 3 for 3mg/ml; n=2 for 6mg/ml) and 56% DMSO treated beads (n=4 for AG1X2) were inserted at the tip of the wing bud using curved forceps. 40 μ L of penicillin-streptomycin was added to the *ex-ovo* embryo (as previously described), the square petri lid and Tupperware lid were placed back onto the box containing the embryo and put back into the incubator. Embryos were incubated to HH30/31 (\approx E6.5) as at this stage, the limbs have grown and skeletal elements have formed (Horakova *et al.*, 2014).

2.7.4 Eye Bead Implantation

Embryos at approximately HH34 (E8) were taken from the incubator and placed under a dissection microscope. At HH34, all papillae have been formed but scleral ossicle induction beneath has not yet began (Franz-Odendaal, 2008). The Tupperware lid and the square petri dish cover were wiped with 70% ethanol. Fine sharp forceps were used to pinch blood vessels close to the area of dissection (i.e. above the eye) before creating an opening in the chorioallantoic membrane to prevent death of the embryo due to blood loss. Using the same forceps, an opening was created in the amniotic sac above the eye. Papilla #10 (Figure 1.1A) was identified and a small incision

was made in the conjunctival epithelium next to the papilla using a tungsten needle. AG1X2 beads pre-soaked in SU5402 (n=3 for 3mg/ml; n=2 for 6mg/ml) or DMSO (n=3) was placed into the incision using curved forceps. A tungsten needle was used to help push the bead in place if required. 40µL of penicillin-streptomycin was added to the *ex-ovo* embryo, the square petri dish lid and Tupperware lid were placed back on to cover the embryo and the container was put back into the incubator (as described previously). Embryos were incubated to HH37 (E11). At this stage, all ossicles have been induced (Franz-Odendaal, 2008).

2.7.5 Microinjections

A microinjection instrument (Eppendorf, FemtoJet express) was used to perform these injections. Prior to injections, the microinjection needles (section 2.6.2) were cleaned by soaking the tip of the needle in 70% ethanol and using the 'clean' option on the instrument. Freshly-made 6mg/mL SU5402 (n=11) or DMSO (n=4) were put into sterile Eppendorf tubes. The tubes were spun briefly at 13000rpm and SU5405 or DMSO was inserted into the needle by placing the tip of the needle into the Eppendorf tube and allowing the solution to move up by capillary action. At HH34, embryos were removed from the incubator and the eye was accessed as previously described Section 2.7.4. Using a tungsten needle, an incision was made close to papilla #10 (Figure 1.1A). The first injection was performed above the incision and the second was performed under the incision. 40µL of penicillin-streptomycin was added to the *ex-ovo* embryo before returning it to the incubator. Embryos were allowed to incubate up to HH37.

2.8 Alkaline-Phosphatase (AP) Staining:

Alkaline phosphatase (AP) staining protocol (Appendix A1 for more details) was adapted from Edsall and Franz-Odenaal (2010). Embryos fixed overnight in 4% PFA were washed in 1x PBS and bisected along the sagittal plane. After the removal of eyelids and the nictitating membrane, embryos were washed in distilled water and placed in tris-malate buffer (pH 8.3) for one hour. The embryos were then stained in the AP substrate solution (Appendix A1) for one hour. This staining technique utilises naphthol AS-TR phosphate (Sigma, N6125) which reacts with the alkaline phosphatase enzyme in the osteoblasts to give a colour reaction. The reaction was stopped by washing the embryos in saturated sodium borate solution. Excess stain was removed from the embryos by placing them overnight in a 3% bleach solution. The embryos were then processed through a graded glycerol series and stored in 80% glycerol.

2.9 Alcian Blue Cartilage Staining:

Wings were dissected from limb bead-implanted embryos and were fixed for one hour in 4% PFA and washed in distilled water followed by dehydration in 70% ethanol for an hour. The wings were stained overnight in Alcian blue (Appendix A2) and then rehydrated in a graded ethanol series to distilled water. The wings were washed for a couple of hours in 1% trypsin/saturated sodium borate solution to remove excess

staining and to digest the tissue surrounding the skeletal element so that it is visible.

The wings were then washed in 1x PBS and stored at 4°C.

2.10 Statistical Analysis:

In microinjection experiments using SU5402 and DMSO (controls), the number of ossicles in the left and right eye were counted after AP staining. Dixon's Q-test was used to test for outliers and once the outliers were removed, an independent two-tailed t-test was carried out using MiniTab to analyse the differences observed in the number of scleral ossicles. The t-test was first done between the left and right eyes of DMSO controls and control no-injection (CNI, data from Hammer, 2016) to make sure that DMSO treated controls were similar to controls that did not receive any treatment. Next, the t-test was carried out between the left and right eyes of SU5402 treated and the DMSO controls groups. The t-test was also carried out between the left and right eyes within each treatment group. A one way ANOVA was conducted between number of ossicles in the right eyes of three treatment groups (CNI, DMSO control and SU5402) to test for significance in variance. Defects observed in the eyes were classified into normal, mild moderate and severe. Fisher's Exact test was performed using SPSS to determine if the differences in the frequencies of the defects between DMSO control and SU5402 treated eyes were statistically significant.

3.0 Results

3.1 *FGFR* *In Situ* Hybridization

3.1.1 Probe Validation

The expression patterns for the isoforms of *FGFRs1-3* were determined for stages of development that encompass both conjunctival papillae (HH30-34) development as well as scleral ossicle development (HH35-37). To optimize the protocol, *in situ* hybridization (ISH) using *BMP2* was performed along with a *FGFR* probe at HH35 since this expression pattern has previously been published by our lab (Jourdeuil and Franz-Odenaal, 2017). The whole mount expression pattern of *BMP2* was identical to that of Jourdeuil and Franz-Odenaal (2017; Appendix C, Figure C3). Strong *BMP2* expression was observed in the conjunctival papillae in the nasal, dorsal and ventral groups. In the temporal group, downregulation of the gene was observed in the conjunctival papillae and in the oval-shaped region of the scleral condensation in the mesenchyme. This gene was used as a positive control for the first three ISH experiments.

Two negative controls were used in each *FGFR* ISH experiment: a no probe control, which received primary digoxigenin labelled antibody but no probe, and a no antibody control which received only probe. Both controls were performed at HH35 and showed no expression in the whole mount eyes (Figure 3.1). The brown signal observed in some parts of the eye represent endogenous alkaline phosphatase and is distinctly different to the purple signal in non-control samples (Figures 3.4 – 3.15). The lack of

expression in the negative controls was confirmed by cryosection, which showed no expression in either the epithelium or the mesenchyme (Figure 3.2).

In this chapter, the expression of each *FGFR* isoform will be discussed individually and a comparison between the genes will be done in Chapter 4. Figure 3.3 shows a schematic of the papillae region, the contiguous region of the papillae and the interpapillary region as well as the superficial and deep mesenchyme. This image serves as a reference for the descriptions of gene expression that follow. Figure plates supporting the gene expression text descriptions are provided at the end of each gene's description to ease reading since all embryonic stages are presented in a single figure panel per gene. Cryosections follow this panel.

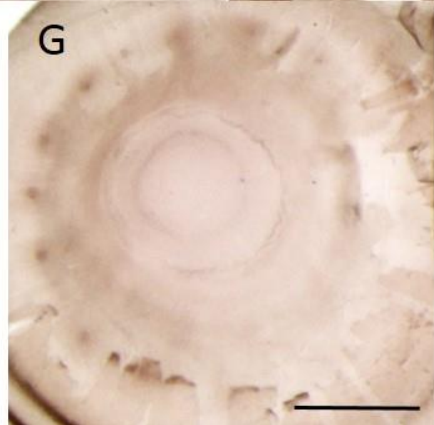
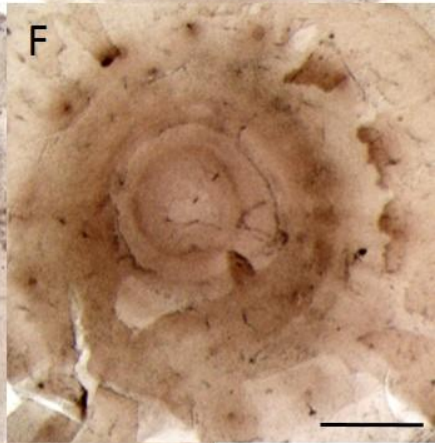
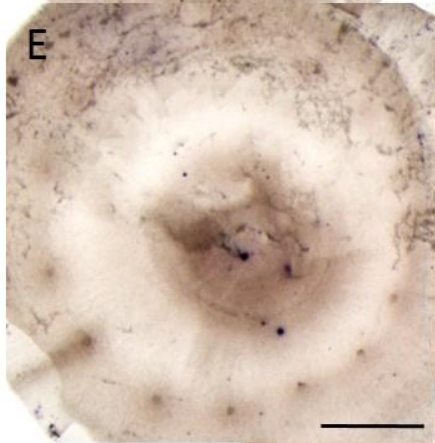
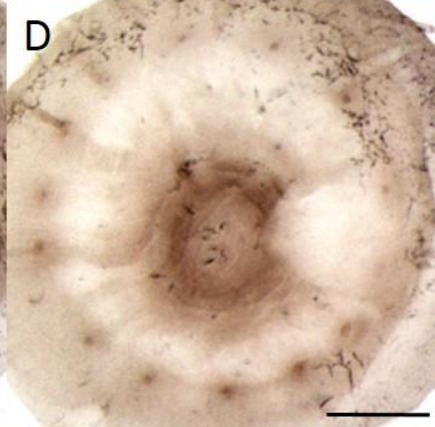
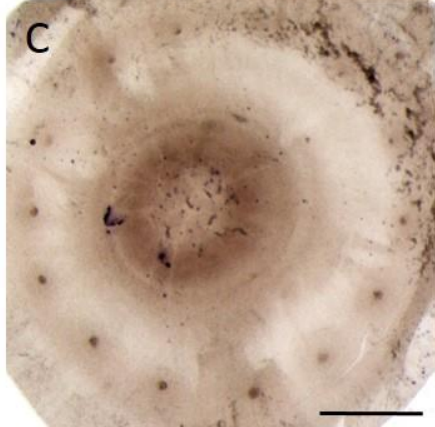
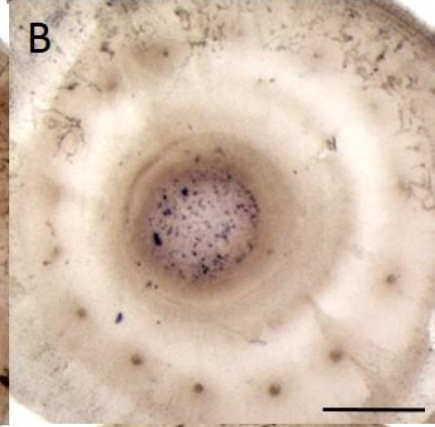
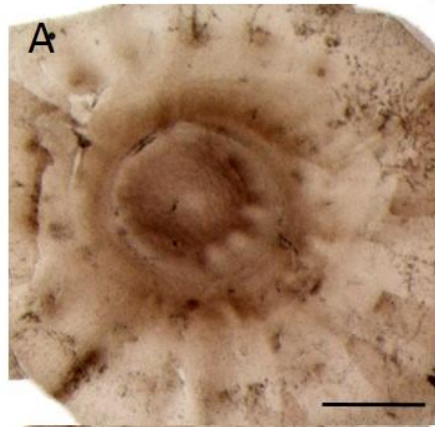


Figure 3.1. *In situ* hybridisation of control embryo eyes at HH35 showing no gene expression. (A) *FGFR1b* probe, received no antibody; (B) *FGFR1c* probe, received no antibody; (C) *FGFR2b* probe, received no antibody; (D) *FGFR2c* probe, received no antibody; (E) *FGFR3b* probe, received no antibody; (F) *FGFR3c* probe, received no antibody; (G) no probe control, received only antibody. Scale bars represent 1mm.

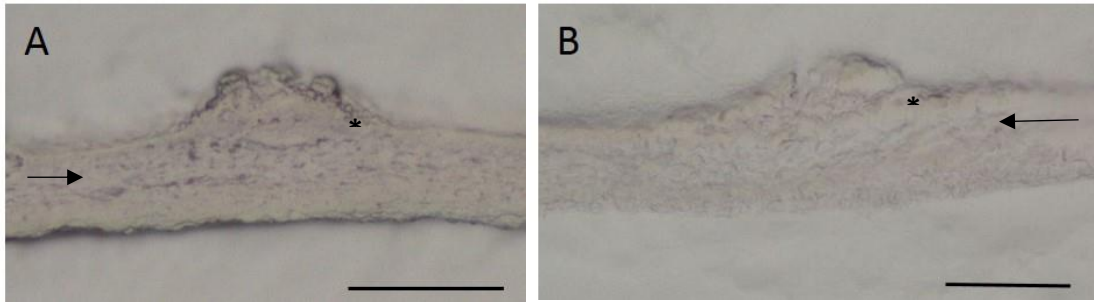


Figure 3.2. Cryosections through conjunctival papillae of control embryo eyes at HH35. Sections show no expression in the epithelium (asterisks) or the mesenchyme (arrow). (A) No antibody control, *FGFR3b* probe; (B) no probe control. Scale bar represents 100 μ m.

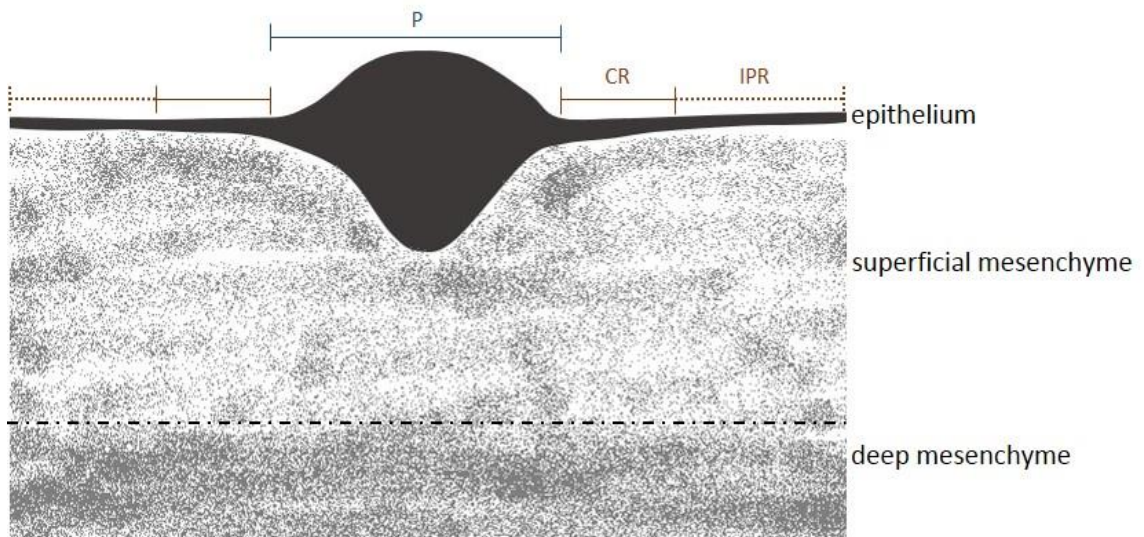


Figure 3.3. A schematic representation of a section through a papilla at HH32/33. This papilla is at Murray stage 2 (Murray, 1943) and shows the epithelium, the superficial and the deep mesenchyme. P: papilla; CR: contiguous region; IPR: interpapillary region. Adapted from Murray (1943).

3.1.2 *FGFR1b* Expression

At HH30, there was strong *FGFR1b* expression in the first conjunctival papilla (papilla #12) that had formed over the ciliary artery (in the temporal region; Figure 3.4A). Low expression was also observed to the left and right of papilla #12 as well as in the nasal region (n=4/6, Figure 3.4A). In two out of six embryo eyes, the papillae beside papilla #12 were more strongly expressed. According to Hamburger and Hamilton (1951) stages of chick embryonic development, at HH30, there are a maximum of two papillae (one papilla forming at the ciliary artery and another beside it). Therefore, the presence of expression in the nasal region was likely marking the position of the next set of papillae. The conjunctival papillae expression became stronger at HH31 (Figure 3.4B). Strong expression of the *FGFR1b* gene was observed in the conjunctival papillae of the temporal region as well as the nasal region (n=5, Figure 3.4B). Less expression was observed in the dorsal region and ventral region, where the next groups of papillae would form. This pattern was also observed at HH32 (n=4/6, Figure 3.4C). In two eyes, at HH32, low expression was observed in the dorsal and ventral regions. Cryosections at HH32 show that the *FGFR1b* gene is primarily expressed in the epithelium with strong expression in the papillae and the CR (Figure 3.5A).

The expression of *FGFR1b* in the conjunctival papillae appeared strongest at HH33 (Figure 3.4D). At this stage, gene expression can also be observed around the papillae. The zone of expression surrounding the conjunctival papillae as well as areas of no expression in the interpapillary region were clearly visible (n=4/6, Figure 3.4D). In 2

of 6 eyes, papillae in the ventral (last) group had less expression and the zone of expression around these papillae was not yet visible. ImageJ was used to measure the diameter of the zone of expression around the papilla at HH33 and indicated an ovoid shape (raw data in Appendix D, Table D5). Cryosections at HH33 show that the *FGFR1b* gene was primarily expressed in the epithelium with strong expression in the papillae and the CR (Figure 3.5B).

At HH34, the expression was downregulated in the temporal group of papilla in all six *FGFR1b* ISH eyes. In three eyes, only papilla #12 (which forms over the ciliary artery) was downregulated (Figure 3.4E) and in others, papilla #12 and its neighbouring papillae were downregulated. A decrease in expression was also observed in the CR in the temporal papillae at this stage. In all papillae, the zone of expression around the papillae was much smaller than that at HH33 (compare Figure 3.4C to 3.4D). In the next two stages of development (HH35 and 36), downregulation of this gene continued. More papillae in the temporal region showed a decrease in expression at HH35 (n=6, Figure 3.4F). At this stage very little expression was observed in the CR surrounding the papillae in the temporal group and a downregulation of the CR was observed around the papillae in the nasal, dorsal and ventral groups. Almost no expression was observed in the temporal region at HH36 (Figure 3.4G). There was a further downregulation of the gene in the papillae in the nasal group and very little expression in the CR around the papillae (n=6, Figure 3.4G). By HH37, there was an almost complete absence of gene expression (n=6, Figure 3.4H).

The intensity of the *FGFR1b* expression was measured across all stages using ImageJ. This analysis showed that the expression in conjunctival papillae near papillae #12 (plus a small part of the CR) was strongest at HH32 (Appendix D, Table D4). From HH30 up until HH32, *FGFR1b* expression was observed in the papillae (including the CR), whereas from HH33 onwards, expression in the CR was visibly separate from the expression in the papillae. Expression of this gene was not observed in the mesenchyme. Whole mount expression showed continual downregulation of this gene from HH34 (Figure 3.4E), however ImageJ measurements indicate that this may occur starting at HH33 (Appendix D, Table D4) at least in the temporal group. The *FGFR1b* gene is significantly downregulated in the temporal group of papillae by HH 35 and completely downregulated by HH37 (Figure 3.4H).

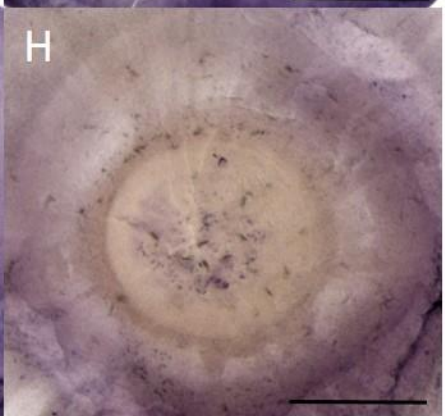
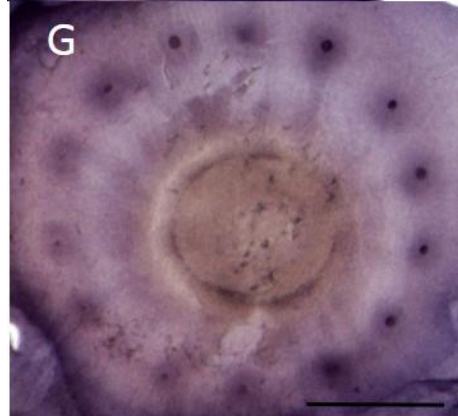
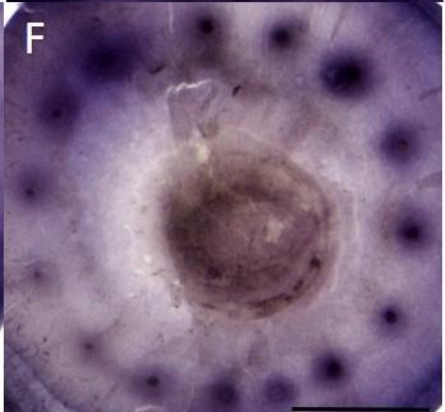
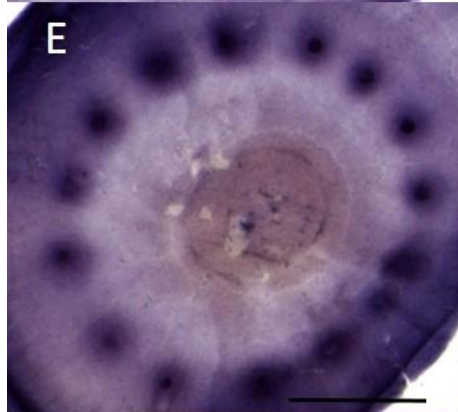
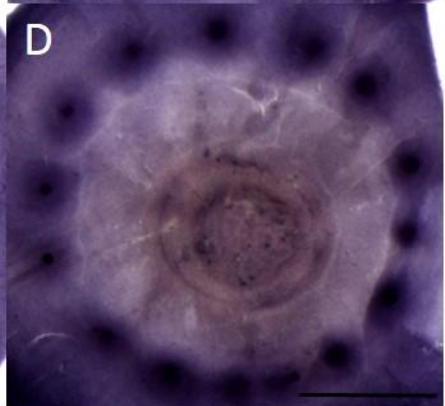
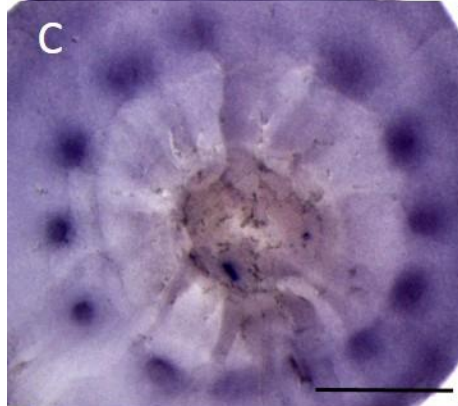
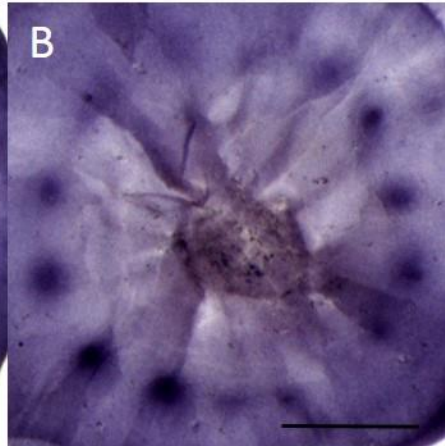
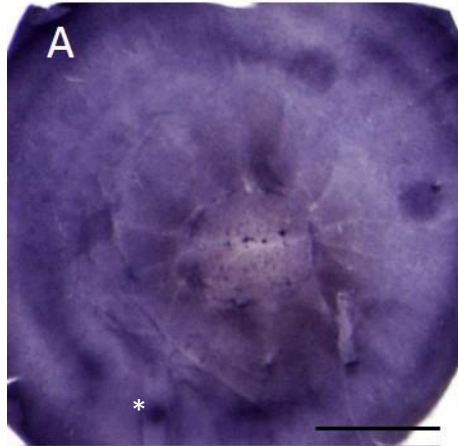


Figure 3.4. *FGFR1b* in situ hybridization from HH30 to HH37 in the chick eye. (A) HH30, strong expression in papilla #12 (indicated by ‘*’ next to the papilla) over the ciliary artery, low expression in neighbouring papilla and in nasal region; (B) HH31, strong expression in temporal and nasal region, low expression in dorsal and ventral region; (C) HH32, strong expression in temporal, nasal and few papillae in dorsal group, low expression in some papillae of dorsal group and ventral group; (D) HH33, very high expression in all conjunctival papillae, expression in the CR observed; (E) HH34, downregulation in papilla #12 and its CR, and a decrease in the expression zone surrounding other papillae; (F) HH35, further downregulation of papillae in temporal region, overall downregulation of zone surrounding papillae; (G) HH36, very little expression in temporal region, downregulation of expression in nasal region, very little expression in zone surrounding papillae; (H) HH37, almost no *FGFR1b* expression observed at this stage. The figures shown are representative of the expression observed in the majority of the embryos. Scale bars are 1mm.

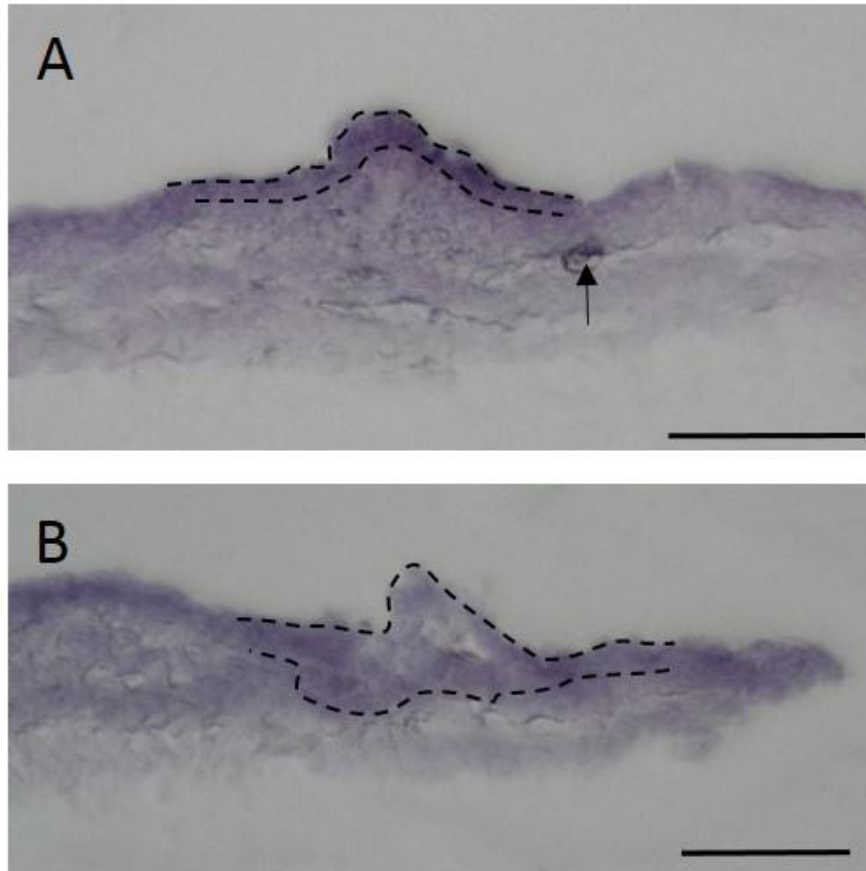


Figure 3.5. Cryosections of *FGFR1b* in situ hybridization. Sections show expression in the papilla and the CR at (A) HH32 and (B) HH33. The papillae and the CR are indicated by dashed lines. Arrow indicates an artifact. Scale bars are 100µm.

3.1.3 *FGFR1c* Expression

Strong *FGFR1c* expression was observed at HH30 in the first papilla (papilla #12) that had formed over the ciliary artery (in the temporal region; Figure 3.6A). Virtually no expression was observed in areas beside papilla #12 and in the nasal region (opposite temporal region) where papillae were still developing, unlike in the previous gene (n=6, Figure 3.6A). At HH31, strong expression was observed in the papillae in the temporal and nasal region (Figure 3.6B). In the dorsal regions, very low expression was observed (n=6, Figure 3.6B). At HH32, the expression was stronger in the dorsal region (where it previously was low) and was not yet present in the ventral region, where the last group of papillae would form (n=6, Figure 3.6C). The cryosection of papillae from the temporal group at this stage showed expression in the papillae, in the CR as well as expression in a small aggregate of cells in the superficial mesenchyme directly beneath the papillae (Figure 3.7A).

According to Hamburger and Hamilton (1951), at HH33, conjunctival papillae have developed in the temporal, nasal, dorsal and ventral regions; the last papilla which forms above the choroid fissure is not yet present. Correlating with this developmental pattern, strong *FGFR1c* expression was observed in all conjunctival papillae and low expression was visible in the area above the choroid fissure where the last papilla was yet to form (n=5/6, Figure 3.6D). One eye at HH33 had no expression in the area where the last papilla would form. At this stage, expression was also observed in the CR surrounding the papillae. Measurement of the diameter of the expression zone around

the papilla using ImageJ at HH33 indicated a wide circular area of expression (raw data in Appendix D, Table D5). At HH34, strong expression was observed in all conjunctival papillae (Figure 3.6E) and similar to HH33, expression was clearly visible in the CR (n=5/6, Figure 3.6E). In one eye, downregulation of expression in the first papilla was observed. Cryosections at HH34 showed expression in the degenerating papillae and the CR of the temporal group as well as in a band of cells in the superficial mesenchyme beneath the papillae (Figure 3.7B). No expression was observed in the deep mesenchyme.

At HH35, two to three papillae from the temporal group were downregulated (Figure 3.6F). There was also an overall decrease in expression in the CR (n=6, Figure 3.6F). At HH36, *FGFR1c* was further downregulated. Very little to no expression was observed in the papillae of the temporal region compared to the other papillae (and the CR) which still had low levels of expression (n=6, Figure 3.6G). At H37, no expression of *FGFR1c* was observed (n=6, Figure 3.6H).

ImageJ analysis of papilla #12 showed that *FGFR1c* expression was observed in the papillae and the CR from HH30 onwards with peak expression at HH32 (Appendix D, Table D4). Additionally, it showed that downregulation begins at HH33. Cryosectioning showed some mesenchymal expression at HH 32 and HH34 directly beneath the papilla. Overall, these results demonstrate that there might be a continual downregulation of this gene, starting somewhere around HH34 or slightly thereafter. Again, no expression is visible at HH37.

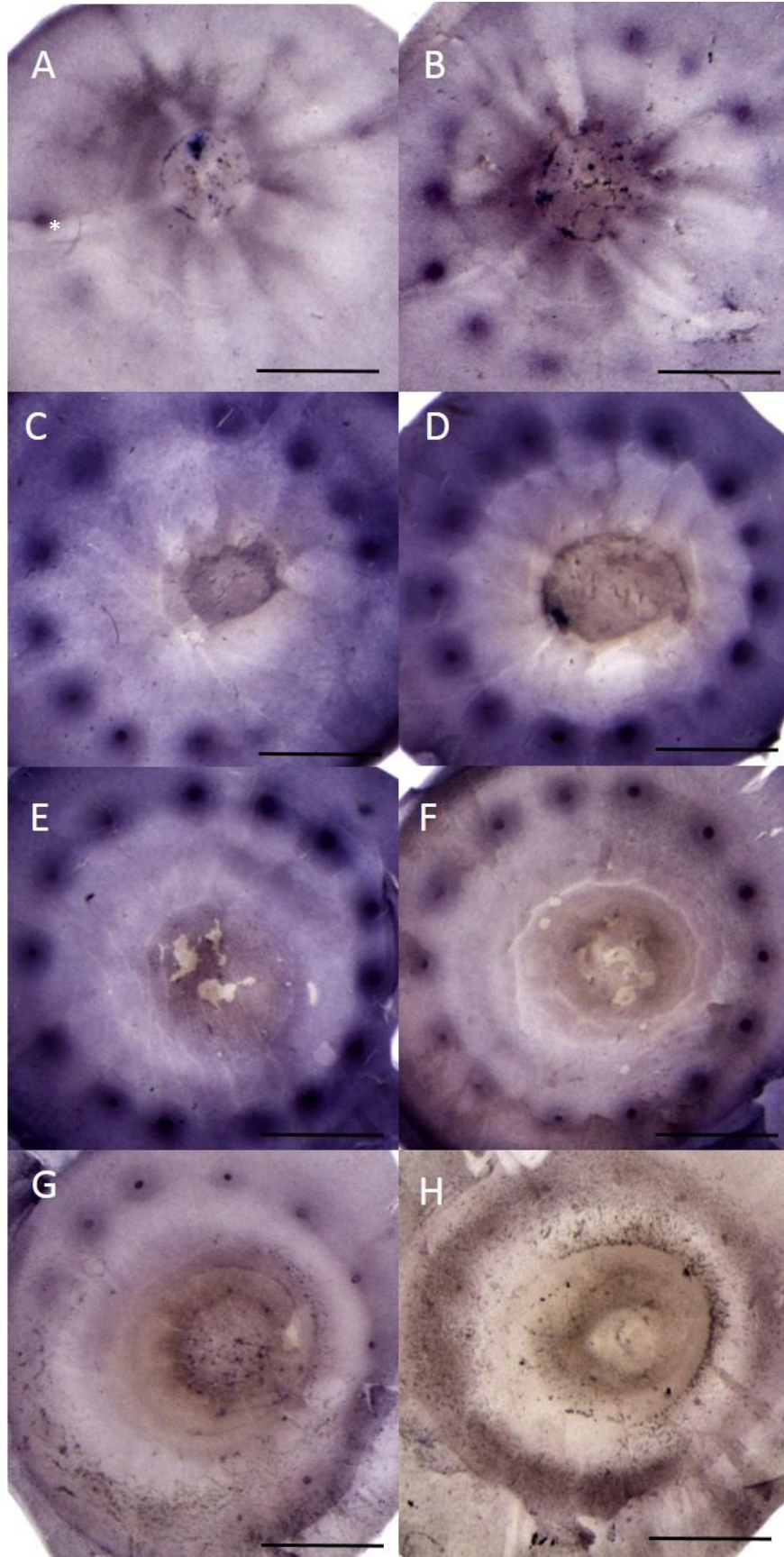


Figure 3.6. *FGFR1c* in situ hybridization from HH30 to HH37 in the chick eye. (A) HH30, strong expression in papilla #12 (asterisk) over the ciliary artery, low expression in neighbouring papillae and in the nasal region; (B) HH31, strong expression in the temporal and nasal region, low expression in the presumptive sites of papillae development; (C) HH32, high expression in the temporal group, strong expression in the nasal region with a few papillae positively stained in the dorsal group; (D) HH33, strong expression in all conjunctival papillae except the last papilla and expression in the CR observed around all the papillae; (E) HH34, strong expression in all conjunctival papillae and in the surrounding CR; (F) HH35, downregulation of papillae in temporal region, and in zone surrounding downregulated papillae; (G) HH36, very little expression in temporal region, downregulation of expression in nasal region, very little expression in the CR; (H) HH37, no *FGFR1c* expression was observed at this stage. These figures are representative of the expression observed in the majority of the embryos. Scale bars are 1mm.

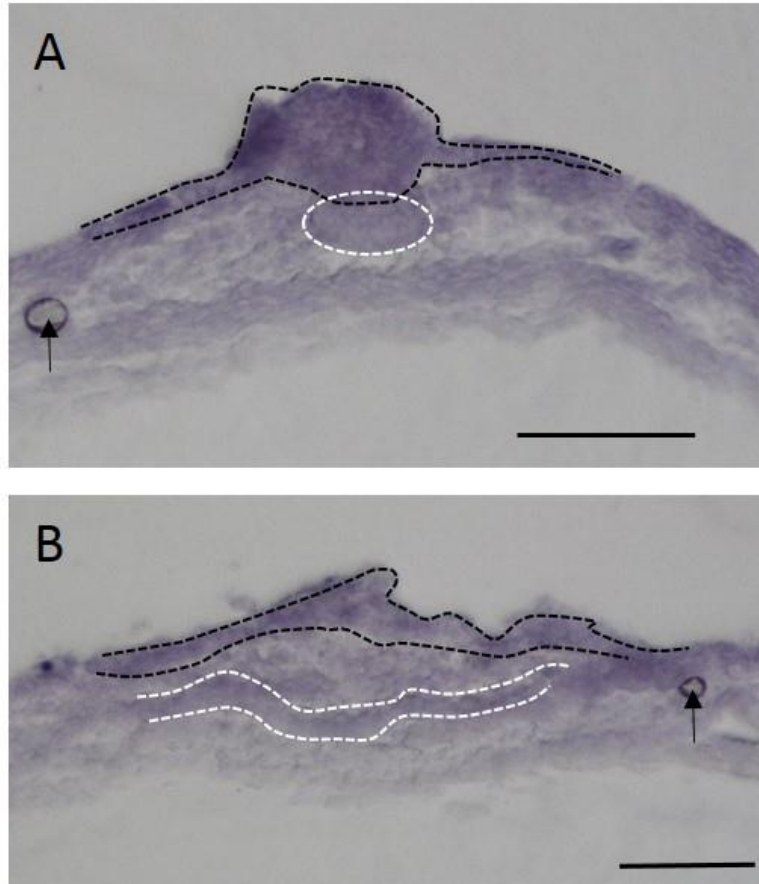


Figure 3.7. Cryosections of *FGFR1c* in situ hybridization. (A) HH32, the section shows expression in the papilla and the CR, expression was also observed in a group of cells in the mesenchyme directly beneath the papilla; (B) HH34, showing expression in a degenerating papilla and in the CR as well as in a band of cells in the superficial mesenchyme. Expression in the mesenchyme is indicated by the white dashed lines, expression in the epithelium is indicated by the black dashed lines. Arrow indicates an artifact. Scale bars are 100µm.

3.1.4 *FGFR2b* Expression

Strong *FGFR2b* expression was observed at the papilla #12 (in the temporal region) over the ciliary artery (n=3/6, Figure 3.8A). In two of six eyes, no expression was visible. In the other eye, strong expression was visible in three papillae of the temporal region and one papilla in the nasal region. As more papillae form in the temporal, nasal, and dorsal regions through HH31 and 32, strong *FGFR2b* expression was visible in conjunctival papillae of these regions (n=6, Figure 3.8B; n=4, Figure 3.8C). At HH32, in one eye, fewer papillae of the nasal and dorsal region showed *FGFR2b* expression and in another eye, more expression was observed in the papillae of the dorsal region. Cryosections of the temporal papillae at HH32 shows expression only in the papillae. No expression was observed in the CR or in the mesenchyme (Figure 3.9A).

Strong *FGFR2b* expression was detected in all conjunctival papillae at HH33 (Figure 3.8D), however, no expression was visible above the choroid fissure, where the last papilla would form at HH34 (n=6, Figure 3.8D). Measurements taken using ImageJ of the diameter of the area of expression around papilla #12 at HH33 showed that *FGFR2b* is expressed in a small ellipse around the papilla (raw data in Appendix D, Table D5). Downregulation of papillae #12 was first observed at HH33. Downregulation continued through to HH34 where a decrease in expression was now observed in all the papillae of the temporal group (n=6, Figure 3.8E). Cryosections of the temporal papillae at this stage showed low levels of expression in the papillae as well as in the CR and no expression in the mesenchyme (Figure 3.9B).

At HH35, further downregulation of the temporal group (n=6) as well as downregulation in conjunctival papillae of the nasal region (n=4/6) was observed (Figure 3.8F). In two of six eyes, downregulation in the nasal region had not yet begun. There was an overall downregulation of gene expression at HH36 (Figure 3.8G) where extremely low expression was visible in the degenerated papillae of the temporal region, very little expression was observed in the degenerating papillae of the nasal region as well as the degenerating papillae of the dorsal and ventral regions (n=6, Figure 3.8G). Although some degenerating papillae are still visible at HH37, almost no gene expression was observed at this stage (n=6, Figure 3.8H).

ImageJ analyses of the intensity of expression at papilla #12 (and a small area of the CR) throughout the stages (HH30-37) indicated that *FGFR2b* is increasing expressed from HH30-32 (Appendix D, Table D4). Cryosections showed that no mesenchymal expression was observed at either HH32 or 34 (Figure 3.9). Similar to what was observed in the whole mount tissue, ImageJ analyses also showed that expression in the temporal papillae was continuously downregulated from HH33 and was switched off by HH37.

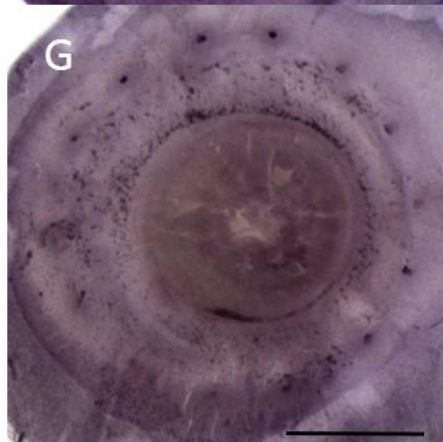
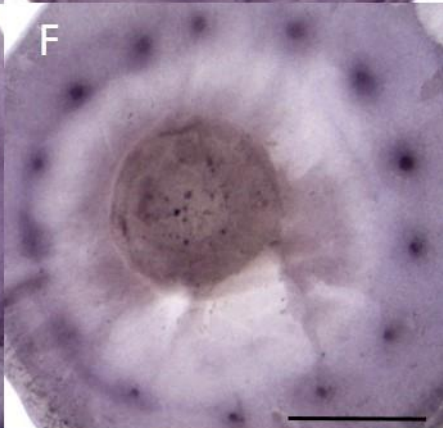
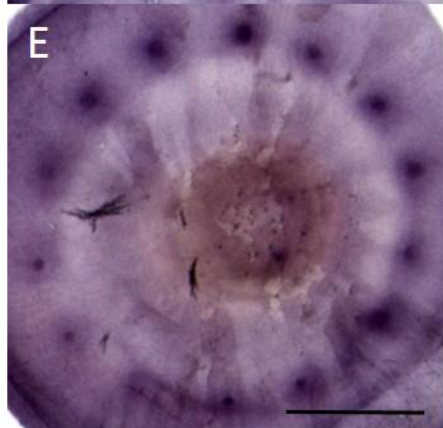
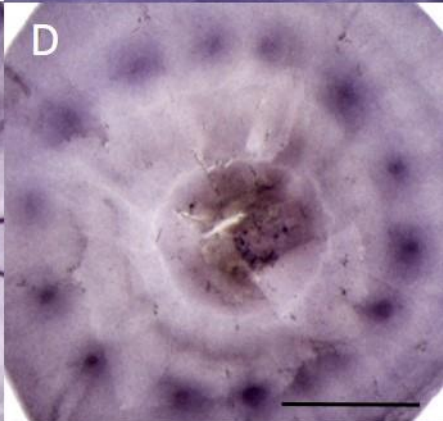
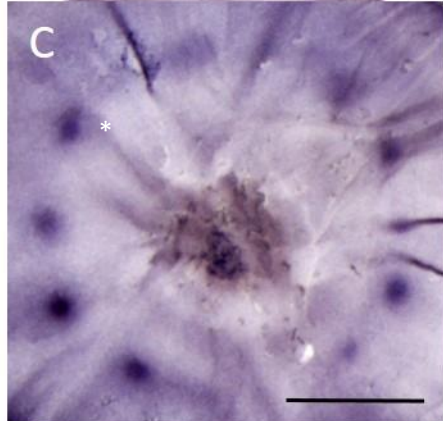
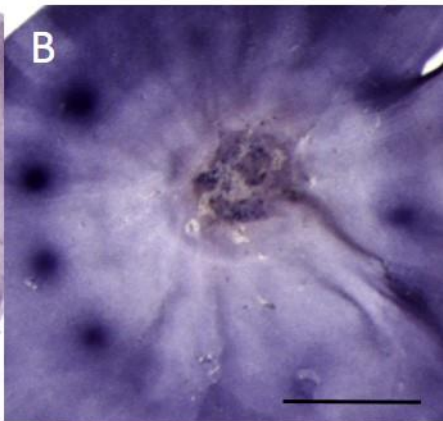
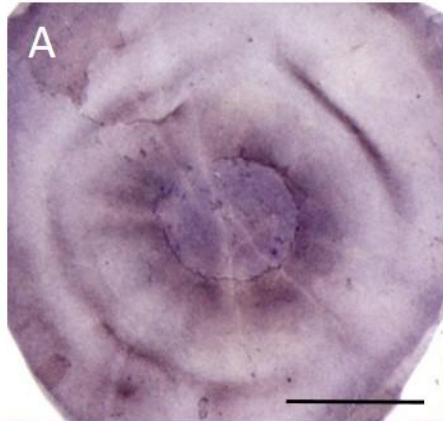


Figure 3.8. *FGFR2b* in situ hybridization from HH30 to HH37 in the chick eye. (A) HH30, strong expression in papilla #12 (asterisk) over the ciliary artery; (B) HH31, strong expression in papillae in the temporal and nasal region; (C) HH32, strong expression observed in the temporal, nasal and the dorsal groups; (D) HH33, downregulation in papilla #12 and no expression in region of the last papilla; (E) HH34, further downregulation of papilla #12; (F) HH35, continued downregulation of papillae in the temporal region and down regulation of papillae in the nasal region; (G) HH36, extremely low expression in the temporal region, very little expression in the nasal region and downregulation in dorsal and ventral regions; (H) HH37, almost no *FGFR2b* expression observed at this stage. These figures are representative of the expression observed in the majority of the embryos. Scale bars are 1mm.

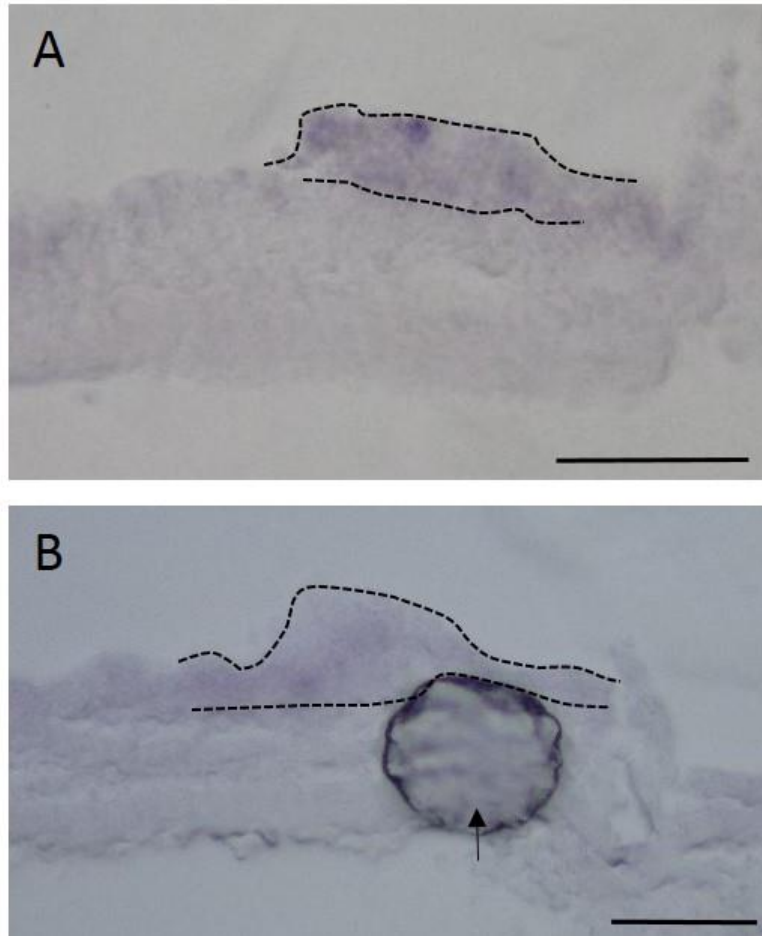


Figure 3.9. Cryosections of *FGFR2b* in situ hybridization. (A) HH32, section shows expression in the papilla but not in the CR or mesenchyme. (B) HH34, expression can be observed in the papilla and a small region of the CR immediately adjacent to the papillae. The papillae and the CR are indicated by dashed lines. Arrows indicate an artifact. Scale bars are 100µm.

3.1.5 *FGFR2c* Expression

At HH30 strong expression was observed in papilla #12 above the ciliary artery (in the temporal region) as well as in the papilla beside it (Figure 3.10A). Low expression was observed in the other temporal papillae as well as in the nasal region (n=5, Figure 3.10A). In one eye, only strong expression was observed in the first two papillae of the temporal group and no other expression was observed. As more papillae form in the temporal and nasal regions at HH31, strong *FGFR2c* expression was observed in the papillae in these regions (Figure 3.10B). At this stage, low expression was observed in the presumptive papillae of the dorsal and ventral regions of the eye (n=4, Figure 3.10B). Two of six eyes had low expression only in the papillae of the nasal region. At HH32, strong gene expression was observed in the conjunctival papillae of the temporal, nasal and dorsal regions (Figure 3.10C). However, no expression was observed at the presumptive sites of papillae formation (n=3, Figure 3.10C). Cryosections of the temporal papillae at this stage showed that *FGFR2c* was expressed in the papillae as well as in the CR (Figure 3.11A). In addition, expression was observed in the superficial mesenchyme, however, no expression was observed in the deep mesenchyme (Figure 3.11A).

At HH33, very strong expression was observed in conjunctival papillae of the nasal, dorsal and ventral groups (Figure 3.10D). At this stage, expression in the last papilla above the choroid fissure was either absent (n=2/6), low (n=3/6) or strong (n=1/6). *FGFR2c* expression also formed a zone surrounding the conjunctival papillae of

the temporal group (Figure 3.10D). Diameter measurements of the expression area around papilla #12 showed that similar to *FGFR2b*, *FGFR2c* was expressed in a small ellipse around the papilla (raw data in Appendix D, Table D5). Papillae in the temporal group had begun to get downregulated at HH33 (n=5/6) and were further downregulated in at HH34. At HH34, downregulation can also be observed in the zone surrounding these temporal papillae (Figure 3.10E). At HH34, a zone of gene expression was now also visible around the conjunctival papillae of the nasal, dorsal and ventral groups (n=6, Figure 3.5E). Cryosections show that at HH34, *FGFR2c* was expressed in the papilla and the CR, however, the expression was absent from the apical region of the papilla (Figure 3.11B). Some expression maybe present in the superficial mesenchyme as well. The presence of expression in the mesenchyme was more visible in the papillae of the nasal group (Appendix C, Figure C4). However, papillae of the nasal group may be developmentally closer to HH33 than HH34 (because of the sequence of papillae development, see section 1.2) and thus the mesenchymal expression as well as expression in the apical part of the papillae are gradually lost as development proceeds. No expression was observed in the deep mesenchyme (Figure 3.11B) at this stage.

At HH35, the expression in the papillae of all groups was further downregulated (n=6, Figure 3.10F). *FGFR2c* expression was completely absent in the area surrounding the papillae in the temporal region. At HH 36, no expression was observed in the temporal region and extremely low expression was observed in the degenerating papillae of other regions (n=6, Figure 3.10G). At HH37, either extremely low expression

was visible in the degenerating papillae of the dorsal and ventral groups (n=3/6) or absolutely no expression was observed (n=3/6, Figure 3.10H).

ImageJ analyses of papilla #12 shows a sudden upregulation at HH34 followed by an extreme downregulation at HH35 (Appendix D, Table D4); no expression intensity could be detected at HH36 and 37. Cryosections of the temporal papillae showed that there was a loss of expression from HH32; where *FGFR2c* was strongly expressed in the papillae, the CR and the superficial mesenchyme, to HH34; where the gene was no longer expressed in the apical region of the papillae and its expression in the superficial mesenchyme is questionable. However, although inconsistent with ImageJ data, these results demonstrate that there was a continual downregulation of this gene from HH33.

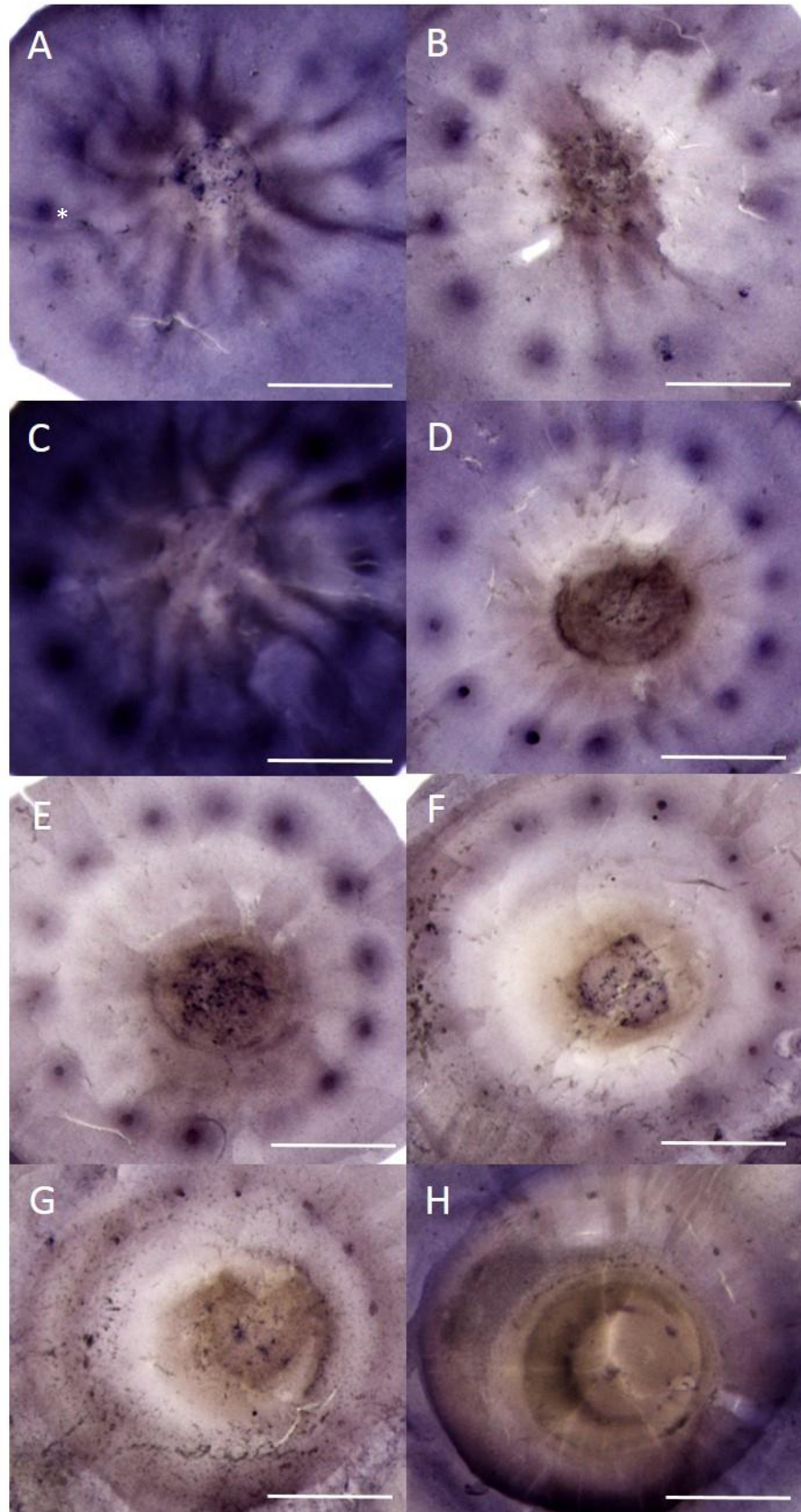


Figure 3.10. *FGFR2c* in situ hybridization from HH30 to HH37 in the chick eye. (A) HH30, strong expression in first two papilla (papilla #12, asterisk), low expression in region beside these papillae and in nasal region; (B) HH31, strong expression in the temporal and nasal region, low expression in presumptive sites of papillae development; (C) HH32, strong expression in the temporal, nasal and in few papillae of the dorsal group; (D) HH33, strong expression in all conjunctival papillae except last papilla and expression visible in the CR of the temporal papillae, downregulation of a few papillae in the temporal region; (E) HH34, further downregulation of papillae in temporal region and its CR, expression in the CR now also visible surrounding all papillae; (F) HH35, downregulation of papillae in the nasal region and very little expression in their CR, overall downregulation in the CR; (G) HH36, very little expression in nasal region, downregulation of papillae in dorsal and ventral regions, complete absence of expression in the CR; (H) HH37, extremely low *FGFR2c* expression observed at this stage. These figures are representative of the expression observed in the majority of the embryos. Scale bars are 1mm.

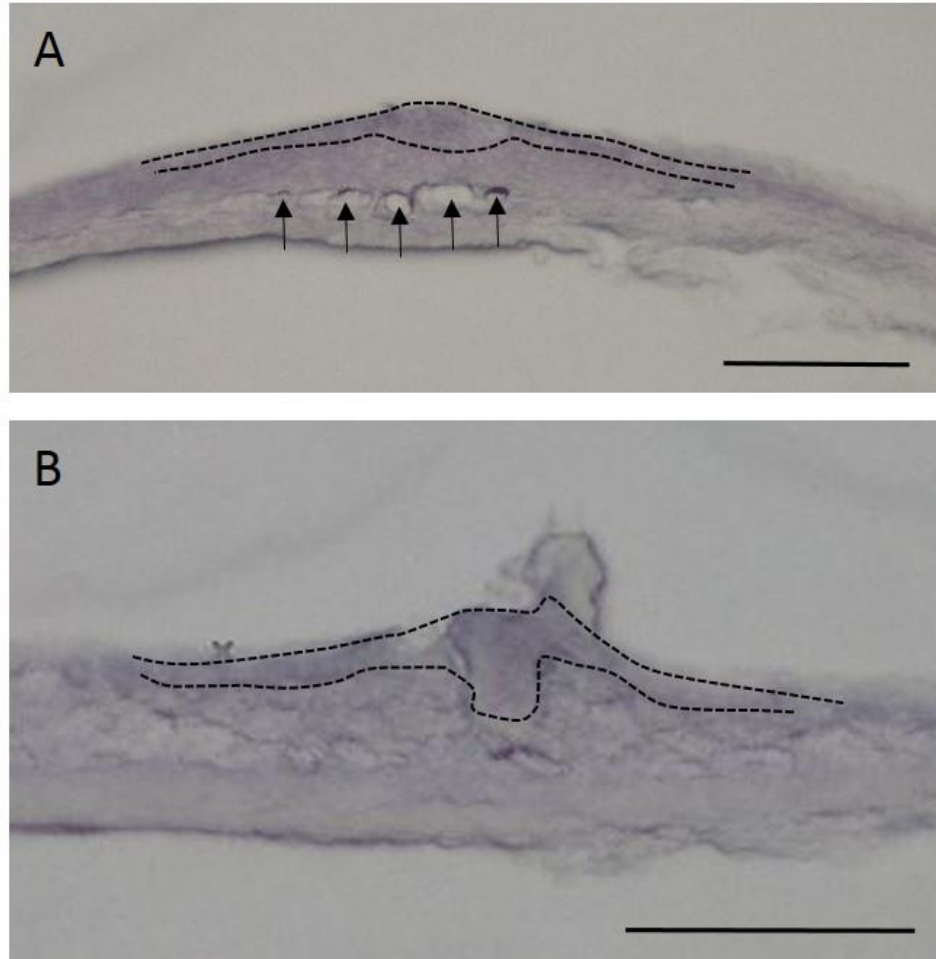


Figure 3.11. Cryosections of *FGFR2c* in situ hybridization. (A) A section at HH32 showing expression in the papilla and the CR as well as the superficial mesenchyme; (B) at HH34, section shows expression in the papilla and the CR, no expression in the apical region of the papilla, expression may be present in the superficial mesenchyme. The papillae and the CR are indicated by the dashed line. Arrows indicate artifacts. Scale bars are 100µm.

3.1.6 *FGFR3b* Expression

At HH30, *FGFR3b* expression was observed in papilla #12 that forms over the ciliary artery (in the temporal region; Figure 3.12A). Low expression was also observed in the presumptive sites of other papillae in the temporal region (n=4/6). In one of six eyes, strong expression was observed in the first two papillae of the temporal region whereas in the other eye, no expression was observed in this region. As conjunctival papillae form in the temporal and nasal regions at HH31, strong expression was observed corresponding to the newly formed papillae (n=6, Figure 3.12B). Similarly at HH32, strong expression was observed in the papillae of the temporal, nasal and dorsal regions (n=6, Figure 3.12C). Cryosections at HH32 indicate that *FGFR3b* was only expressed in the papilla and a small part of the CR (Figure 3.13A). No *FGFR3b* expression was observed in the mesenchyme (Figure 3.13A).

At HH33 in four out of the six eyes, no *FGFR3b* expression was observed in a few conjunctival papillae in the dorsal group as well as in the papillae in the ventral region (Figure 3.12D). In two eyes, papillae in the dorsal region showed low expression. ImageJ analyses was used to measure the diameter of the zone of expression around papilla #12 at HH33 and indicated an ovoid spatial expression zone (raw data in Appendix D, Table D5). At HH34, strong expression was observed in all conjunctival papillae (n=6, Figure 3.6E). Cryosections of the temporal papillae at this stage revealed the presence of expression in the papillae, a small part of the adjacent CR as well as in a band of cells in the superficial mesenchyme directly under the papilla (Figure 3.13B).

At HH35, expression in the first one to three papillae that formed in the temporal region was downregulated, particularly in the CR (n=6, Figure 3.6F). At HH36, very little expression was visible in the papillae of the temporal region and downregulation was observed in the papillae of the nasal region (n=6, Figure 3.6G). At HH37, either no *FGFR3b* expression was observed (n=4/6) or very little expression was observed in the degenerating papillae of the dorsal and ventral regions (n=2/6, Figure 3.6H).

ImageJ analysis of papilla #12 shows that *FGFR 3c* expression was observed in the papillae and the CR from HH30 with peak expression at HH31(Appendix D, Table D4). The analysis indicated that after a slight downregulation at HH32, the expression was stable until HH34 after which further downregulation was observed. Cryosectioning showed the appearance of expression in the mesenchyme directly beneath the papillae at HH34 which was absent at HH32. In all, these results demonstrate that there might be a continual downregulation of this gene, starting somewhere around HH34. ImageJ analysis was unable to detect any expression at HH37 in papilla #12.

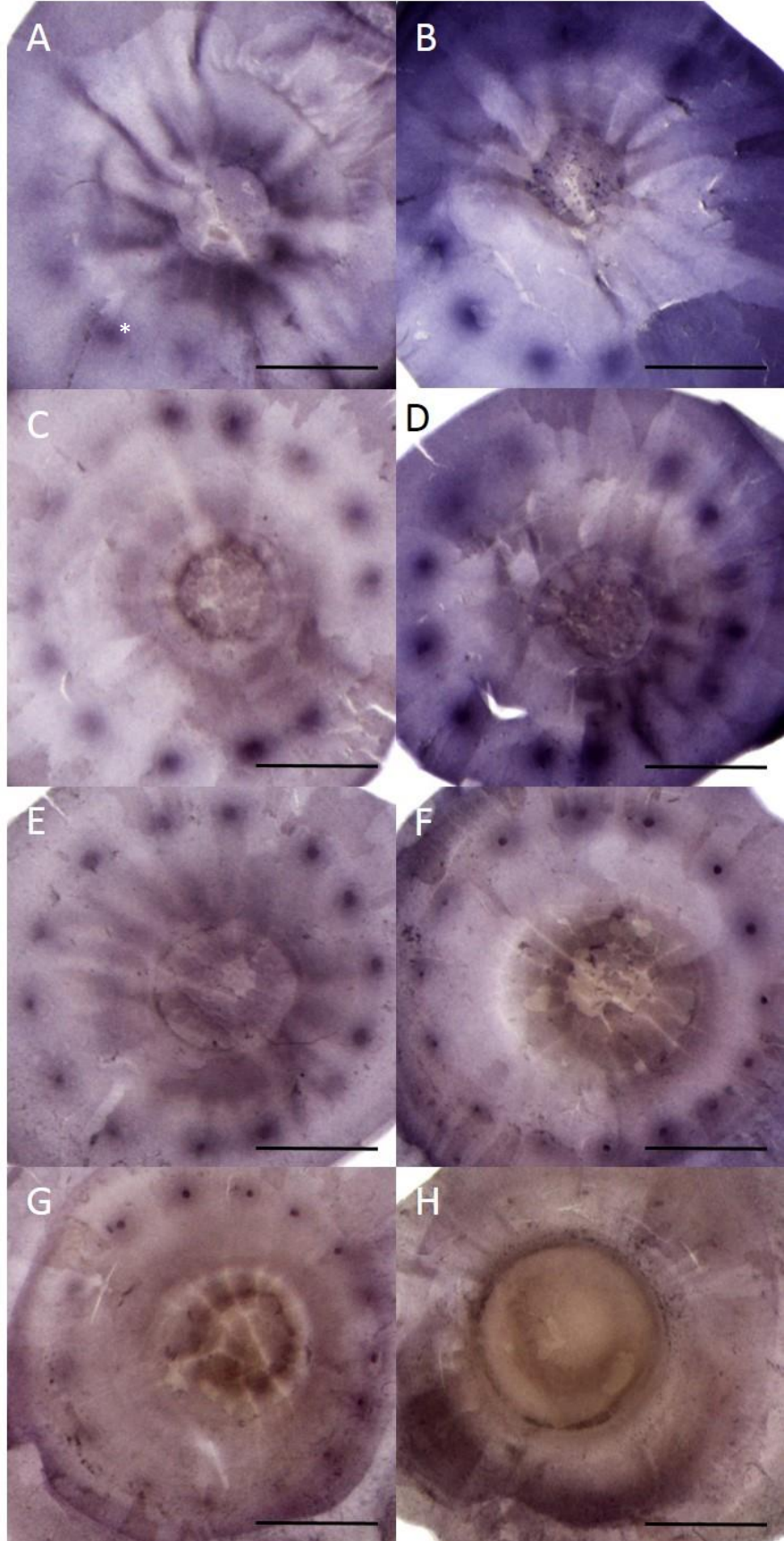


Figure 3.12. *FGFR3b* in situ hybridization from HH30 to HH37 in the chick eye. (A) HH30, strong expression in the first two papilla, low expression in the region beside these papilla and in the nasal region; (B) HH31, strong expression in the temporal and nasal region; (C) HH32, strong expression in the temporal, nasal and few papillae in dorsal group (D) HH33, strong expression in papillae of the temporal, nasal and dorsal regions; (E) HH34, strong expression in all conjunctival papillae; (F) HH35, downregulation of the papillae in the temporal region; (G) HH36, very little expression in papillae of the temporal region and downregulation of papillae in nasal region; (H) HH37, no *FGFR3b* expression observed at this stage. These figures are representative of the expression observed in the majority of the embryos. The asterisk in (A) indicates papilla #12. Scale bars are 1mm.

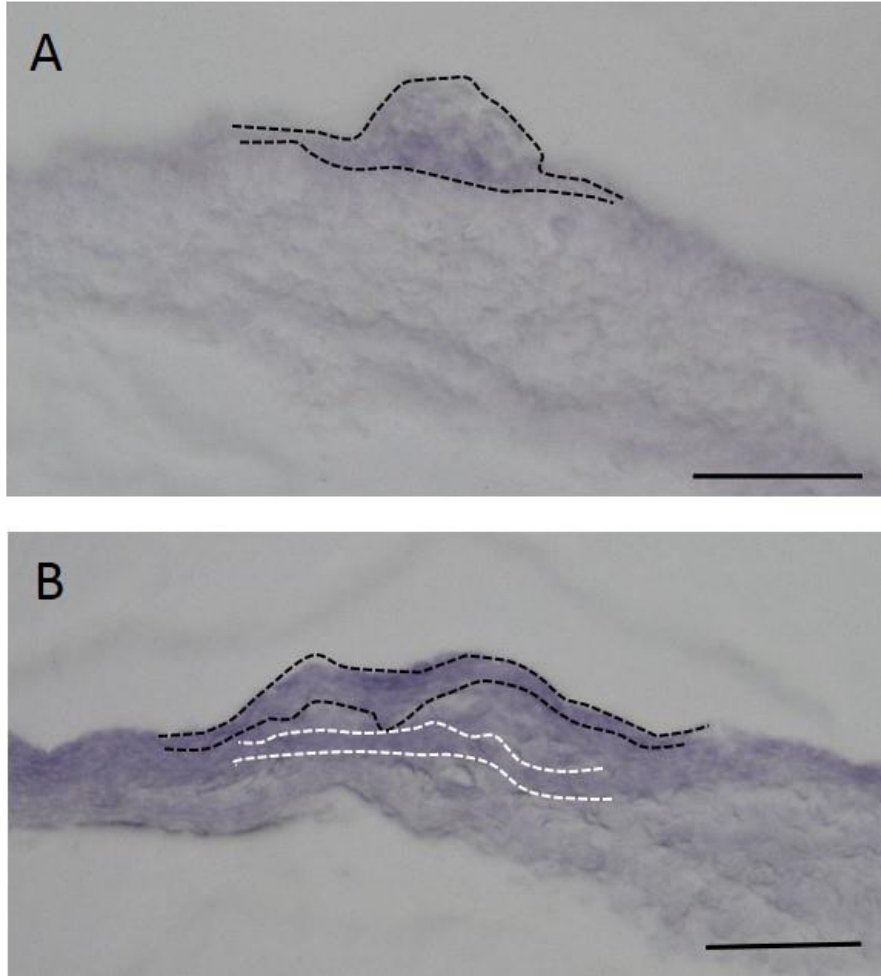


Figure 3.13. Cryosections of *FGFR3b* in situ hybridization. (A) HH32, section showing expression in the papilla and a small part of the CR. (B) HH34, section showing expression in the papilla and the CR as well as in a band of cells in the mesenchyme beneath the papilla. Black dashed lines indicate papillae and the CR. Mesenchyme is indicated by white dashed lines. Scale bars are 100µm.

3.1.7 *FGFR3c* Expression

At HH30, very low *FGFR3c* expression was observed in papilla #12 that forms over the ciliary artery (in the temporal region; n=6; Figure 3.14A). Low expression was also observed at sites of presumptive papillae formation in both the temporal and the nasal regions (n=5/6; Figure 3.14A). In one eye, no expression was observed in the nasal region. At HH31, the papillae in the temporal and nasal regions that had low expression at HH30, now have strong expression (n=6; Figure 3.14B).

As more papillae are formed in the nasal, dorsal and ventral regions at HH32 and 33, strong *FGFR3c* expression is observed in the conjunctival papillae corresponding to these papillae (n=6; Figure 3.14B and C respectively). Cryosections of the temporal papillae at HH32 showed that *FGFR3c* was expressed in the papillae and the CR as well as in the superficial and deep mesenchyme beneath the region of epithelial expression (Figure 3.15A). At HH33, although the last papilla above the choroid fissure has not yet formed either no expression (n=2/6) or low expression was observed at this site (n=4/6; Figure 3.14D). Diameter measurements of the expression area around the papilla showed that similar to *FGFR1c*, *FGFR3c* was expressed in a wide circle around the papilla (raw data in Appendix D, Table D5). Strong *FGFR3c* expression was observed in all conjunctival papillae at HH34 (Figure 3.14E). At this stage the first papilla #12 (in the temporal region) has become downregulated compared to others in the ring (n=6; Figure 3.14E). In comparison to HH32, cryosections at HH34 reveal that *FGFR3c* is no

longer expressed in the mesenchyme but is restricted to the papilla and a small CR (Figure 3.15B).

More papillae of the temporal region were downregulated at HH35 (Figure 3.14F). At this stage, papillae of the nasal region have also started to downregulate this gene (n=5/6; Figure 3.14F). In one eye, gene expression in the papillae of the nasal region were not downregulated. Further downregulation was observed at HH36 (Figure 3.14G) where no expression was observed in the papillae of the temporal region and extremely diminished expression was observed in the papillae of the nasal, dorsal and the ventral regions (n=6; Figure 3.14G). At HH37, no *FGFR3c* expression could be observed (n=6; Figure 3.14H).

ImageJ analysis of the intensity of expression at papilla #12 (and a small area of the CR) indicated that *FGFR3c* is upregulated from HH30 to 33, after which it is downregulated (Appendix D, Table D4). Cryosections at HH32 showed expression in the temporal papillae, the CR and throughout the mesenchyme. However, at HH34, the expression was limited to the papilla only. In summary, these results demonstrate that there is a continual downregulation of this gene from HH33/34 (E7.5-8).

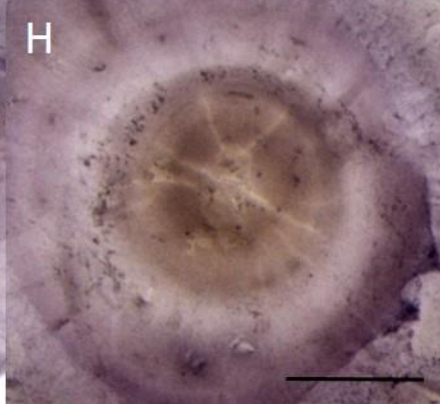
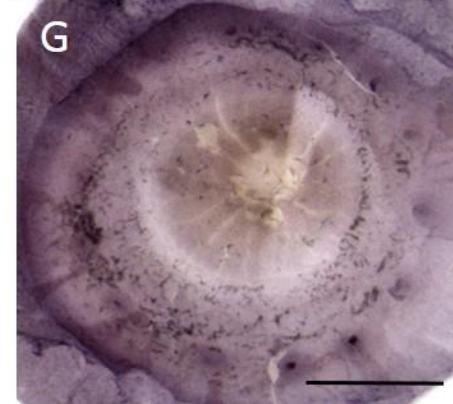
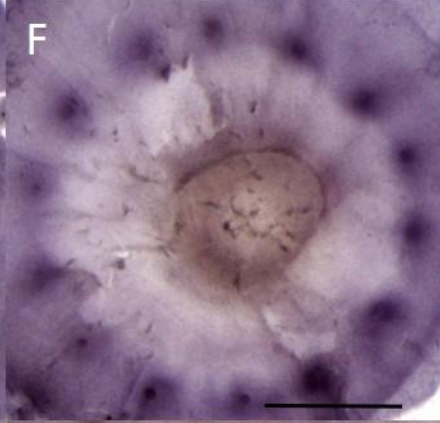
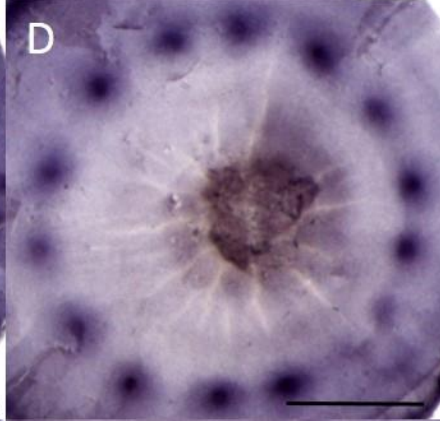
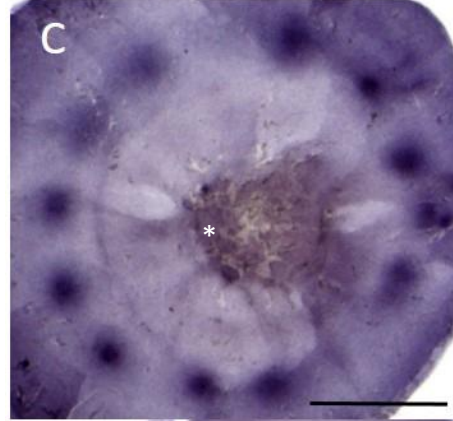
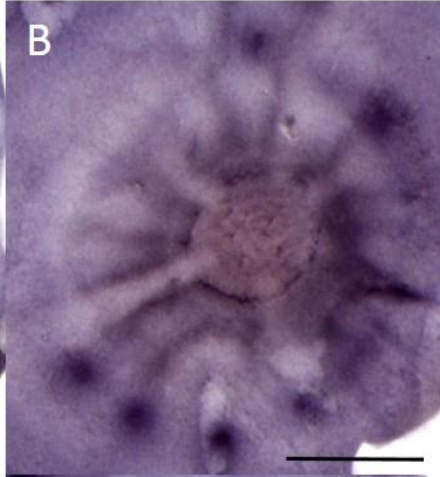
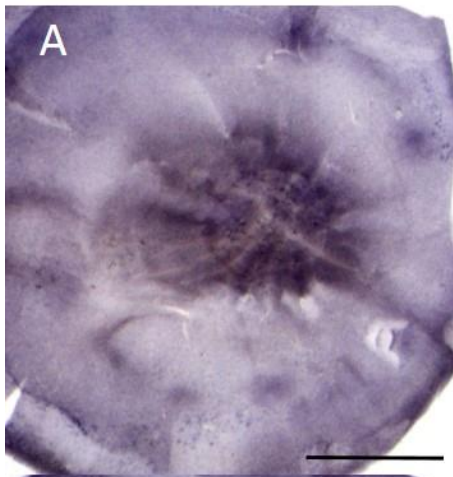


Figure 3.14. *FGFR3c* in situ hybridization from HH30 to HH37 in the chick eye. (A) HH30, low expression is observed in first papilla over the ciliary artery (asterisk) and in the neighbouring papillae as well as in the nasal region; (B) HH31, strong expression in the papillae of the temporal and nasal region; (C) HH32, strong expression in the papillae of the temporal, nasal and a few papillae in dorsal group; (D) HH33, very high expression in all conjunctival papillae and low expression at site of last papilla; (E) HH34, downregulation in the first papilla of the temporal region; (F) HH35, further downregulation of papillae in the temporal region and downregulation of papillae in the nasal region; (G) HH36, no expression in temporal region, almost no expression in nasal, dorsal and ventral regions; (H) HH37, no *FGFR3c* expression observed at this stage. These figures are representative of the expression observed in the majority of the embryos. Scale bars are 1mm.

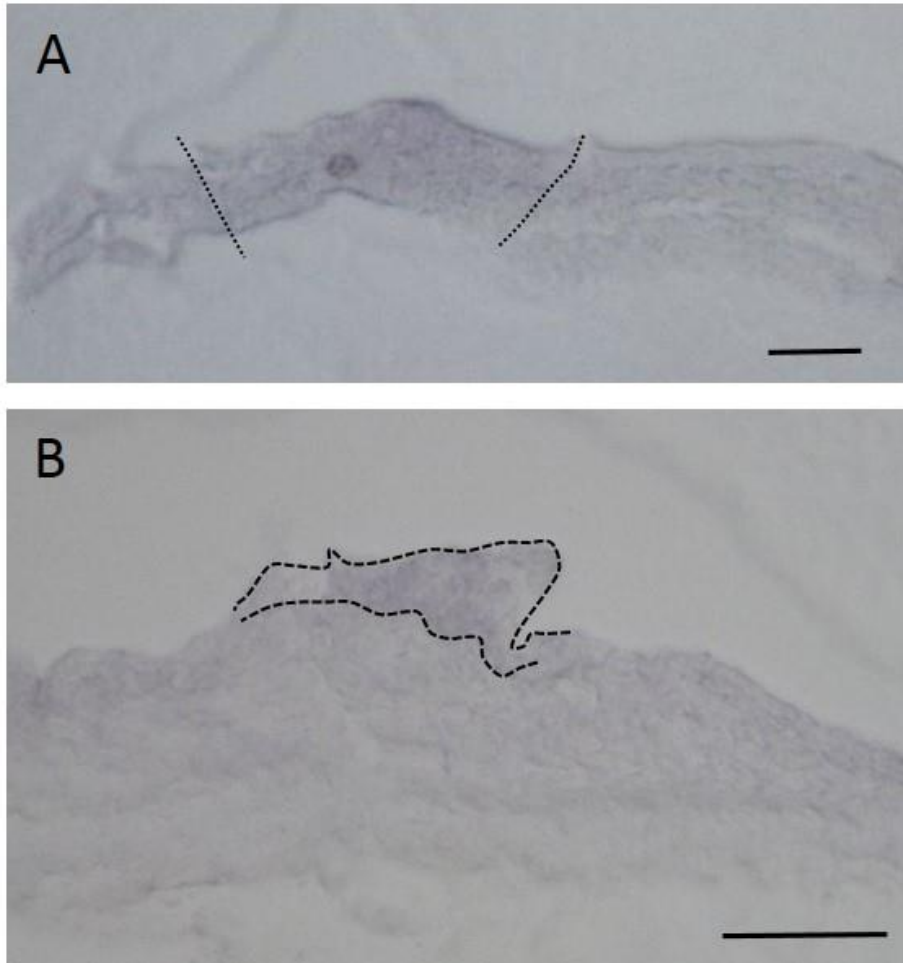


Figure 3.15. Cryosections of *FGFR3c* in situ hybridization. (A) HH32, section showing the area of expression in the papilla and the CR as well as the mesenchymal region beneath (indicated by dotted lines). The photograph was taken at 4x magnification as this was the only magnification at which the low expression could be photographed and therefore shows a much larger area of the section. (B) HH34, section showing expression in the papilla and the CR (indicated by dashed lines). Scale bars are 100µm.

3.2 Bead Implantation

3.2.1 Effect of SU5402 Treatment on Limb Development

The SU5402 inhibitor was first tested using Affi-gel blue beads. Beads soaked in the 3mg/ml SU5402 (n=3) were implanted into the right wing buds at HH20/21. Embryos were grown to HH29/30, their wings were dissected and stained with Alcian blue. Measurements of the length of the radius, ulna and humerus showed that the average length of these cartilages were similar for both the right implanted limb and the left unimplanted limb. Therefore it was determined that the inhibitor had no effect on limb development (Appendix D, Table D1). Therefore, this bead type with the inhibitor was not used further.

To ensure that the SU5402 inhibitor worked in conjunction with the AG1X2 beads, prior to treatment in the eye, these beads were also soaked in the inhibitor and implanted into the right wing buds at HH20/21 (at 3mg/ml SU5402, n=3, and at 6mg/ml SU5402, n=2). Beads soaked in DMSO (n=4) were used as a negative control; the untreated wing bud of the left side of the embryo was also analysed. However one of the four control DMSO-treated embryos was a conjoined twin (sharing one head between two bodies) and therefore resulted in a total of five measurements (in one of which, the right wing bud was also an untreated control). After bead implantation, embryos were grown to HH29/30, wings were then dissected, stained with Alcian blue (section 2.9). The total length of the cartilaginous portion of the humerus, radius and ulna were then measured. The average length of the radius, ulna and humerus of DMSO

treated controls (n=5) was $0.84\text{mm} \pm 0.17$, $1.10\text{mm} \pm 0.11$ and $1.16\text{mm} \pm 0.05$, respectively, in the right bead implanted wing (Figure 3.16A). In the contralateral untreated left wing, these elements measured $0.93\text{mm} \pm 0.14$, $1.14\text{mm} \pm 0.10$ and $1.17\text{mm} \pm 0.13$, respectively, (Table 3.1). T-test carried out between the DMSO treated right (bead implanted) and left (unimplanted) limbs showed no statistical difference (T-Test; $T=-0.32$, $p=0.763$, $df=5$; Appendix E3). At 3mg/ml SU5402, in two out of the three embryos, all skeletal elements were either missing or only the ulna was absent (Figure 3.16B). A similar effect was seen in embryos implanted with beads soaked in 6mg/ml SU5402 (Figure 3.16C). In one of the implanted right wing, only the ulna was present and in the other, the radius was extremely thin and almost absent. The left wing of the same embryos had normally developed cartilages (Figure 3.16D). The average lengths of the radius, ulna and humerus in the left limb of embryos 6mg/ml SU5402 bead implantation were $1.15\text{mm} \pm 0.05$, $1.05\text{mm} \pm 0.15$ and $0.96\text{mm} \pm 0.14$ (Table 3.1). The left wing of the SU5402 treated embryos were not statistically different from the left limb of DMSO control embryos (T-Test; $T=-1.42$, $p=0.215$, $df=5$). The right wings of SU5402 treated embryos clearly show that the SU5402 soaked on AG1X2 beads has an effect on limb development and leads to either abnormal or no cartilage formation.

Table 3.1. Measurements of wing cartilages at HH29/30 after AG1X2 bead implantation at HH20/21. *embryo was a conjoined twin joined at the head.

	Left Unimplanted Wing (mm)			Right Implanted Wing (mm)		
	Radius	Ulna	Humerus	Radius	Ulna	Humerus
DMSO- Control	1.2	1.34	1.3	1.1	1.3	1.2
	*0.87	*1.1	*1.2	*0.58	*1.06	*1.06
			*Cut during			
	*0.82	*1.1	dissection	*0.77	*0.96	*1.2
	0.87	1.06	0.96	0.87	1.06	1.2
	0.87	1.1	1.2	0.87	1.1	1.15
Average	0.93	1.14	1.17	0.84	1.10	1.16
Standard Deviation	0.14	0.10	0.13	0.17	0.11	0.05
3mg/ml- SU5402	1.2	1	1.2	0.9	absent	0.9
	1.3	1	1.4	1.3	0.9	1.2
	1.3	1	1.4	all bones absent		
Average	1.27	1	1.33	1.1	0.9	1.05
Standard Deviation	0.05	0	0.09	0.2	0	0.15
6mg/ml- Su5402	1.1	0.9	1.1	1.1 (Thin- almost absent)		1.1
	1.2	1.2	0.82	absent	0.7 0.91	absent
Average	1.15	1.05	0.96	1.1	0.81	1.1
Standard Deviation	0.05	0.15	0.14	0	0.12	0

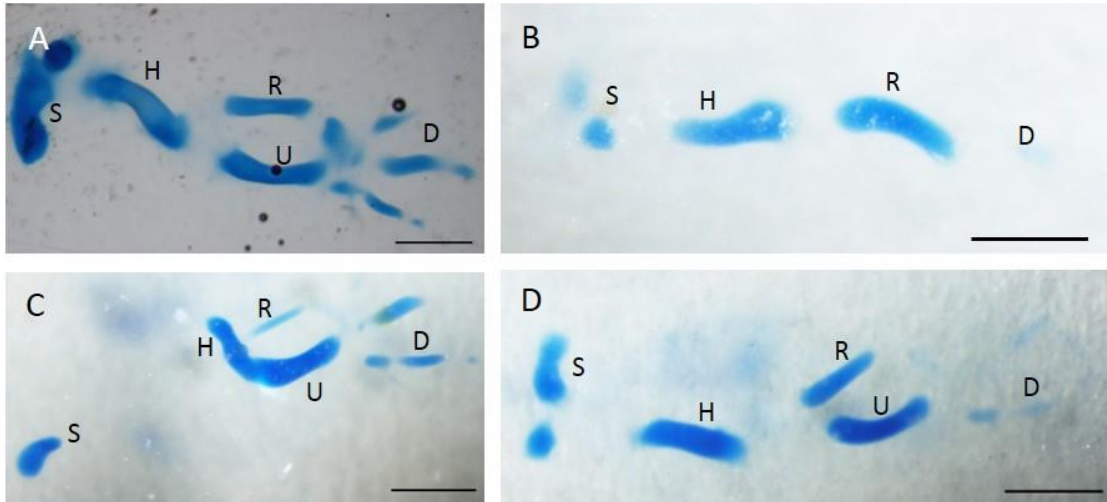


Figure 3.16. Alcian blue cartilage staining of wing limbs. (A) DMSO treated control, all skeletal elements are normally developed in right wing; (B) 3mg/ml SU5402, ulna is absent in right wing; (C) 6mg/ml SU5402, radius is thin to almost absent in right wing; (D) Left control wing of embryo implanted with 6mg/ml SU5402 showing normally developed skeletal elements. S: Scapula, H: Humerus, R: Radius, U: Ulna, D: Digits. Scale bars are 1mm.

3.2.2 Effect of SU5402 on Scleral Ossicle Development

AG1X2 beads soaked in 3mg/ml (n=3) and 6mg/ml (n=2) SU5402 were implanted next to a papilla at HH34 (section 2.7.4). Controls included beads soaked in DMSO (n=3) as well as the left untreated eye. Embryos were incubated for three days and then stained for the presence of alkaline phosphatase, which can be used as a proxy of skeletogenic condensation development.

In all three samples of DMSO treated embryos both the left and the right eyes had a similar staining and ossicle patterning (Figure 3.17A). All embryos had the same

number of ossicles in the right (DMSO treated) and the left (untreated) eye except for one which had a difference of one ossicle (Table 3.2); however this is within the normal range of asymmetry between eyes (Franz-Odendaal, 2008). When implanted with 3mg/ml SU5402, no abnormal ossicles were observed and both eyes had the same number of ossicles (n=3, Table 3.2). In one embryo, however, one ossicle was clearly missing from the ring (Figure 3.17B). However, when this was compared with the unimplanted left eye, it also had one missing ossicle. Therefore, it was deduced that this result was not due to the SU5402. Similarly, when embryos were implanted with 6mg/ml SU5402, no difference in ossicle number was observed (n=2, Table 3.2). No abnormal ossicles were present either (Figure 3.17C). Therefore, treatment of papillae with SU5402 at HH34 using the bead implantation technique had no effect on scleral ossicle development.

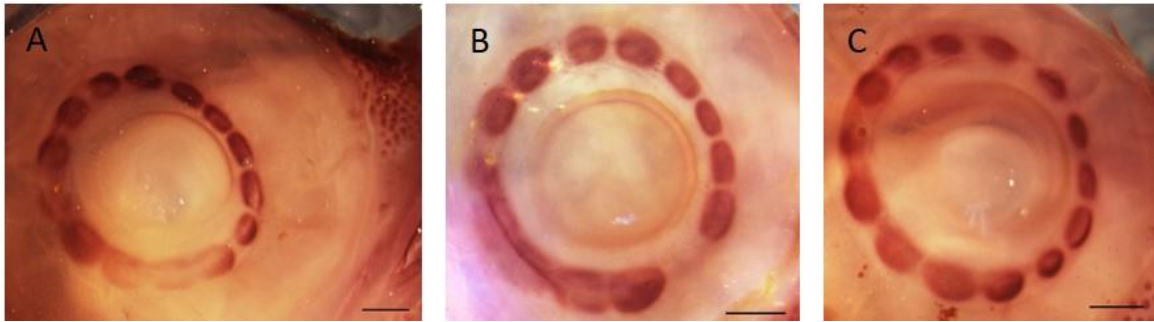


Figure 3.17. Representative right eyes implanted with AG1X2 beads at HH34 and stained for AP at HH37. (A) Control DMSO-treated eye, showing normal scleral condensations; (B) 3mg/ml SU5402-treated eye with 13 ossicles and one missing ossicle; (C) 6mg/ml SU5402 treated eye showing normal scleral condensations. All images are oriented with the beak to the right. Scale bars are 1mm.

Table 3.2. Number of scleral condensations at HH37 in the left and right eyes of embryos that were implanted with AG1X2 beads soaked in either DMSO, 3mg/ml SU5402 or in 6mg/ml SU5402. Left eyes were untreated in each embryo.

Treatment	Unimplanted Left Eye	Implanted Right Eye
Control – DMSO	14	14
	13	14
	14	14
3mg/ml SU5402	14	14
	13	13
	14	14
6mg/ml SU5402	14	14
	14	14

3.3 Microinjections

Microinjections were performed using 6mg/ml SU5402 (n=11) at HH34, embryos were then incubated for three days and stained for alkaline phosphatase (AP). Controls included a DMSO treated right eye (n=4) and the untreated left eyes. For each embryo, the number of ossicles was counted after AP staining in the left and right eyes. Defects were observed in some embryos, and hence eyes were classified as either normal or having a mild, moderate or severe defect (Figure 3.18) after Hammer (2016).

Classification was based on the following criteria: normal, where no abnormalities were

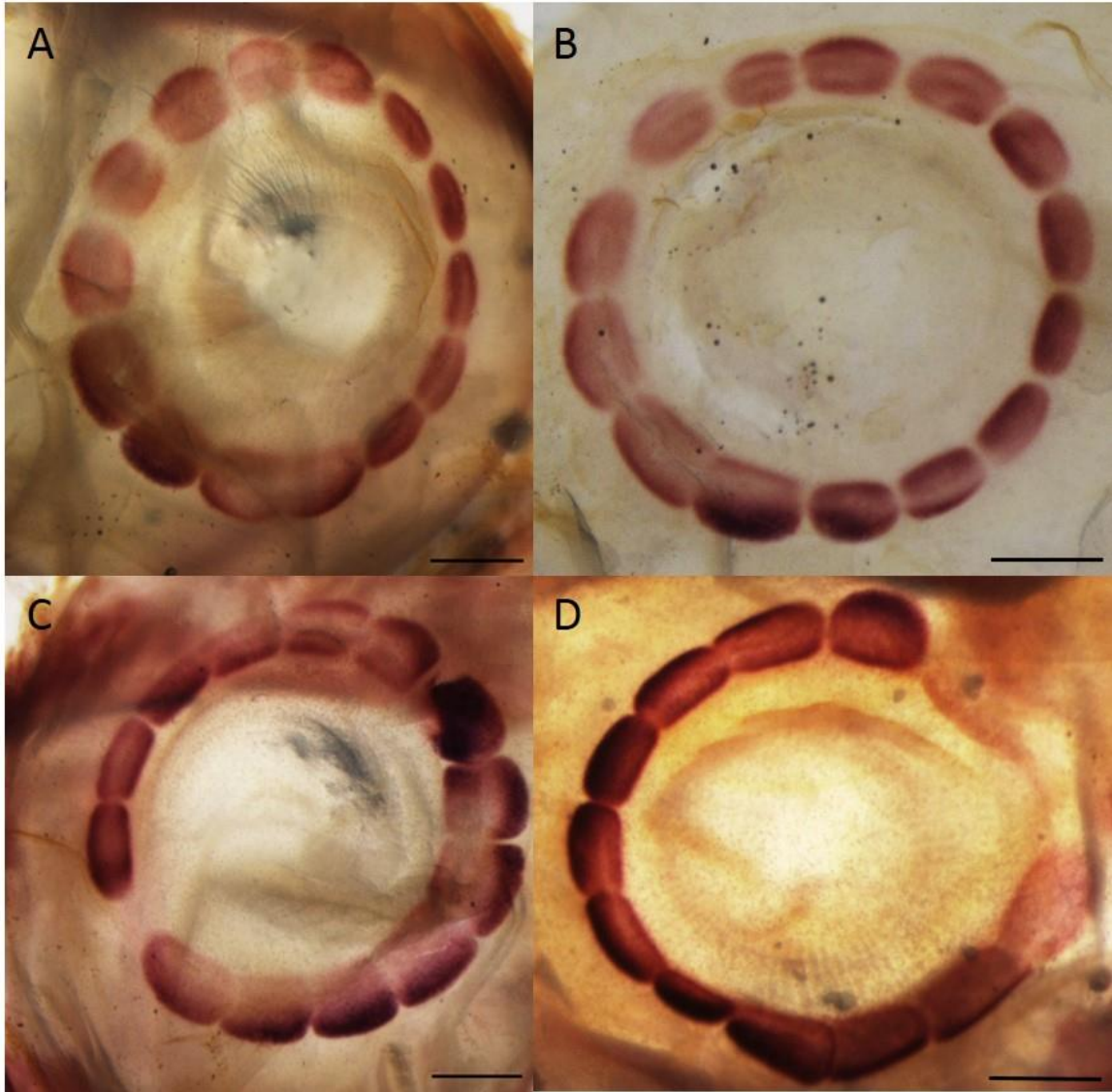


Figure 3.18. Examples of the classification of defects observed in scleral condensations after microinjection with 6mg/ml SU5402 at HH34 and stained for AP at HH37. (A) normal, no defects; (B) mild, small gaps between ossicles; (C) moderate, one missing ossicle; (D) severe, more than one missing ossicle. Scale bars are 1mm.

observed (Figure 3.18A); mild, those with small ossicles or a small gap (Figure 3.18B); moderate, those with one missing ossicle (Figure 3.18C); severe, those that had more than one missing ossicle or formed a large gap in the ring (Figure 3.18D). In this section the microinjection data is first qualitatively (section 3.3.1, 3.3.2 and 3.3.3) and then quantitatively (section 3.3.4) analysed.

3.3.1 Control Microinjections

In control DMSO injected embryos, 50% of the right eyes were normal, and 50% had defects (Figure 3.19, Table 3.3). Of those with defects, 25% (1 out of 4) had a small gap and was therefore classified as having a mild defect and 25% (1 out of 4) had more than one missing ossicle and was therefore categorized as having a severe defect (Table 3.2). The average number of ossicle in the right eye was 13.5 ± 0.87 (n=4). Similarly, in the contralateral untreated left eyes of the DMSO treated embryos, 50% of the eyes were normal, and 50% had defects (Figure 3.19). Again, one eye (25%) had unusually small ossicles and was therefore classified as mild and 25% (1 out of 4) had more than one missing ossicle and was classified as severe (Table 3.3). In the left eyes, the average number of ossicles was 13.25 ± 1.92 (n=4). An independent t-test between the treated right and the untreated left eye for DMSO controls showed no statistical difference (T-test; $T=-0.21$, $p=0.843$, $DF=6$). A second set of controls that received no injections (CNI; data from Hammer, [2016]; Appendix D, Table D3) was also used. The average number of ossicles in the right eye of CNI was 14.28 ± 0.45 and 14.45 ± 0.5 (n=11) in the left eye. No statistical difference was found between the right eyes of DMSO and CNI groups (T-

Table 3.3. Frequency of the different categories of defects observed in eyes microinjected with DMSO and 6mg/ml SU5402.

	Normal	Mild	Moderate	Severe	n
Control DMSO injected right eye	2	1	0	1	4
Control DMSO left eye	2	1	0	1	4
6mg/ml SU5402 injected right eye	7	4	0	0	11
6mg/ml SU5402 left eye	6	1	2	0	9

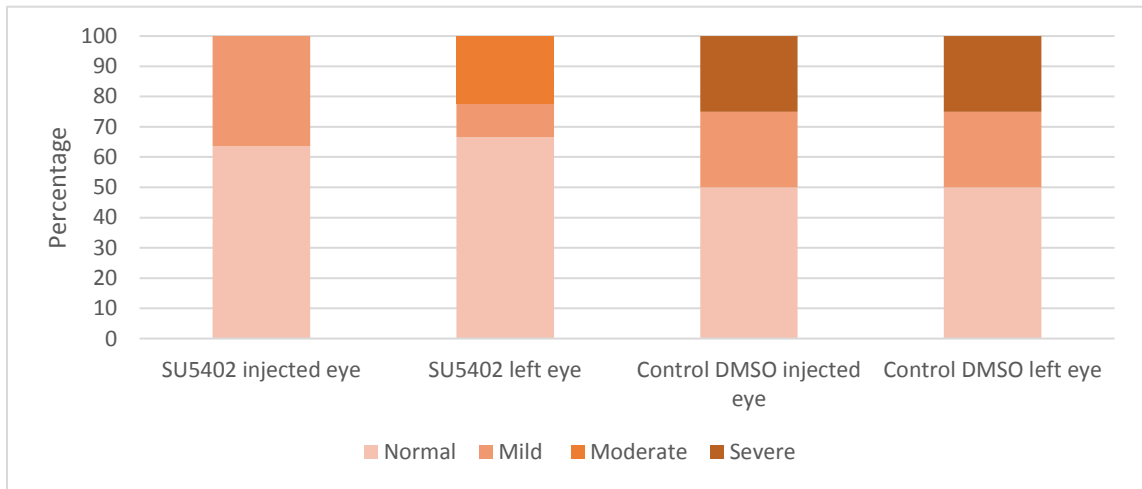


Figure 3.19. Percentage of eyes with each defect (mild, moderate and severe) observed in scleral condensations at HH37 in each group of microinjected eyes. SU5402 injected and left eyes as well as control DMSO injected and left eyes.

Test; $T=2.11$, $p=0.055$, $DF=13$). Similarly, no statistical difference was found when an independent t-test was performed between the contralateral left (untreated) eye of DMSO control and CNI (T test; $T=1.80$, $p=0.096$, $DF=13$). Since no difference was observed between DMSO control and CNI eyes, it was therefore deduced that DMSO itself did not have any effect.

3.3.2. SU5402 Microinjections

In the right SU5402 injected eyes, 63.64% of the eyes appeared normal (7 out of 11) and 36.36% (4 out of 11) had mild defects (Figure 3.19; Table 3.3). In those with mild defects, all the eyes had one unusually small ossicle. The average number of ossicles in the right SU5402 treated eyes was 14.18 ± 0.39 ($n=11$) with no moderate or severe abnormalities observed in any of the eyes. Surprisingly, the left (untreated) eyes, displayed mild, moderate as well as severe abnormalities. Two had severe defects with less than 10 papillae; these two eyes were determined to be outliers using the Dixon's Q-test at 95% confidence (Appendix E1) and were therefore not included in further analyses. Another two eyes had one missing ossicle, having a total 13 ossicles and were both categorized as moderately defective (two out of nine, 22.22%, Table 3.3). Omitting the outliers, 66.67% of the left untreated eyes were normal (6 out of 9). 11.11% (1 out of 9) had one small ossicle and was classified as having mild defect and 22.22% (2 out of 9) had moderate defects, where one eye had one missing ossicle and another had a small gap as well as a missing ossicle (Table 3.3). The average number of ossicles in the untreated left eye was 13.77 ± 0.42 ($n=9$) when the outliers were omitted. When an

independent t-test was performed, no statistical difference was found in the number of ossicles between the right and left eyes of SU5402 injected eyes (T-Test; $T=-0.96$, $p=0.362$ DF=9).

3.3.3 Comparison of Defects in DMSO and SU5402

A Fisher's Exact test was performed on the frequencies of normal, mild, moderate and severe defects in the right and left eyes of DMSO and SU5402 injections treatment groups (Appendix E1). No statistical difference was found in the various classification of defects between the right eyes of the two treatment groups (Fisher's Exact Test; $p=0.429$) or the left eyes of the two treatment groups (Fisher's Exact Test; $p=0.432$).

Overall, these analyses show that, although some defects were observed in the AP stained ossicles of DMSO and SU5402 treated eyes, these treatments have similar effect on scleral ossicle development.

3.3.4. Comparison of Number of Ossicles in DMSO and SU5402 Microinjections

In the majority of embryos both eyes had the same number of ossicles. The exception is one of the DMSO control injections and one of the SU5402 injected eyes (Table 3.4). In one control injection, the right eye had 14 ossicles and the left eye had 15 ossicles; in one of the SU5402 injected eyes, one embryo had 15 ossicles in the right eye and 14 ossicles in the left (Table 3.4). These counts are within the normal range of asymmetry for chicken embryos (Franz-Odendaal, 2008) and therefore were considered developmentally normal.

Table 3.4. Number of ossicles at HH37 in left and right microinjected eye of DMSO control group and 6mg/ml SU5402 group. The average number of ossicles \pm standard deviation is given, both with and without the outlier. No significant difference was found between the two treatment groups. * indicates eyes were determined outliers using Dixon's Q-test.

	DMSO Control		6mg/ml SU5402	
	Left eye	Injected right eye	Left eye	Injected right eye
	10	12	14	14
	14	14	13	15
	14	14	10*	14
	15	14	14	14
			14	15
			14	14
			7*	14
			13	14
			14	14
			14	14
			14	14
Average \pm S.D	13.25 \pm 1.92	13.5 \pm 0.82	12.82 \pm 2.21 (with outlier) 13.78 \pm 0.42 (without outlier)	14.18 \pm 0.39

For the DMSO control, the average number of ossicles was 13.5 ± 0.87 for the right eye (Table 3.4) compared to 14.18 ± 0.39 in the right eye of embryos treated with SU5402 (Table 3.4). In the contralateral untreated left eyes, the average number of ossicles was 13.25 ± 1.92 for DMSO treated control embryos (Table 3.4; Figure 3.20). In the case of SU5402 injected eyes, the average number of ossicles for the untreated left eye was 12.82 ± 2.21 when the outliers were included and 13.78 ± 0.42 when the outliers were omitted (Table 3.4).

An independent two sample t-test was carried out between each injection group (DMSO control and SU5402) to determine if there was any significant difference (Appendix E2). The independent t-test between the right treated eye of DMSO and SU5402 injected embryos showed no statistical significance (T-Test; $T=-2.02$, $p=0.065$, $DF=13$). When the test was carried out between the left eyes of DMSO and SU5402, again, no statistical difference was observed (T-Test; $T=-0.51$, $p=0.637$, $DF=4$).

A one way ANOVA was performed on the number of ossicles in the right eyes of the three treatment groups (CNI, DMSO control and SU5402) to confirm that there was no statistical difference between the three groups (ANOVA; $F=3.096$, $p=0.064$; Appendix E4). Overall, these analyses show that not only are the two controls (DMSO controls and CNI) similar but there is also no statistical difference between SU5402 treated and control eyes.

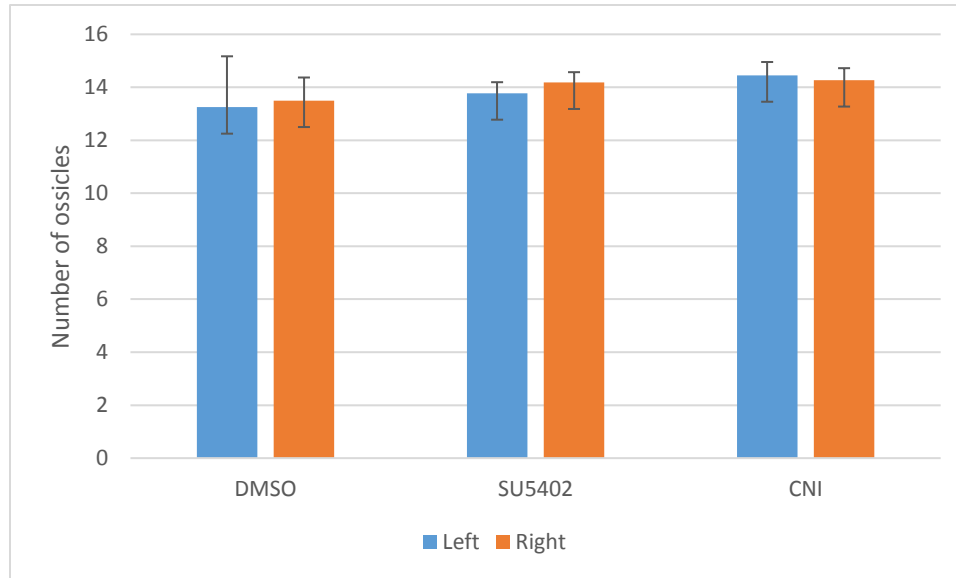


Figure 3.20. Average number of ossicles in left and right eyes for each group of microinjections. DMSO control and 6mg/ml SU5402 compared to CNI (Appendix D, Table D3; for data on CNI from Hammer, 2016) plotted with outliers omitted and standard deviations. No significant difference was found between or within the treatment groups (see text for details).

4.0 Discussion

4.1 *In Situ* Hybridization of *FGFRs*

In the sections below, the expression of *FGFR* isoforms is discussed in light of current literature and is divided into early (HH30-31), mid (HH32-34) and late (HH35-37) stages of the scleral ossicle developmental system. Schematics in this section represent observed whole mount expression comparing all *FGFRs* at these stages. ImageJ analysis was used to quantify the changes in expression at papilla #12 through HH30-37 for each of the genes. It appears that ImageJ was able to identify minor changes in the expression and thus the analysis showed some differences compared to what was observed in the whole mount.

4.1.1 *FGFR* Expression at Early Stage

All isoforms of *FGFRs*1-3 were expressed in papilla #12 at HH30 with low expression observed in neighbouring papillae in the temporal group as well as in the nasal region (opposite the temporal region). These areas of low expression mark the positions for future papillae development (Figure 4.1). The only exception to this was *FGFR2b* which, at HH30, was only expressed in papillae #12 and did not show any expression in future papillae development sites. Thus I conclude that *FGFR2b* is expressed slightly after the other isoforms, but in the same general pattern. This is in contrast to my hypothesis which stated that only *FGFRs* 1c, 3c and 2b would be observed prior to papillae formation.

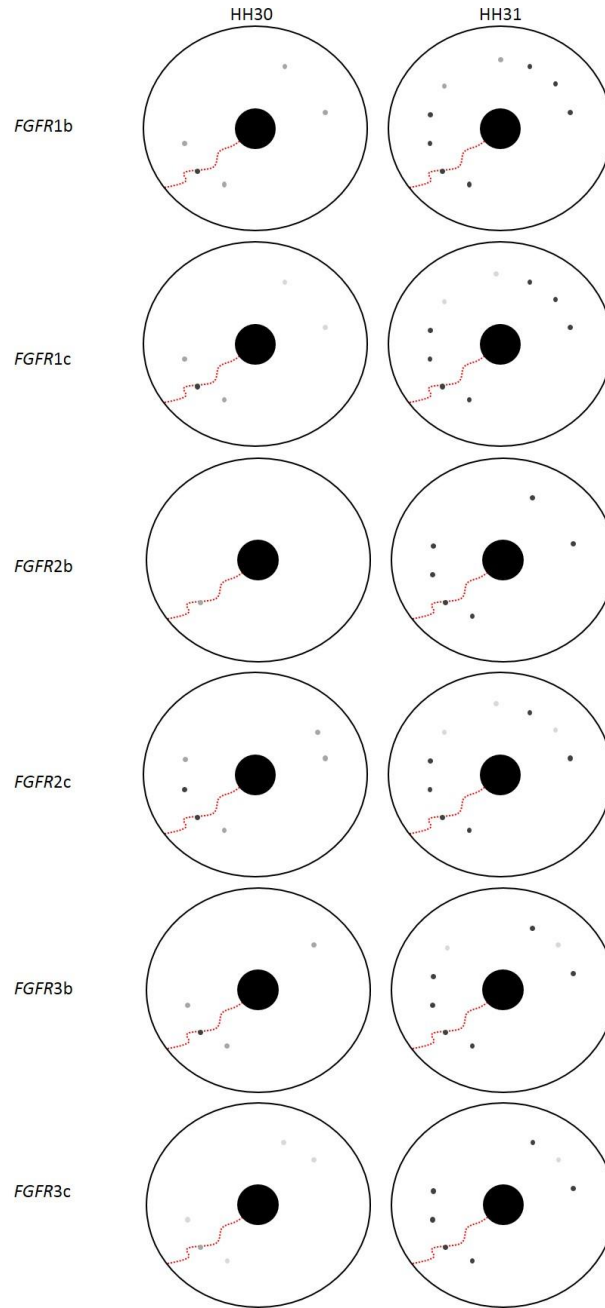


Figure 4.1. Schematic showing comparative expression of FGFR isoforms at early stage (HH30-31) of scleral ossicle developmental system. Key to the schematic is in Appendix C, Figure C4.

A similar pattern was observed at HH31. *FGFRs* 1b, 1c, 2c, 3b, and 3c were strongly expressed in conjunctival papillae of the temporal and nasal regions, whereas low expression of these genes was observed in regions marking sites of future papillae development (Figure 4.1). Again, *FGFR2b* was expressed only in the papillae that had already developed and showed no expression in future papillae development sites. Some variations can be observed between the expressions of each of the genes. However, this variation is limited to the number of papillae present, and thus demonstrates the variations in expression from an early point in the stage to a later point in the same stage.

During developmental processes such as the feather and tooth, the FGF pathway is required to induce placode formation. In feathers, the development begins by formation of a dense dermis and establishment of a feather dermis tract (Lin et al., 2006). Upon the formation of feather tracts, morphogens such as FGFs, BMP and HH, distribute themselves to form the bud and inter-bud regions. One of the first genes to be expressed during feather development is β -catenin (Lin et al., 2006). β -catenin is expressed in the mesenchyme prior to, and is thought to be required for feather tract formation. It is later expressed in the epithelium during feather tract formation (Normaly et al., 1999). Other early markers include *FGFR1* and *Wnt6* (Mandler and Neubüser, 2004). As mentioned earlier (section 1.4), *FGFR1* is expressed in the mesenchyme of feather tracts prior to bud formation (Noji et al, 1993). Using dominant negative forms of *FGFR1* and 2 in chick embryos, Mandler and Neubüser (2004)

reported that in the absence of *FGFR1* and *2*, feather development was inhibited. When the FGF pathway was inhibited using *SU5402* in explants with established buds, *BMP* and *SHH*, which are early markers of placode formation were not expressed. Similarly, *FGFR1*, *Wnt6* and *β -catenin* were not expressed when explants (prior to placode formation) were inhibited with *SU5402* demonstrating that the FGF pathway is important for feather placode formation (Mandler and Neubüser, 2004) and that the FGF pathway interacts with *BMP* and *HH*, two gene families we know are present in the scleral ossicle system (Duench and Franz-Odenaal, 2012). Interestingly, Jourdeuil and Franz-Odenaal (2016) reported the expression of *β -catenin* at HH30 in the epithelium during conjunctival papillae development and hypothesised that similar to feather development, *β -catenin* may be involved in preconditioning the epithelium to receive signals from the mesenchyme prior to papillae formation. Early expression of *FGFRs*, as shown in this thesis, may be involved in epithelial thickening in a similar manner as in feather formation and thus may be required for conjunctival papillae induction together with *β -catenin*.

During tooth development, *FGFR1c* is expressed in the mesenchyme prior to epithelial thickening (Porntaveetus *et al*, 2011) and once formed, *FGFR2b* is expressed in the epithelial thickening (Kettunen *et al.*, 1998). *FGFR2b* is also expressed in the apical ectodermal ridge of the chick limb buds (Noji *et al.*, 1993; Sheeba *et al.*, 2010) and chick with deleted IgIII domain of *FGFR2b* did not form limbs (Xu *et al.*, 1998). Similarly, in my

study, *FGFR2b* expression was only observed in the conjunctival papillae once they were induced and after other isoforms.

4.1.2 *FGFR* Expression at Mid Stage

Although the whole mount expression of *FGFR* isoforms is similar at HH30/31 (with the exception of *FGFR2b*), differences in the expression pattern start to appear at HH32/33 (Figure 4.2). This can be observed in both the whole mount eyes as well as in the cryosections. At HH32, conjunctival papillae of the temporal and nasal groups as well as some papillae of the dorsal group show strong expression for all *FGFR* isoforms (Figure 4.2). However, low gene expression for *FGFRs* 1b, 1c, 2c and 3c, but not 2b and 3b, was observed in future sites of papillae development in the dorsal and ventral regions (Figure 4.2). This is not unusual for *FGFR2b* since it is only expressed once the papillae have formed. On the other hand, the absence of low expression of *FGFR3b* in areas of future papillae sites at HH32 is most likely due to the use of embryonic eyes that were at an early HH32 stage. On the other hand, embryonic eyes used for the ISH of *FGFRs* 1, 2, and 3c were at HH32.5 or HH32.75 stage. This is supported by expression pattern observed at HH30 and 31 where low levels of *FGFR3b* expression can be observed marking the presumptive site of papillae development.

Cryosections of the temporal papillae at HH32 give further insight into the differences in expression of *FGFR* isoforms. At HH32/33, *FGFR1b* was expressed in the papillae as well as in the CR. Whereas at HH32, *FGFR1c* was expressed in the papillae (and the CR) as well as in a small aggregate of cells in the superficial mesenchyme

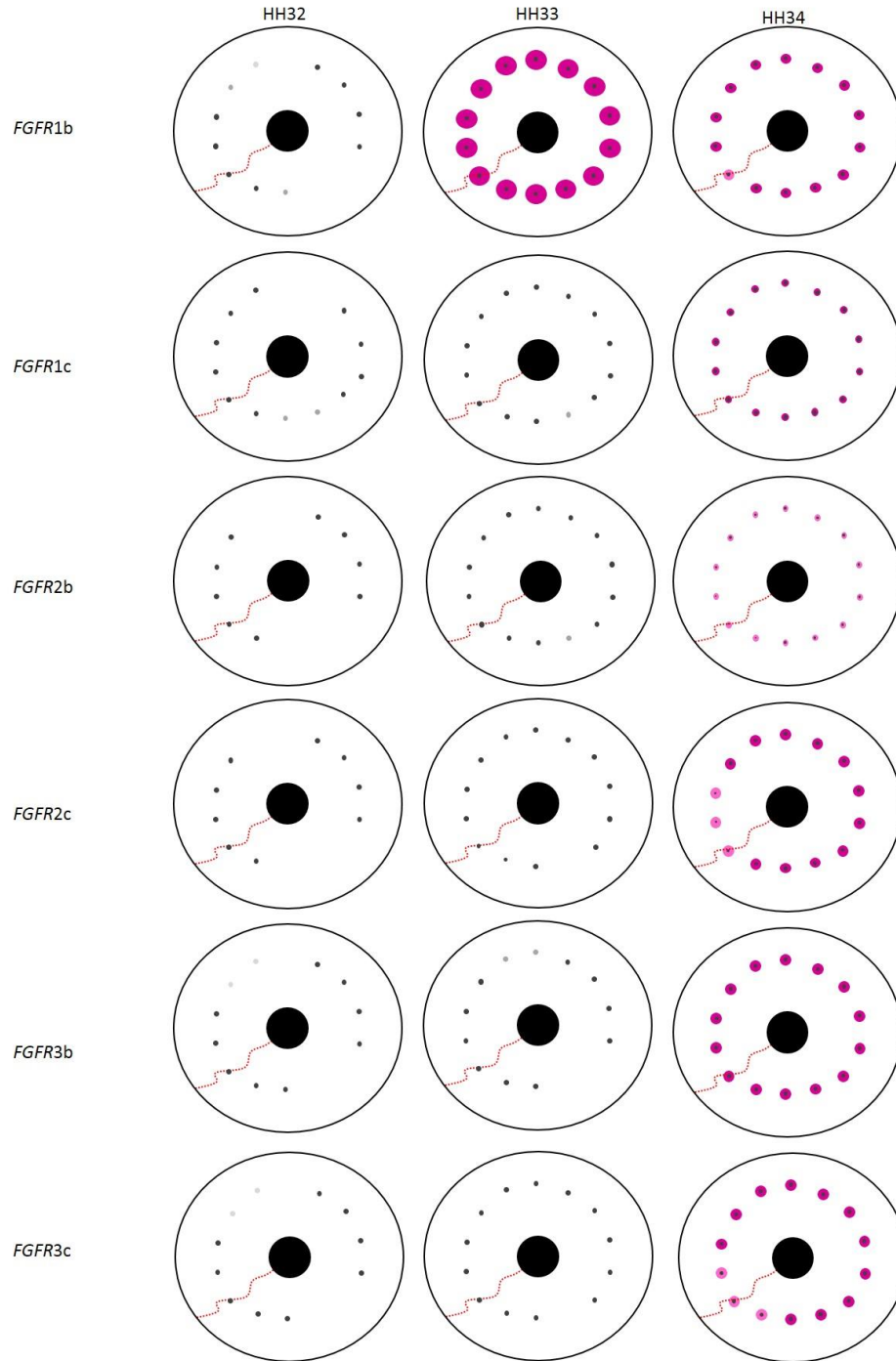


Figure 4.2. Schematic showing comparative expression of FGFR isoforms at mid stage (HH32-34) of scleral ossicle developmental system. Key to the schematic is in Appendix C, Figure C4.

directly beneath the papillae. This is interesting because Murray (1943) described the presence of condensations in the mesenchyme at Murray stage 2 and 3 in the form of a “thick-disc”, a shape similar to that observed expressing *FGFR1c* (Figure 3.7A). The expression of *FGFR2b* on the other hand is observed only in the papillae and no expression is observed in the CR. *FGFR2c* is expressed both in the papillae (and its CR) as well as in the superficial mesenchyme and the expression in the mesenchyme is limited to the same length of expression as in the epithelium. *FGFR3b* expression at this stage is observed in the conjunctival papillae as well as in a small CR. In comparison, at HH32, *FGFR3c* is diffusely expressed in the papillae, its CR, as well as throughout the mesenchyme beneath. All FGFR isoforms are expressed in the papilla region at HH32 and FGFRs 1c, 2c, and 3c are also expressed in the mesenchyme.

All conjunctival papillae have developed at HH33 except for the last papilla (papilla #1), which develops over the choroid fissure at HH34. All *FGFR* isoforms are expressed in this pattern at HH33. In addition low expression of *FGFRs* 1b, 1c, 2c, and 3b was observed at this stage in the region over the choroid fissure indicating position of future papilla development (Figure 4.2). Again, this expression was not observed for *FGFR2b* since it is expressed once the papillae have formed. The expression of *FGFR3b* was not similar to those of *FGFR1b*, 1c, 2c and 3c in that the conjunctival papillae at HH33 for *FGFR3b* did not form a complete circle with one missing papilla over the choroid fissure (Figure 4.2). Instead, low expression was observed at papillae of the dorsal and ventral groups. This may be attributed to using embryonic eyes from early

HH33 for *FGFR3b* WMISH as compared to the embryonic eyes used for WMISH of the other *FGFR* isoforms. However, with a sample number of six, this seems unlikely. Therefore, it is more likely that *FGFR3b* may not be as intensely expressed as the other genes. A similar observation was made when the intensity of expression was measured in papilla #12 through all the stages (Appendix D, Table D4). At HH33, expression for all *FGFR* isoforms can be observed in the CR in a zone of expression around the papillae. The zone of expression around the papillae observed for all *FGFRs* was present in an oval shape and differed in size for each of the isoforms (Figure 4.3). ImageJ was used to measure the field of expression in papilla #12 and its CR at HH33 (raw data in Appendix D, Table D5). *FGFR1b* showed a large zone of expression at HH33 compared to the other *FGFR* isoforms. Overall, strong expression of *FGFRs* 1 and 3 was observed in the papillae at HH33, whereas at the same stage, downregulation of *FGFR2b* and 2c was observed in the temporal group of papillae.

For several of the *FGFR* isoforms, downregulation in the temporal group of papillae begins at HH34. For *FGFR1b*, downregulation in the temporal group observed at HH34 is accompanied by an overall downregulation in the CR surrounding all the papillae (Figure 4.2). Similarly, for *FGFR3c*, downregulation of papilla #12 was first observed at HH34. In the case of *FGFR1c* and 3b, it is likely that downregulation in the temporal group begins at either a late HH34 or early HH35 since no downregulation is observed at HH34. The zone of expression in the CR surrounding the papillae for *FGFR1c* and 2b at HH34 are much smaller compared to *FGFR1b*, 2b and both isoforms of *FGFR3*.

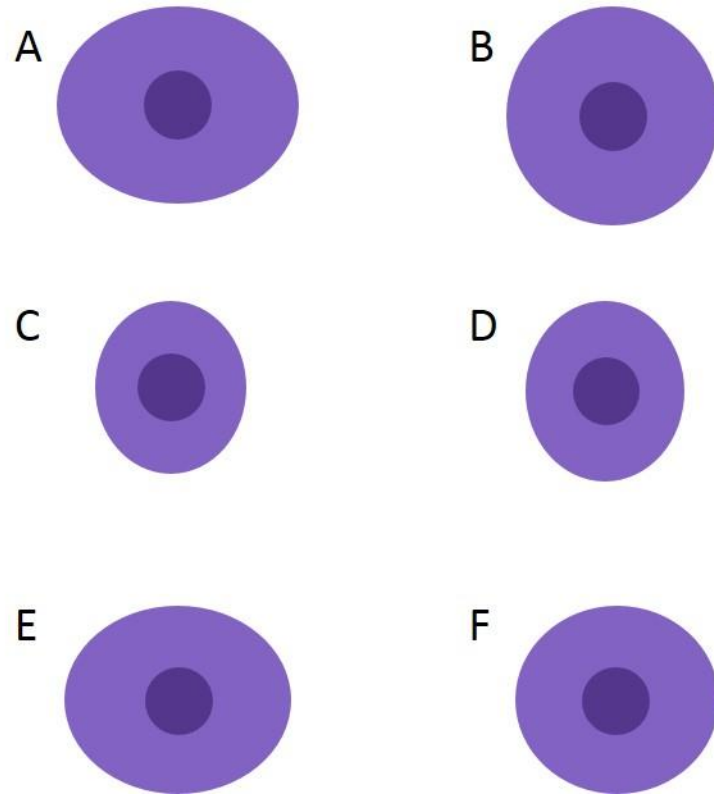


Figure 4.3. Schematic diagram showing the field of expression for *FGFRs* surrounding papilla #12 at HH33. (A) *FGFR1b*; (B) *FGFR1c*; (C) *FGFR2b*; (D) *FGFR2c*; (E) *FGFR3b*; (F) *FGFR3c*. Image J was used to measure the field of expression (Appendix D, Table D5). Papillae are in dark purple and the CR is in light purple.

For *FGFR2b* and *2c*, further downregulation of the temporal region was observed. Therefore, although downregulation of *FGFR2b* and *2c* begun at HH33, the downregulation of all *FGFR* isoforms can be observed in the temporal group of papillae. At HH32-36, although feather buds express *FGFRs*, they undergo anterior-posterior polarization and bud elongation (Widelitz *et al.*, 1999; Chen *et al.*, 2015) becoming morphologically different from conjunctival papillae and therefore it is difficult to compare these systems at these stages.

Cryosections of the temporal group at HH34 gives further insight into the spatial expression pattern of each of the isoforms. *FGFR1b* was expressed in the papillae as well as in the CR. In the superficial mesenchyme, where *FGFR1c* expression was observed at HH32 in a small aggregate of cell, at HH34, the expression was now present in a band of cell beneath the papilla. *FGFR2b* was expressed in the papillae and expression in a small CR was also observed. On the other hand, at the same stage, *FGFR2c* was expressed in the papillae and its CR and some expression may be present in the superficial mesenchyme. Interestingly, no expression was observed in the apical region of the papillae at this stage for this gene. For *FGFR3b*, where no mesenchymal expression was observed at HH32, at HH34, a small band of cells directly beneath the papillae show expression of this gene. In comparison, the opposite occurs in the case of *FGFR3c*. At HH32, *FGFR3c* expression was observed throughout the mesenchyme, whereas at HH34 this gene is expressed only in the papillae. These data show that expression of *FGFRs1c*,

2c, 3b and 3c changed in the epithelium and mesenchyme between HH32 and 34 whereas no such changes were observed in the case of *FGFRs*1b, and 2b.

FGFRs 1 and 2 are expressed in skeletal condensations in the mesenchyme during intramembranous ossification (Delezoide *et al.*, 1998) and conditional inactivation of *FGFR2* in mice showed that *FGFR2* is required for the proliferation of osteoprogenitor cells (Yu *et al.*, 2003). Similarly, using mouse models, Iskei *et al.* (1999) showed that *FGFR1* may be involved in pre-osteoblast differentiation whereas *FGFR2* may be required for the proliferation of osteoprogenitors. It is therefore possible that the presence of *FGFR1c* and 2c in the mesenchyme during scleral ossicle development may be playing a similar role.

4.1.3 *FGFR* Expression at Late Stage

Contrary to my hypothesis, which stated that all *FGFRs* would be expressed later during scleral ossicle development, an overall downregulation of *FGFR* expression was observed from stages 35 to 37, such that by HH37, no *FGFR* expression was observed (Figure 4.4). In *FGFR1b* WMISH eyes, downregulation in the temporal papillae had begun at HH34. Continued downregulation in the temporal as well as downregulation of the nasal, dorsal and ventral papillae was observed. This was accompanied by an overall decrease in expression in the CR of these papillae (Figure 4.4). Further downregulation for this gene was observed at HH36. A similar pattern was observed for *FGFR3c*, where downregulation of the gene was first observed at HH34 and continued downregulation in the temporal, nasal, dorsal and ventral regions was observed at HH35 and 36. In the

case of *FGFRs* 2b and 2c however, downregulation of the genes was first observed earlier at HH33. Therefore by HH35, very little *FGFR2* expression was observed in the temporal group of papillae and no temporal expression was observed at HH36. This was also confirmed through intensity measurements of papilla #12 using ImageJ, as very low intensity values were obtained for *FGFR2b* and intensity could not be determined for *FGFR2c* at HH36. Downregulation was first observed in ISH eyes of *FGFR1c* and 3b at HH35. However, since at this stage several of the papillae of the temporal group were downregulated, downregulation might have begun either at late HH34 or early HH35. Despite the different time points at which downregulation begins for each of the *FGFR* isoforms, all *FGFRs* have no expression at HH37 (Figure 4.4).

Skeletogenic condensations in the mesenchyme during chick scleral ossicle formation can be first observed at HH36 with mineralization occurring after HH37 and observed by HH38 (Franz-Odendaal, 2008). In addition, the role of *FGFRs* in osteoblast lineage show that *FGFRs* 1 and 2 are involved in the proliferation of pre-osteoblasts and in the differentiation of osteoblasts (Long, 2012). Therefore, it is not surprising that *FGFR1* and 2 expression was downregulated during the stages of matrix deposition (HH35 onwards) in chick scleral ossicles. Mice deficient in *FGFR3* had an increase in unmineralized tissue and increased osteoblast and osteocyte number in long bones showing that *FGFR3* plays an important role in mineralization (Valverde-Franco *et al.*, 2004). *FGFR3* downregulation was observed in chick WMISH eyes at HH35 to 37 when matrix deposition is taking place. It is possible the *FGFR3* expression is once again

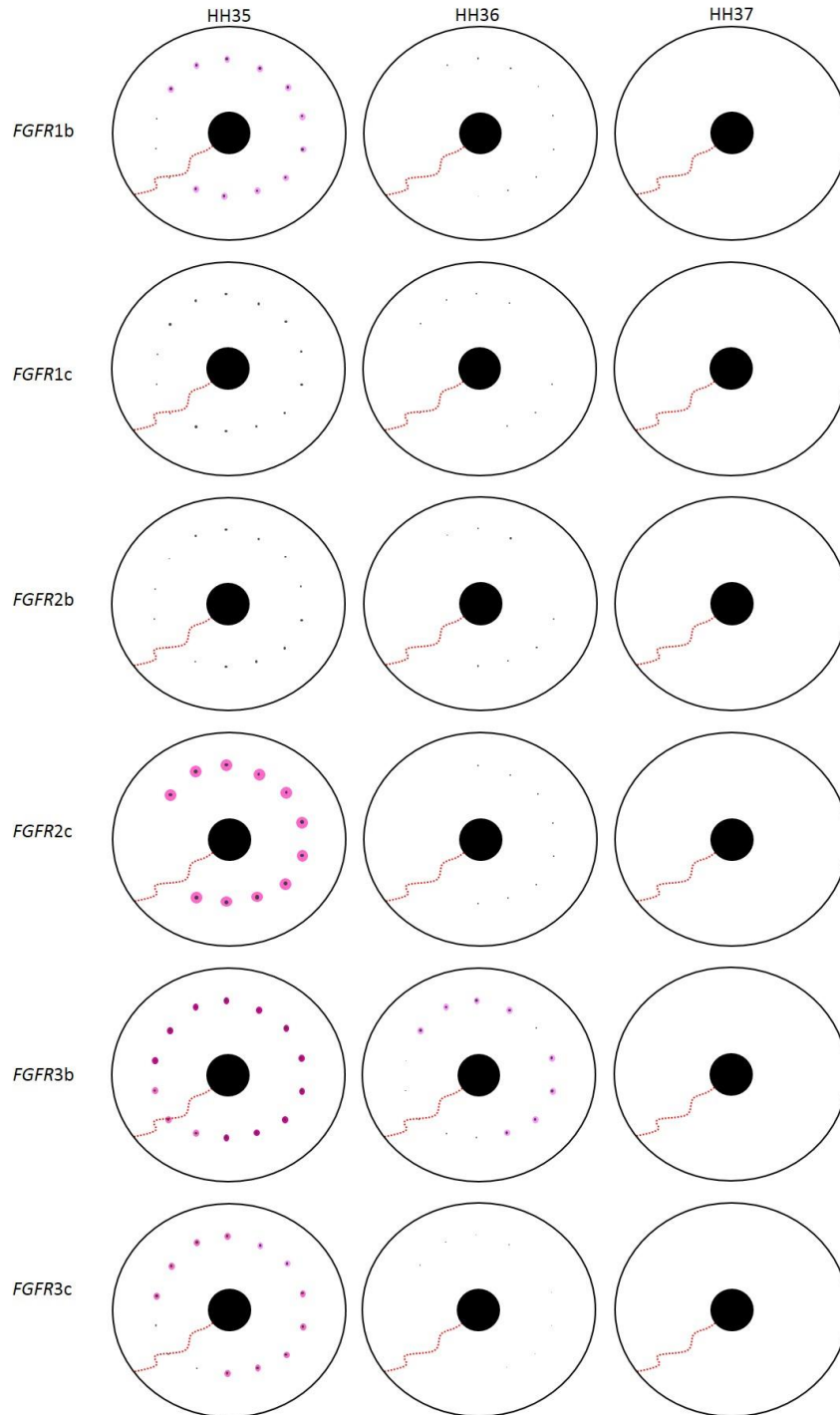


Figure 4.4. Schematic showing comparative expression of FGFR isoforms at late stage (HH35-37) of scleral ossicle developmental system. Key to the schematic is in Appendix C, Figure C4.

upregulated at the stages of osteoid deposition (HH38 onwards), however, these stages were not examined in this study.

Several studies have shown that the FGF and BMP pathway interact with each other throughout development. Previous studies in the chick scleral ossicle system have identified the expression of BMP2 and SHH in the papillae as well as IHH, which was expressed in the papillae as well as the mesenchyme (Duench and Franz-Odenaal, 2012). All three genes were found to be expressed between HH35 and 36, stages when ossicle induction is taking place. During some processes, like chondrogenesis in limb development, the FGF and BMP act as antagonists (Yoon *et al.*, 2006; Guo and Wong, 2009) whereas in other processes, such as hepatocyte differentiation, they act in synergy (Yanai *et al.*, 2008). In feather development, BMP was observed in the feather primordia once FGFs are no longer expressed (Jung *et al.*, 1998). In addition, exogenous BMP inhibited *FGFR1* expression in the chick dermis (Normaly and Morgan, 1998). Interestingly, at HH35, when BMP expression was first observed in the chick conjunctival papillae (Duench and Franz-Odenaal, 2012), *FGFRs* are being downregulated. Therefore, it is possible that in the chick scleral ossicle system, the FGF and the BMP pathway work opposite each other. SHH and FGF on the other hand, form a positive feedback loop during limb bud outgrowth in the chick. FGF8 and later FGF4 are involved in maintaining SHH in the zone of polarizing activity (Crossley *et al.*, 1996; Laufer *et al.*, 1994). In turn, SHH maintains FGF4 in the apical ectodermal ridge (Scherz *et al.*, 2004). In early mouse development, FGFs also induce the release of SHH during left-right

determination (Tanaka *et al.*, 2005). In the scleral ossicle system, *FGFRs* are downregulated at the time that *SHH* was expressed (HH35 and 36; Franz-Oudendaal, 2008), indicating that they might work opposite each other. Although the above mentioned studies show that *FGFs* interact with *SHH*, it is unclear whether this interaction occurs in the scleral ossicle system.

A recent study in our lab has also investigated the role of vasculature in the development of scleral ossicles (Jabalee and Franz-Oudendaal, 2015) as vascularization plays an important role in bone development and the first papillae forms above the ciliary artery. Avascular zones are present beneath each papillae (at HH34.5) and as the papillae degenerate, the area beneath the papillae becomes highly vascularized showing that vascularization does not occur until osteogenesis has begun (Jabalee and Franz-Oudendaal, 2015). Vascular endothelial growth factor A (*Vegfa*) is required for angiogenesis (Otrock *et al.*, 2007). In the chick sclera, diffuse expression of *Vegfa* was observed in the epithelium, superficial mesenchyme but it was most strongly observed in the papillae at HH35 (Jabalee and Franz-Oudendaal, 2015). As the papillae degenerate, the expression of *Vegfa* also decreases until it completely disappears by HH38.5 (Jabalee and Franz-Oudendaal, 2015). *FGF2* is also an important factor involved in angiogenesis and was the first pro-angiogenic molecule identified (Flokman *et al.*, 1984; Cross and Claesson-Welsh, 2001). The importance of *FGF* in vasculature is shown by inactivating the *FGF2* gene in mice which resulted in mice with decreased vascular zone and low blood pressure (Dono *et al.*, 1998; Cross and Claesson-Welsh, 2001). Not only is *FGF2*

involved in the proliferation and migration of endothelial cells, by working upstream of VEGF, FGF2 also induces VEGF expression in the endothelial cells (Seghezzi *et al.*, 1998). However, once VEGF is expressed, it no longer requires FGF signalling (Murakami and Simons, 2008). *FGFR1* is also expressed in the endothelium and is important for vasculature development and maintenance (Lee and Swain, 2000). In addition a recent study looking at the role of FGF pathway in blood and lymphatic vasculature showed that the FGFs are crucial for vasculature development and act by controlling the metabolic pathway (Yu *et al.*, 2017). Since FGFs are involved upstream of VEGF, it is possible that *FGFRs* are expressed first during conjunctival papillae development and become downregulated in later stages once they have induced VEGF. However, this seems unlikely because: i) *FGFRs1b*, *1c*, *2b*, *2c* and *3b* expression was not observed in a diffuse manner in the mesenchyme and therefore these *FGFR* probes likely did not bind to vascular endothelial cells in the mesenchyme, ii) although *FGFR3c* was diffusely expressed in the mesenchyme at HH32, it was only expressed beneath the area of the papilla and its CR, iii) in addition to inducing VEGF, FGF and VEGF are synergistically involved in vascular development (Seghezzi *et al.*, 1998) and therefore one would expect that *FGFRs* would be expressed in a similar pattern to *Vegfa* in the scleral ossicle system from HH35-37 (Jabalee and Franz-Odenaal, 2015). However, my data shows that this is not the case. In summary, it seems unlikely that *FGFRs* act upstream of *Vegfa* in the scleral ossicle system.

To understand how *FGFRs* interact with previously identified genes in the scleral ossicle system, experiments involving the inhibition of FGF/FGFR pathway, for example by using chemical inhibitors such as LY2874455 should be carried out. How inhibition of the FGF/FGFR pathway results in changes in expression of *BMP*, *HH* and *VEGF* as well as changes in vasculature development should also be studied.

4.1.4 Summary of *FGFR* Expression

The overall expression of *FGFR* is best described by looking at how expression varies in papilla #12 (and a small area of its contiguous region) through the stages of the scleral ossicle system (HH30-37) for each of the isoforms. Quantitative analysis of the intensity of expression of the *FGFR* isoforms shows that the intensity of *FGFR1b* and *1c* at papillae #12 increases from HH30 to 32 and a continuous decrease in intensity is observed from HH33 to 37 (raw data in Appendix D, Table D4). This is somewhat similar to what was observed in the WMISH eyes, the only difference is that downregulation in *FGFR1b* was observed at HH34 whereas in *FGFR1c* it was at HH35. However, prior to HH33, expression for both genes was observed in the general papillae area (papilla + CR) and at HH33, the expression in the CR was distinct from the expression in the papillae. It is likely that the CR is downregulated first and therefore the expression can be seen separately from the papillae and that this downregulation in the CR was quantified by ImageJ and shown as a decrease in the total level of intensity. A similar pattern of intensity is observed for *FGFR2b* where intensity increases from HH30 to 32 and then a decrease is observed from HH33 to 37. This was also observed in the WMISH eyes,

where downregulation was observed at HH33. For *FGFR2c*, an increase in intensity is observed at HH31 after which an almost stable value of intensity is observed until HH33. There is however, a sudden increase in intensity at HH34 which is unexpected as downregulation was observed at HH33. This is supported by cryosections which show absence of *FGFR2c* expression in the apical region of the papillae in the temporal as well as in the nasal group (Appendix C, Figure C2) at HH34. In the case of *FGFR3b*, a decrease in intensity is first observed at HH32, this is followed by an almost stable value of intensity until HH34 after which further decrease in intensity is observed. For *FGFR3c*, a steady increase in intensity is observed until HH33 which is then followed by a steady decrease in intensity. The pattern of intensity is somewhat similar to what was observed in the WMISH eyes, with the exception that the downregulation in the temporal papillae was observed at HH35 in for *FGFR3b* and at HH34 for *FGFR3c*. The pattern of intensity for each *FGFR* isoform is summarized in Table 4.1. Overall, the intensity values provide a good estimate for the time when downregulation begins for each *FGFR* isoform. Analyses using quantitative RT-PCR would give a more accurate indication for the changes in the level of FGFR expression in the different areas of the eye tissue.

4.1.5 FGFR Expression in the Interpapillary Regions

Apart from the transmembrane bound 'b' and 'c' isoforms, *FGFRs* can also undergo splicing to form secreted versions of the receptor. Tomlinson *et al.* (2005) reported the presence of a secreted form of *FGFR3* expressed in the urothelium and that the secreted form inhibits FGF1 induced cell proliferation. A secreted form of

Table 4.1. Intensity of expression of each FGFR isoform in papilla #12 and its CR from HH30 to 37. '+' is used to indicate the level of intensity with more plus signs to show more intensity. Values are left blank where ImageJ was unable to determine intensity.

	HH stage							
	30	31	32	33	34	35	36	37
FGFR1b	+	+++	++++	+++	+++	++	+	+
FGFR1c	+	++	+++	+++	++	+	+	
FGFR2b	++	++	++++	+++	++	+	+	+
FGFR2c	+	++	++	++	++++	+		
FGFR3b	+++	+++	++	++	++	+	+	
FGFR3c	+	++	+++	++++	++++	++	+	

FGFR1 binds to both FGF1 and 2 (Duan *et al.*, 1992) and are mostly found in the endothelial cells. These secreted forms of *FGFRs* are involved in inhibiting *FGFR* signalling. Chick WMISH eyes for all *FGFR* isoforms show extremely low levels of expression in the interpapillary region. It is also possible that secreted forms of *FGFRs* may be present in the eye epithelium bound to and sequestering important FGF ligands, thereby inhibiting *FGFR* signalling in the interpapillary area. *FGFRs* may also be involved in the spacing of papillae and interpapillary regions in the chick eye by varying FGF/*FGFR* signalling.

4.1.6 Spatial Expression of FGFR Isoforms

Transmembrane bound isoforms are usually present in a tissue specific manner, where the 'b' isoform is usually expressed in the epithelium and the 'c' isoform is expressed in the mesenchyme. Cryosections show that typical to this tissue specificity,

FGFR1b and 2b were expressed in the epithelium. However, isoform tissue specificity might not be very stringent. Both *FGFR3b* and 3c isoforms were found in the normal as well as carcinoma cells of the urothelium (Tomlinson *et al.*, 2004). In addition, fibroblast cells can express both *FGFR3b* and 3c isoforms (Werner *et al.*, 1993). *FGFRs* 2c and 3c are both expressed in the retinal pigmented epithelium (Alizadeh *et al.*, 2003) and *FGFR2c* expression is also observed in the corneal epithelium (Wilson *et al.*, 1993). *FGFR3c* is also expressed in the prostatic epithelium (Nickel, 1999) as well as the undifferentiated epithelial cells in mouse intestine (Vidrich *et al.*, 2004). Therefore, it is not completely unexpected that, in the scleral ossicle system, *FGFR3b* was observed in the mesenchyme at HH34 and that at the same stage, the expression of *FGFR1c*, 2c and 3c was observed in the epithelium. However, there are no previous studies showing expression of *FGFR1c* in the epithelium. The expression of *FGFR1c* in the epithelium should be further explored, for example by using western blot to confirm the presence or absence of the protein.

4.1.7 Possible FGFs involved in the scleral ossicle system

The FGF-FGFR signalling pathway typically works such that an FGF in the epithelium activates another FGF in the mesenchyme and vice versa (Ornitz and Itoh, 2015). Due to the presence of all FGFRs in the epithelium, there are several FGFs that could binding to these FGFRs (Table 1). The most likely candidates however are FGFs 2, 4, 8, 10 and 18 and 20.

The role of FGFs in processes requiring epithelial-mesenchymal interactions and placode formation such as in limb, calvariae, feather and tooth will be discussed next, together with any insights that can be obtained for the scleral ossicle system based on these other systems. In limb development, ectopic FGF10 was able to induce expression of ectodermal *FGF8* upon removal of the apical ectodermal ridge and application of ectopic FGF8 induced expression of mesodermal *FGF10* (Ohuchi *et al.*, 1997). Therefore, it was concluded that FGF10 is the initial signal required for induction of FGF8 in the ectoderm. The FGF8 in turn helps to maintain the required levels of FGF10 in the underlying mesenchyme (Ohuchi *et al.*, 1997). Mutant mice lacking FGF10 were unable to develop all components of the fore-and hind-limbs (including the rudimentary iliac bone) and also had absent apical ectodermal ridge and regions of zone polarizing activity (Sekine *et al.*, 1999). Sun *et al.* (2000) showed that FGF does not affect the apical ectodermal ridge. They suggest that the hypoplastic phenotype observed in the forelimb of double knock-out mice of FGF4 and FGF8 was due to a decrease in the number of progenitor cells available and that this may be due to the influence of FGF8 in cell adhesion there by limiting the number of cells available for migration into the condensation area (Sun *et al.*, 2000). These studies show that FGF10 in the mesenchyme is required for epithelial thickening and induction of FGF8 in the epithelium. It is therefore possible that FGFs 8 and 10 are expressed early in conjunctival papillae development. FGF8 binds to FGFR1c whereas FGF 10 binds to FGFR1b and 2b.

During intramembranous bone development, FGF18 was required for proliferation of osteogenic mesenchyme cells as well as for their progression towards terminal differentiation to osteoblasts in the calvariae (Ohbayashi *et al.*, 2002). In mice embryos, FGF18 was expressed in the coronal sutures as well as at the dorsal rims of the parietal bones, but not in the sutural mesenchyme (Hajihosseini and Heath, 2002). Mice deficient in FGF18 had defective proliferation and differentiation mechanisms which resulted in delay of ossification and therefore in delay of calvarial development and suture closure (Ohbayashi *et al.*, 2002). FGF2, 4 and 9 were also expressed in calvarial sutures. FGF2 promotes osteogenic cell proliferation (Rice *et al.*, 2000) and lack of FGF2 prevents osteogenesis (Greenwald *et al.*, 2001). Beads releasing exogenous FGF4 at the osteogenic front caused suture closure and fusion, however, application of FGF4 on the mid-sutural mesenchyme only caused an increase in the thickness of the tissue (Kim *et al.*, 1998). Therefore, FGF4 may direct cell proliferation. FGF9 was found to be expressed in the dura mater as well as the calvarial mesenchyme (Kim *et al.*, 1998). With respect to osteogenic potential, FGF 2 and 18 are extremely important, since in their absence there is a delay in skull development as well as suture closure. However, not much else is known about the involvement of FGFs in intramembranous bone development. Since scleral ossicles are also intramembranous bones, FGF2, 4, 18 (along with FGF 8 and 10) might be expressed during HH32-34. FGF2 binds to all FGFRs except for 2b. FGF 4 binds to all 'c' isoforms whereas FGF18 binds to FGFR2c and 3c (Table 1.1).

During feather development, FGF2 and 4 promote bud formation (Song *et al.*, 2004). Normally, during feather formation, first detection of FGF10 is possible at HH stage 29 and can be observed as spots (Taoa *et al.*, 2002). Normal chick explants treated with FGF10 blocking antibodies prior to placode formation resulted in no new bud formation and no *Bmp2* or *Shh* expression detection. Therefore, showing that FGF10 is required for feather placode development (Mandler and Neubuser, 2004). *Scaleless* mutant chicken not only lack scales and feathers but also have only 2-4 scleral ossicles (Blanck *et al.*, 1981) as compared to the 14-16 in *Gallus* and therefore the recent discovery of a mutation in FGF20 (Well *et al.*, 2012) may be an indication of the role of FGF 20 in scleral ossicle development. These studies provide further support for the involvement of FGF10 in epithelial thickening and its possible role early during conjunctival papillae development. During HH32-34, FGF20 might also be expressed along with the aforementioned FGFs 2, 4, 8, 10 and 18. FGF20 binds to FGFR1c and 2c (Table1.1).

An overview of the FGFs and FGFRs involved in tooth development is given in section 1.4. Briefly, FGF10 was detected in the epithelium and in the mesenchyme even before the initial bud stage (Kettunen *et al.*, 2000). FGFs 17, 8 and 9 were also expressed prior to epithelial thickening and FGFs 8 and 9 were expressed until epithelial budding (Kettunen *et al.*, 1998; Porntaveetus *et al.*, 2011). During the epithelial thickening, FGF10 was weakly expressed in the mesenchyme (Kettunen *et al.*, 2000) and FGF18 was weakly expressed on the buccal side (Porntaveetus *et al.*, 2011). At the bud stage, the

expression of FGFs 10, 18 and 20 were observed (Porntaveetus *et al.*, 2011) along with FGF4, 8 and 9 (Kettunen *et al.*, 1998). The expression of FGFs in tooth development also indicate the possibility of the expression of FGFs2, 4, 8, 10 18 and 20 during conjunctival papillae development.

By collectively looking at these studies, it is likely that FGF8 and 10 are expressed at HH30-31, early during conjunctival papillae development. During HH32-34, FGF2, 4, 8, 10, 18 and 20 might be expressed and in the late stage of the scleral ossicle developmental system, due to the downregulation of FGFRs, FGFs should also be downregulated. It would be interesting to look at the spatial and temporal expression of FGFs 2, 4, 8, 10, 18 and 20 due to their role in similar developmental processes requiring epithelial-mesenchymal interactions and placode formation.

4.2 Inhibition of the FGF Pathway

Several studies show that the FGF-FGFR signaling is inhibited by SU5402 (Sanz-Ezquerro and Tickle, 2003; Kawakami *et al.*, 2004; Tirosh-Finkel *et al.*, 2010; Sato and Nakamura, 2004 are just a few). Horakova *et al.*, (2014) reported that when AG1X2 beads soaked with 0.3mg/ml and 0.5mg/ml SU5402 were implanted into the chick wing bud at HH20-21, only a few embryos had smaller wings. This was attributed mostly to a thinner and shorter humerus. However, at higher concentrations (0.74 and 1mg/ml SU5402) the majority of the embryos had shorter wings with complete loss of one or several skeletal elements. In this thesis, SU5402 was first tested using affigel blue beads. Beads implanted into the wing bud at HH20/21 did not show any abnormal skeletal

development. SU5402 was next tested using AG1X2 beads. These SU5402 soaked beads were similarly implanted into the wing bud at HH20/21 and as previously reported by Horakova *et al.* (2014), high concentrations of SU5402 (3 and 6mg/ml) resulted in a complete loss of one or several skeletal elements. However, when AG1X2 beads soaked in SU5402 were implanted next to a conjunctival papillae at HH34, no effect on the development of scleral ossicles was observed. The likely explanation for this is that the AG1X2 beads could not be inserted completely under the papilla and almost half the bead was above the epithelial surface. This was because of their large size of 100-150µm; a bead size of 70-80µm is best suited for implanting under the papillae (Jabalee, 2014). With the bead not completely embedded, the SU5402 might not have efficiently released into the tissue. Because when correctly implanted, SU5402 treated beads resulted in abnormal formation of skeletal elements in the limb, it is more likely that it was the size of the bead and not the concentration of SU5402 that was responsible for the no effect that was observed on scleral ossicle development. Therefore, the method of microinjection was next used to release the inhibitor into the tissue.

The structure of the corneal epithelial tissue was such that it would block the needle and prevent the direct release of inhibitor into the tissue. Hence, an alternative procedure was used which required making a small incision next to a papilla, injecting the inhibitor above the incision and allowing the inhibitor to settle onto the tissue. Results using this procedure were inconclusive (results section 3.3). This procedure seems inefficient since it is possible that the inhibitor diffused into the amniotic fluid

before it could be taken up by the tissue. In addition, as all FGFRs are downregulated from HH34-37, it is possible that the FGF pathway is not involved in scleral ossicle induction, instead, an effect might be observed if microinjections were carried out at HH30/31 when conjunctival papillae development is taking place and when there is strong FGFR expression. Moreover, although SU5402 is often used as a broad range FGFR inhibitor, it preferentially inhibits FGFR1 over FGFRs 2 or 3. A broad range inhibitor such as LY2874455 which binds to all FGFRs could be used instead to give a more definitive idea of whether the FGF pathway is involved during scleral ossicle induction. However, a t-test between right injected eyes of DMSO and SU5402 had a p value of 0.055. Therefore, it is possible that there is some difference between the two treatment groups and that this difference could be more distinct with a higher sample size. Currently, studies in our lab are looking at culturing chick embryo eyes *in vitro*, this could provide an easier method of releasing SU5402. The role of FGF/FGFR pathway can be also be studied using a combination of exogenous FGF bead implantation, electroporation, siRNA (Katahira and Nakamura, 2003) and using other chemical inhibitors such as NF449, PD161570 and PD173074 (Horakova *et al.*, 2014) and observing the effect at HH36 and 37.

5.0 Summary and Conclusion

FGF/FGFRs play important roles throughout development. Although extensive research is present examining *FGF/FGFR* expression and function in endochondral bone development, very little work has been done to study their role in intramembranous bones. In this study I reported the expression patterns of 'b' and 'c' isoforms of *FGFRs*1-3 during conjunctival papillae development and scleral ossicle induction. A common pattern is seen in their expression where all *FGFRs* are expressed at HH30 and are completely downregulated by HH37. Interestingly, all *FGFR* isoforms were expressed in the papilla and their CR. It is likely that FGF-FGFR signalling is involved in the patterning, as well as the development of the conjunctival papillae. Comparable to other studies looking at expression of *FGFRs* in bone development and osteoblast lineage, *FGFRs*1c and 2c were expressed spatially and temporally during mesenchymal condensation and preosteoblast proliferation, indicating that *FGFRs* may be involved in the early stages of scleral ossicle development (i.e. establishment of the condensation). Interestingly, all *FGFRs* were downregulated from HH34-37 and no *FGFR* expression was observed at HH37, showing that *FGFRs* are mostly likely not involved during matrix deposition. *FGFR* expression may reappear later at HH38/38.5 during stages of mineralization, however, these stages were beyond the scope of this research. However, further experiments need to be carried out to determine the role of *FGFRs* in the scleral ossicle system. Through inhibitory experiments, I also attempted to provide insight into the role of FGF pathways during scleral ossicle development. Unfortunately, bead implantation and

microinjection methods were unsuccessful in releasing the SU5402 inhibitor into the desired tissue area.

Significantly, this study was able to identify another potential important gene family, namely the FGF family, in the development of the scleral ossicle system. Studies investigating the expression of FGF ligands in the scleral ossicle system would create a more wholesome understanding of the possible *FGF/FGFR* interactions. Furthermore, since FGFs often work with other morphogens such as BMP, HH and Wnt, studying how changes in *FGF/FGFR* affect BMP, HH, and Wnt expression as well as vasculature would provide insight into some of the interactions that govern the development of this fascinating scleral ossicle system as well as the development of intramembranous bones and non-neurogenic placodes.

Literature Cited:

Alizadeh, M., Miyamura, N., Handa, J. T., & Hjelmeland, L. M. (2003). Human RPE cells express the FGFR2IIIc and FGFR3IIIc splice variants and FGF9 as a potential high affinity ligand. *Experimental Eye Research*, 76(2), 249-256.

Blanck, C. E., McAleese, S. R., & Sawyer, R. H. (1981). Morphogenesis of conjunctival papillae from normal and scaleless chick embryos. *The Anatomical Record*, 199(2), 249-257.

Bonaventure, J. (1998). FGFR3 (fibroblast growth factor receptor 3). *Atlas Genetics and Cytogenetics in Oncology and Haematology*, 2(1), 12-13.

Browaeys-Poly, E., Blanquart, C., Perdereau, D., Antoine, A. F., Goenaga, D., Luzy, J. P., ... & Burnol, A. F. (2010). Grb14 inhibits FGF receptor signaling through the regulation of PLC γ recruitment and activation. *FEBS Letters*, 584(21), 4383-4388.

Camps, M., Nichols, A., & Arkinstall, S. (2000). Dual specificity phosphatases: a gene family for control of MAP kinase function. *The FASEB Journal*, 14(1), 6-16.

Chen, C. F., Foley, J., Tang, P. C., Li, A., Jiang, T. X., Wu, P., ... & Chuong, C. M. (2015). Development, regeneration, and evolution of feathers. *Annual Review of Animal Biosciences*, 3(1), 169-195.

Cloney, K., & Franz-Odenaal, T. A. (2015). Optimized ex-ovo culturing of chick embryos to advanced stages of development. *JoVE (Journal of Visualized Experiments)*, (95), e52129-e52129.

Cohn, M. J., Izpisua-Belmonte, J. C., Abud, H., Heath, J. K., & Tickle, C. (1995). Fibroblast growth factors induce additional limb development from the flank of chick embryos.

Cell, 80, 739-749.

Cordero, D. R., Brugmann, S., Chu, Y., Bajpai, R., Jame, M., & Helms, J. A. (2011). Cranial neural crest cells on the move: Their roles in craniofacial development. *American*

Journal of Medical Genetics Part A, 155(2), 270-279.

Coulombre, A. J., & Coulombre, J. L. (1973). The skeleton of the eye: II. Overlap of the scleral ossicles of the domestic fowl. *Developmental Biology*, 33(2), 257-267.

Coulombre, A. J., Coulombre, J. L., & Mehta, H. (1962). The skeleton of the eye: I.

Conjunctival papillae and scleral ossicles. *Developmental Biology*, 5(3), 382-401.

Couly, G. F., Coltey, P. M., & Le Douarin, N. M. (1993). The triple origin of skull in higher vertebrates: a study in quail-chick chimeras. *Development*, 117(2), 409-429.

Cross, M. J., & Claesson-Welsh, L. (2001). FGF and VEGF function in angiogenesis:

signalling pathways, biological responses and therapeutic inhibition. *Trends In*

Pharmacological Sciences, 22(4), 201-207.

Crossley, P. H., Minowada, G., MacArthur, C. A., & Martin, G. R. (1996). Roles for FGF8 in

the induction, initiation, and maintenance of chick limb development. *Cell*, 84(1), 127-

136.

De Robertis, E. M., & Kuroda, H. (2004). Dorsal-ventral patterning and neural induction in *Xenopus* embryos. *Annual Review of Cell and Developmental Biology*, 20, 285-308.

Delezoide, A. L., Benoist-Lasselín, C., Legeai-Mallet, L., Le Merrer, M., Munnich, A., Vekemans, M., & Bonaventure, J. (1998). Spatio-temporal expression of FGFR 1, 2 and 3 genes during human embryo-fetal ossification. *Mechanisms of Development*, 77(1), 19-30.

Dono, R., Texido, G., Dussel, R., Ehmke, H., & Zeller, R. (1998). Impaired cerebral cortex development and blood pressure regulation in FGF-2-deficient mice. *The EMBO Journal*, 17(15), 4213-4225.

Dorey, K., & Amaya, E. (2010). FGF signalling: diverse roles during early vertebrate embryogenesis. *Development*, 137(22), 3731-3742.

Duan, D. S., Werner, S., & Williams, L. T. (1992). A naturally occurring secreted form of fibroblast growth factor (FGF) receptor 1 binds basic FGF in preference over acidic FGF. *Journal of Biological Chemistry*, 267(23), 16076-16080.

Duench, K., & Franz-Odenaal, T. A. (2012). BMP and Hedgehog signaling during the development of scleral ossicles. *Developmental Biology*, 365(1), 251-258.

Eswarakumar, V. P., Lax, I., & Schlessinger, J. (2005). Cellular signaling by fibroblast growth factor receptors. *Cytokine & Growth Factor Reviews*, 16(2), 139-149.

Eswarakumar, V. P., Monsonego-Ornan, E., Pines, M., Antonopoulou, I., Morriss-Kay, G. M., & Lonai, P. (2002). The *Il1c* alternative of *Fgfr2* is a positive regulator of bone formation. *Development*, *129*(16), 3783-3793.

Evans, D. J., & Noden, D. M. (2006). Spatial relations between avian craniofacial neural crest and paraxial mesoderm cells. *Developmental Dynamics*, *235*(5), 1310-1325.

Fletcher, R. B., & Harland, R. M. (2008). The role of FGF signaling in the establishment and maintenance of mesodermal gene expression in *Xenopus*. *Developmental Dynamics*, *237*(5), 1243-1254.

Folkman, J., Shing, Y., Sullivan, R., Butterfield, C., Murray, J., & Klagsbrun, M. (1984). Heparin affinity-purification of a tumor derived capillary endothelial cell growth factor. *Science*, *223*, 1296-1300.

Franz-Odenaal, T. A. (2008). Toward understanding the development of scleral ossicles in the chicken, *Gallus*. *Developmental Dynamics*, *237*, 3240-3251

Franz-Odenaal, T. A. (2010). Induction and patterning of intramembranous bone. *Frontiers in Bioscience (Landmark Edition)*, *16*, 2734-2746.

Franz-Odenaal, T. A., & Vickaryous, M. K. (2006). Skeletal elements in the vertebrate eye and adnexa: morphological and developmental perspectives. *Developmental Dynamics*, *235*(5), 1244-1255.

Franz-Odenaal, T. A., Hall, B. K., & Witten, P. E. (2006). Buried alive: how osteoblasts become osteocytes. *Developmental Dynamics*, 235(1), 176-190.

Fyfe, D. M., & Hall, B. K. (1983). The origin of the ectomesenchymal condensations which precede the development of the bony scleral ossicles in the eyes of embryonic chicks. *Journal of Embryology and Experimental Morphology*, 73, 69-86.

Gilbert, S.F. (2000). *Developmental biology* (6th Ed.). Sinauer Associates. Sunderland, MA.

Goetz, R., Beenken, A., Ibrahimi, O. A., Kalinina, J., Olsen, S. K., Eliseenkova, A. V., ... & Yu, X. (2007). Molecular insights into the klotho-dependent, endocrine mode of action of fibroblast growth factor 19 subfamily members. *Molecular and Cellular Biology*, 27(9), 3417-3428.

Greenwald, J. A., Mehrara, B. J., Spector, J. A., Warren, S. M., Fagenholz, P. J., Smith, L. P., ... & Longaker, M. T. (2001). *In vivo* modulation of FGF biological activity alters cranial suture fate. *The American Journal of Pathology*, 158(2), 441-452.

Gross, J. B., & Hanken, J. (2008). Review of fate-mapping studies of osteogenic cranial neural crest in vertebrates. *Developmental Biology*, 317(2), 389-400.

Guo, X., & Wang, X. F. (2009). Signaling cross-talk between TGF- β /BMP and other pathways. *Cell Research*, 19(1), 71-88.

- Hajihosseini, M. K., & Heath, J. K. (2002). Expression patterns of fibroblast growth factors-18 and -20 in mouse embryos is suggestive of novel roles in calvarial and limb development. *Mechanism of Development, 113*, 79-83.
- Hall, B. K. (1975). Evolutionary consequences of skeletal differentiation. *American Zoologist, 15*(2), 329-350.
- Hall, B.K. (2005). Bones and Cartilage: developmental and evolutionary skeletal biology. Elsevier (USA) Ltd. San Diego, CA.
- Hall, B. K. (1981). Specificity in the differentiation and morphogenesis of neural crest-derived scleral ossicles and of epithelial scleral papillae in the eye of the embryonic chick. *Journal of Embryology and Experimental Morphology, 66*, 175-190.
- Hall, B. K., & Miyake, T. (1992). The membranous skeleton: the role of cell condensations in vertebrate skeletogenesis. *Anatomy and Embryology, 186*(2), 107-124.
- Hall, B. K., & Miyake, T. (1995). Divide, accumulate, differentiate: cell condensation in skeletal development revisited. *International Journal of Developmental Biology, 39*(6), 881-893.
- Hall, B. K., & Miyake, T. (2000). All for one and one for all: condensations and the initiation of skeletal development. *BioEssays, 22*(2), 138-147.
- Hamburger, V., & Hamilton, H. L. (1951). A series of normal stages in the development of the chick embryo. *Journal of Morphology, 88*(1), 49-92.

Hammer, C. L. (2016). Investigating the development of chick conjunctival papillae and scleral ossicles following hydrocortisone injections. M.Sc. Thesis. Saint Mary's University.

Hanafusa, H., Torii, S., Yasunaga, T., & Nishida, E. (2002). Sprouty1 and Sprouty2 provide a control mechanism for the Ras/MAPK signalling pathway. *Nature Cell Biology*, 4(11), 850-858.

Haÿ, E., Marie, P. J., & Debiais, F. (2002). Regulation of human cranial osteoblast phenotype by FGF-2, FGFR-2 and BMP-2 signaling. *Histology and Histopathology*, 17(3), 877-885.

Hecht, J. T., & Francomano, L Z, C. A. (1995). A recurrent mutation in the tyrosine kinase domain of fibroblast growth factor receptor 3 causes hypochondroplasia. *Nature Genetics*, 10.

Horakova, D., Cela. P., Krejci, P., Balek, L., Balkova, S. M., Matalova, E. & Buchtova, M. (2014). Effect of FGFR inhibitors on chick limb development. *Development, Growth and Differentiation*, 56, 555-572.

Huret, J. L. (2009). FGFR1 (fibroblast growth factor receptor 1). *Atlas Genetics and Cytogenetics in Oncology and Haematology*, 13(11), 821-840.

Iseki, S., Wilkie, A. O., & Morriss-Kay, G. M. (1999). Fgfr1 and Fgfr2 have distinct differentiation-and proliferation-related roles in the developing mouse skull vault. *Development*, 126(24), 5611-5620.

Itoh, N., & Ornitz, D. M. (2004). Evolution of the Fgf and Fgfr gene families. *Trends in Genetics*, 20(11), 563-569.

Jabalee, J. P. (2014). The role of vasculature during the development of intramembranous bones of the chick, *Gallus gallus*. M.Sc. Thesis. Dalhousie University.

Jabalee, J., Hillier, S., & Franz-Odenaal, T. A. (2013). An investigation of cellular dynamics during the development of intramembranous bones: the scleral ossicles. *Journal of Anatomy*, 223(4), 311-320.

Jacob, A. L., Smith, C., Partanen, J., & Ornitz, D. M. (2006). Fibroblast growth factor receptor 1 signaling in the osteo-chondrogenic cell lineage regulates sequential steps of osteoblast maturation. *Developmental Biology*, 296(2), 315-328.

Jourdeuil, K., & Franz-Odenaal, T. A. (2016). Gene expression analysis during the induction and patterning of the conjunctival papillae in the chick embryonic eye. *Gene Expression Patterns*, 22(1), 30-36.

Jourdeuil, K., & Franz-Odenaal, T. A. (2017). A wide temporal window for conjunctival papillae development ensures the formation of a complete sclerotic ring. *Developmental Dynamics*, 246(5), 381-391.

Katahira, T., & Nakamura, H. (2003). Gene silencing in chick embryos with a vector-based small interfering RNA system. *Development, Growth & Differentiation*, 45(4), 361-367.

Katoh, M. (2009). FGFR2 (fibroblast growth factor receptor 2). *Atlas Genetics and Cytogenetics in Oncology and Haematology*, 13(7), 477-482.

Kawakami, Y., Esteban, C. R., Matsui, T., Rodríguez-León, J., Kato, S., & Belmonte, J. C. I. (2004). Sp8 and Sp9, two closely related buttonhead-like transcription factors, regulate Fgf8 expression and limb outgrowth in vertebrate embryos. *Development*, 131(19), 4763-4774.

Kettunen, P., Karavanova, I., & Thesleff, I. (1998). Responsiveness of developing dental tissues to fibroblast growth factors: Expression of splicing alternatives of FGFR1, -2, -3, and of FGFR4; and stimulation of cell proliferation by FGF-2, -4, -8, and -9. *Development Genetics*, 22, 374-385.

Kettunen, P., Laurikkala, J., Itäranta, P., Vainio, S., Itoh, N., & Thesleff, I. (2000). Association of FGF-3 and FGF-10 with signalling networks regulating tooth morphogenesis. *Development Dynamics*, 219, 322-332.

Kim, H.-J., Rice, D. P. C., Kettunen, P. J., & Thesleff, I. (1998). FGF-, BMP- and Shh-mediated signalling pathways in the regulation of cranial suture morphogenesis and calvarial bone development. *Development*, 125, 1241-1251.

Kimonis, V., Gold, J. A., Hoffman, T. L., Panchal, J., & Boyadjiev, S. A. (2007). Genetics of craniosynostosis. In *Seminars In Pediatric Neurology* 14(3), 150-161, WB Saunders.

Laufer, E., Nelson, C. E., Johnson, R. L., Morgan, B. A., & Tabin, C. (1994). Sonic hedgehog and Fgf-4 act through a signaling cascade and feedback loop to integrate growth and patterning of the developing limb bud. *Cell*, *79*(6), 993-1003.

Lee, S. H., Schloss, D. J., & Swain, J. L. (2000). Maintenance of vascular integrity in the embryo requires signaling through the fibroblast growth factor receptor. *Journal of Biological Chemistry*, *275*(43), 33679-33687.

Lewandoski, M., Sun, X., & Martin, G. R. (2000). Fgf 8 signalling from the AER is essential for normal limb development. *Nature Genetics*, *29*, 460-463.

Lin, C. M., Jiang, T. X., Widelitz, R. B., & Chuong, C. M. (2006). Molecular signaling in feather morphogenesis. *Current Opinion in Cell Biology*, *18*(6), 730-741

Long, F. (2012). Building strong bones: molecular regulation of the osteoblast lineage. *Nature reviews Molecular cell biology*, *13*(1), 27-38.

Mandler, M., & Neubuser, A. (2004). FGF signaling is required for initiation of feather placode development. *Development*, *131*(14), 3333-3343.

McCloy, R. A., Rogers, S., Caldon, C. E., Lorca, T., Castro, A., & Burgess, A. (2014). Partial inhibition of Cdk1 in G2 phase overrides the SAC and decouples mitotic events. *Cell Cycle*, *13*(9), 1400-1412.

Miki, T., Bottaro, D. P., Fleming, T. P., Smith, C. L., Burgess, W. H., Chan, A. M., & Aaronson, S. A. (1992). Determination of ligand-binding specificity by alternative

splicing: two distinct growth factor receptors encoded by a single gene. *Proceedings of the National Academy of Sciences*, 89(1), 246-250.

Mohammadi, M., Olsen, S. K., & Goetz, R. (2005). A protein canyon in the FGF–FGF receptor dimer selects from an a la carte menu of heparan sulfate motifs. *Current Opinion In Structural Biology*, 15(5), 506-516.

Murakami, M., & Simons, M. (2008). Fibroblast growth factor regulation of neovascularization. *Current opinion in hematology*, 15(3), 215.

Murray, P. D. (1943). The development of the conjunctival papillae and of the scleral bones in the embryo chick. *Journal of Anatomy*, 77(Pt 3), 225-240.

Nicholson, K. M., & Anderson, N. G. (2002). The protein kinase B/Akt signalling pathway in human malignancy. *Cellular Signalling*, 14, 381-395.

Nickel, J. C. (1999). Textbook of prostatitis. ISIS Medical Media. CRC Press. UK.

Nishita, J., Ohta, S., Bleyl, S. B., & Schoenwolf, G. C. (2011). Detection of isoform-specific fibroblast growth factor receptors by whole-mount in situ hybridization in early chick embryos. *Developmental Dynamics*, 240(6), 1537-1547.

Noji, S., Koyama, E., Myokai, F., Nohno, T., Ohuchi, H., Nishikawa, K., & Taniguchi, S. (1993). Differential expression of three chick FGF receptor genes, FGFR1, FGFR2 and FGFR3, in limb and feather development. *Progress in Clinical and Biological Research*, 383, 645-654.

Noramly, S., Freeman, A., & Morgan, B. A. (1999). Beta-catenin signaling can initiate feather bud development. *Development*, *126*(16), 3509-3521.

Nutt, S. L., Dingwell, K. S., Holt, C. E., & Amaya, E. (2001). *Xenopus* Sprouty2 inhibits FGF-mediated gastrulation movements but does not affect mesoderm induction and patterning. *Genes & Development*, *15*(9), 1152–1166.

Ohbayashi, N., Shibayama, M., Kurotaki, Y., Imanishi, M., Fujimori, T., Itoh, N., & Takada, S. (2002). FGF18 is required for normal cell proliferation and differentiation during osteogenesis and chondrogenesis. *Genes and Development*, *16*, 870-879.

Ohuchi, H., Nakagawa, T., Yamamoto, A., Araga, A., Ohata, T., Ishimaru, Y. ,... & Noji, S. (1997). The mesenchymal factor, FGF10, initiates and maintains the outgrowth of the chick limb bud through interaction with FGF8, an apical ectodermal factor. *Development*, *124*, 2295-2244.

Olsen, S. K., Ibrahimi, O. A., Raucci, A., Zhang, F., Eliseenkova, A. V., Yayon, A., ... & Mohammadi, M. (2004). Insights into the molecular basis for fibroblast growth factor receptor autoinhibition and ligand-binding promiscuity. *Proceedings of the National Academy of Sciences of the United States of America*, *101*(4), 935-940.

Ornitz, D. M., & Itoh, N. (2001). Fibroblast growth factors. *Genome Biology*, *2*(3), 3005.3001 - 3005.3012.

Ornitz, D. M., & Itoh, N. (2015). The fibroblast growth factor signaling pathway. *Wiley Interdisciplinary Reviews: Developmental Biology*, *4*(3), 215-266

Ornitz, D. M., & Marie, P. J. (2002). FGF signaling pathways in endochondral and intramembranous bone development and human genetic disease. *Genes & Development, 16*(12), 1446-1465.

Otrock, Z. K., Mahfouz, R. A., Makarem, J. A., & Shamseddine, A. I. (2007). Understanding the biology of angiogenesis: review of the most important molecular mechanisms. *Blood Cells, Molecules, and Diseases, 39*(2), 212-220.

Palmoski, M. J., & Goetinck, P. F. (1970). An analysis of the development of conjunctival papillae and scleral ossicles in the eye of the scaleless mutant. *Journal of Experimental Zoology Part A: Ecological Genetics and Physiology, 174*(2), 157-164.

Peters, K. G., Werner, S., Chen, G., & Williams, L. T. (1992). Two FGF receptor genes are differentially expressed in epithelial and mesenchymal tissues during limb formation and organogenesis in the mouse. *Development, 114*(1), 233-243.

Pinto, C. B., & Hall, B. K. (1991). Toward an understanding of the epithelial requirement for osteogenesis in scleral mesenchyme of the embryonic chick. *Journal of Experimental Zoology Part A: Ecological Genetics and Physiology, 259*(1), 92-108.

Polanska, U. M., Fernig, D. G., & Kinnunen, T. (2009). Extracellular interactome of the FGF receptor-ligand system: complexities and the relative simplicity of the worm. *Developmental Dynamics, 238*(2), 277-293.

Porntaveetus, T., Otsuka-Tanaka, Y., Basson, M. A., Moon, A. M., Sharpe, P. T., & Ohazama, A. (2011). Expression of fibroblast growth factors (Fgfs) in murine tooth development. *Journal of Anatomy*, *218*(5), 534-543, .

Pownall, M.E. & Isaacs, H.V. (2010). FGF Signalling in Vertebrate Development. Morgan & Claypool Life Sciences. San Rafael, CA.

Revest, J. M., DeMoerlooze, L., & Dickson, C. (2000). Fibroblast growth factor 9 secretion is mediated by a non-cleaved amino-terminal signal sequence. *Journal of Biological Chemistry*, *275*(11), 8083-8090.

Rice, D.P., Aberg, T., Chan, Y., Tang, Z., Kettunen, P.J., Pakarinen, L., Maxson, R.E., Thesleff, I. (2000). Integration of FGF and TWIST in calvarial bone and suture development. *Development*, *127*(9), 1845–1855.

Santagati, F., & Rijli, F. M. (2003). Cranial neural crest and the building of the vertebrate head. *Nature Reviews Neuroscience*, *4*(10), 806-818.

Sanz-Ezquerro, J. J., & Tickle, C. (2003). Fgf signaling controls the number of phalanges and tip formation in developing digits. *Current biology*, *13*(20), 1830-1836.

Sarabipour, S., & Hristova, K. (2016). Mechanism of FGF receptor dimerization and activation. *Nature Communications*, *7*, 10262.

Sasaki, A., Taketomi, T., Kato, R., Saeki, K., Nonami, A., Sasaki, M., ... & Yoshimura, A. (2003). Mammalian Sprouty4 suppresses Ras-independent ERK activation by binding to Raf1. *Nature cell biology*, 5(5), 427-432.

Sato, T., & Nakamura, H. (2004). The Fgf8 signal causes cerebellar differentiation by activating the Ras-ERK signaling pathway. *Development*, 131(17), 4275-4285.

Scherz, P. J., Harfe, B. D., McMahon, A. P., & Tabin, C. J. (2004). The limb bud Shh-Fgf feedback loop is terminated by expansion of former ZPA cells. *Science*, 305(5682), 396-399.

Schlessinger, J., Plotnikov, A. N., Ibrahimi, O. A., Eliseenkova, A. V., Yeh, B. K., Yayon, A., ... & Mohammadi, M. (2000). Crystal structure of a ternary FGF-FGFR-heparin complex reveals a dual role for heparin in FGFR binding and dimerization. *Molecular cell*, 6(3), 743-750.

Seghezzi, G., Patel, S., Ren, C. J., Gualandris, A., Pintucci, G., Robbins, E. S., ... & Mignatti, P. (1998). Fibroblast growth factor-2 (FGF-2) induces vascular endothelial growth factor (VEGF) expression in the endothelial cells of forming capillaries: an autocrine mechanism contributing to angiogenesis. *The Journal of cell biology*, 141(7), 1659-1673.

Sekine, K., Ohuchi, H., Fujiwara, M., Yamasaki, M., Yoshizawa, T., Sato, T., ... & Kato, S. (1999). Fgf 10 is essential for limb and lung formation. *Nature Genetics*, 21, 138-141.

Sivak, J. M., Petersen, L. F. & Amaya, E. (2005). FGF signal interpretation is directed by Sprouty and Spred proteins during mesoderm formation. *Developmental Cell*, 8(5), 689-701

Song, H. K., Lee, S. H., & Goetinck, P. F. (2004). FGF-2 signaling is sufficient to induce dermal condensations during feather development. *Developmental Dynamics*, 231(4), 741-749. doi: 10.1002/dvdy.20243

Song, H., Wang, Y., & Goetinck, P. F. (1996). Fibroblast growth factor 2 can replace ectodermal signalling for feather development. *Proceedings of the National Academy of Science of the United States of America*, 93(19), 10246-10249

Sun, X., Mariani, F. V., & Martin, G. R. (2002). Functions of FGF signalling from the apical ectodermal ridge in limb development. *Nature*, 418, 501-508.

Superti-Furga, A., Steinmann, B., Gitzelmann, R., Eich, G., Giedion, A., Bucher, H. U., & Wissler, J. (1995). A glycine 375-to-cysteine substitution in the transmembrane domain of the fibroblast growth factor receptor-3 in a newborn with achondroplasia. *European Journal of Pediatrics*, 154(3), 215-219.

Tanaka, Y., Okada, Y., & Hirokawa, N. (2005). FGF-induced vesicular release of Sonic hedgehog and retinoic acid in leftward nodal flow is critical for left–right determination. *Nature*, 435(7039), 172-177.

Taoa, H., Yoshimotoa, Y., Yoshiokaa, H., Nohnob, T., Nojia, S., & Ohuchia, H. (2002).

FGF10 is a mesenchymally derived stimulator for epidermal development in the chick embryonic skin. *Mechanisms of Development*, 116, 39-49.

Thisse, B., & Thisse, C. (2005). Functions and regulations of fibroblast growth factor signaling during embryonic development. *Developmental Biology*, 287(2), 390-402.

Tirosh-Finkel, L., Zeisel, A., Brodt-Ivenshitz, M., Shamai, A., Yao, Z., Seger, R., ... & Tzahor, E. (2010). BMP-mediated inhibition of FGF signaling promotes cardiomyocyte differentiation of anterior heart field progenitors. *Development*, 137(18), 2989-3000.

Toledo, L. M., Lydon, N. B., & Elbaum, D. (1999). The structure-based design of ATP-site directed protein -kinase inhibitors. *Current Medicinal Chemistry*, 6(2), 775-805.

Tomlinson, D. C., L'Hôte, C. G., Kennedy, W., Pitt, E., & Knowles, M. A. (2005).

Alternative Splicing of Fibroblast Growth Factor Receptor 3 Produces a Secreted Isoform That Inhibits Fibroblast Growth Factor–Induced Proliferation and Is Repressed in Urothelial Carcinoma Cell Lines. *Cancer research*, 65(22), 10441-10449.

Torii, S., Kusakabe, M., Yamamoto, T., Maekawa, M., & Nishida, E. (2004). Sef is a spatial regulator for Ras/MAP kinase signaling. *Developmental cell*, 7(1), 33-44.

Ueda, Y., Hirai, S.-I., Osada, S.-I., Suzuki, A., Mizuno, K., & Ohno, S. (1996). Protein kinase C activates the MEK-ERK pathway in a manner independent of Ras and dependent on Raf. *The Journal of Biological Chemistry*, 271(38), 23512-23519

Väänänen, H. K., Zhao, H., Mulari, M., & Halleen, J. M. (2000). The cell biology of osteoclast function. *Journal of Cell Science*, *113*(Pt 3), 377-381.

Valverde-Franco, G., Liu, H., Davidson, D., Chai, S., Valderrama-Carvajal, H., Goltzman, D., ... & Henderson, J. E. (2004). Defective bone mineralization and osteopenia in young adult *FGFR3*^{-/-} mice. *Human molecular genetics*, *13*(3), 271-284.

Vidrich, A., Buzan, J. M., Ilo, C., Bradley, L., Skaar, K., & Cohn, S. M. (2004). Fibroblast growth factor receptor-3 is expressed in undifferentiated intestinal epithelial cells during murine crypt morphogenesis. *Developmental dynamics*, *230*(1), 114-123.

Wells, K. L., Hadad, Y., Ben-Avraham, D., Hillel, J., Cahaner, A., & Headon, D. J. (2012). Genome-wide SNP scan of pooled DNA reveals nonsense mutation in *FGF20* in the scaleless line of featherless chickens. *BMC Genomics*, *13*, 257.

Werner, S., Weinberg, W., Liao, X. I. A. N. G., Peters, K. G., Blessing, M., Yuspa, S. H., ... & Williams, L. T. (1993). Targeted expression of a dominant-negative FGF receptor mutant in the epidermis of transgenic mice reveals a role of FGF in keratinocyte organization and differentiation. *The EMBO Journal*, *12*(7), 2635.

Widelitz, R. B., Jiang, T. X., Chen, C. W., Stott, N. S., & Chuong, C. M. (1999). Wnt-7a in feather morphogenesis: involvement of anterior-posterior asymmetry and proximal-distal elongation demonstrated with an in vitro reconstitution model. *Development*, *126*(12), 2577-2587.

Wilson, S. E., He, Y. G., Weng, J., Zieske, J. D., Jester, J. V., & Schultz, G. S. (1994). Effect of epidermal growth factor, hepatocyte growth factor, and keratinocyte growth factor, on proliferation, motility and differentiation of human corneal epithelial cells. *Experimental Eye Research*, 59(6), 665-678.

Wolpert, L. (1998). Pattern formation in epithelial development: the vertebrate limb and feather bud spacing. *Philosophical Transactions of the Royal Society of London. Series B, Biological Sciences*, 353(1370), 871-875.

Xu, X., Weinstein, M., Li, C., Naski, M., Cohen, R. I., Ornitz, D. M., ... & Deng, C. (1998). Fibroblast growth factor receptor 2 (FGFR2)-mediated reciprocal regulation loop between FGF8 and FGF10 is essential for limb induction. *Development*, 125(4), 753-765.

Yanai, M., Tatsumi, N., Hasunuma, N., Katsu, K., Endo, F., & Yokouchi, Y. (2008). FGF signaling segregates biliary cell-lineage from chick hepatoblasts cooperatively with BMP4 and ECM components in vitro. *Developmental Dynamics*, 237(5), 1268-1283.

Yoon, B. S., Pogue, R., Ovchinnikov, D. A., Yoshii, I., Mishina, Y., Behringer, R. R., & Lyons, K. M. (2006). BMPs regulate multiple aspects of growth-plate chondrogenesis through opposing actions on FGF pathways. *Development*, 133(23), 4667-4678.

Yu, K., Xu, J., Liu, Z., Sasic, D., Shao, J., Olson, E. N., ... & Ornitz, D. M. (2003). Conditional inactivation of FGF receptor 2 reveals an essential role for FGF signaling in the regulation of osteoblast function and bone growth. *Development*, 130(13), 3063-3074.

Yu, P., Wilhelm, K., Dubrac, A., Tung, J. K., Alves, T. C., Fang, J. S., ... & Zhang, J. (2017).

FGF-dependent metabolic control of vascular development. *Nature*, 545(7653), 224-228.

Zhang, D., Ighaniyan, S., Stathopoulos, L., Rollo, B., Landman, K., Hutson, J., Newgreen,

D. (2014). The neural crest: A versatile organ system. *Birth Defects Research Part C:*

Embryo Today: Reviews, 102(3), 275-298.

Zhang, X., Ibrahimi, O. A., Olsen, S. K., Umemori, H., Mohammadi, M., & Ornitz, D. M.

(2006). Receptor specificity of the fibroblast growth factor family. The complete

mammalian fgf family. *Journal of Biological Chemistry*, 281(23), 15694-15700.

Zhao, Y., & Zhang, Z. Y. (2001). The mechanism of dephosphorylation of extracellular

signal-regulated kinase 2 by mitogen-activated protein kinase phosphatase 3. *Journal of*

Biological Chemistry, 276(34), 32382-32391.

Appendix A: Protocols

Appendix A1: Chick Alkaline Phosphatase Staining Protocol:

Collection of embryos:

1. Fix embryo head at desired stage overnight at 4°C in 4% PFA made in 1x PBS
2. Next day, wash 3 times in 1xPBS for 15mins each at room temperature and store at 4°C until needed for staining

Alkaline phosphatase staining:

1. Dissect the heads into half and remove the eyelid and nictitating membrane
2. Place dissected heads in glass vials and wash 3 times in distilled water for 15mins each at room temperature
3. Place heads in Tris- Maleate Buffer (pH8.3) for 1 hour at room temperature
 - While waiting, make AP substrate solution (make in glass vial, in fume hood, in dark)
4. Place heads in AP substrate solution for 1 hour at room temperature
5. Wash heads 3 times in saturated sodium borate water for 15 mins each at room temperature
6. Place heads overnight in 3% bleach solution at room temperature
7. In the morning, process embryos to 80% glycerol in 1%KOH at room temperature
 - 1 hour in 25%/75% glycerol in 1%KOH
 - 1 hour in 50%/50% glycerol in 1%KOH

- Store in 80%/20% glycerol in 1%KOH at 4°C

Solution compositions:

4% Paraformaldehyde (PFA) – 500ml

20g PFA (Sigma, P6148)

Add 450mL 1x PBS, add one NaOH pellet (Sigma, S5881) and dissolve over heated stir plate in fume hood

pH to 7.4 and top up to 500ml with 1xPBS

Aliquot and store in -20°C

Tris-Maleate Buffer (pH8.3) – 100ml:

2.24g Tris Base (Roche, 03 118 142001)

2.2g Maleic Acid (Sigma, M0375)

70ml dH₂O

pH to 8.3 with NaOH, top up to 100ml with dH₂O

1% KOH – 100ml

1g Potassium hydroxide (Sigma, 221473)

100ml dH₂O

Saturated Sodium Borate Water – 100ml:

5g Sodium tetraborate decahydrate (Sigma, B9876)

100ml dH₂O

Alkaline phosphate substrate solution (make in dark glass vial in the fume hood):

0.01g Naphthol-AS-TR-phosphate (Sigma, N6125)

0.008g Fast Blue (Sigma, D9805)

1ml N,N dimethyl formamide (Sigma, 319937)

10ml Tris Maleate buffer

3% bleach solution – 20ml:

2ml 3% hydrogen peroxide (Pharmasave, commercial drug store)

18ml 1% KOH

25% glycerol in 1% KOH – 50ml:

12.5ml glycerol (VWR, CABDH1172)

37.5ml 1%KOH

50% glycerol in 1% KOH – 50ml:

25ml glycerol

25ml 1% KOH

80% glycerol in 1% KOH – 50ml:

40ml glycerol

10ml 1% KOH

Appendix A2: Alcian Blue Cartilage Staining:

1. Fix embryo wings in 4% PFA at 4°C for 1hour
2. Wash 3x15mins in dH₂O
3. Dehydrate in 70% EtOH for 1hour at room temperature
4. Stain in Alcian blue overnight at room temperature
5. Serially rehydrate stained limbs:
 - 1 hour at room temperature in 100% EtOH
 - 1 hour at room temperature in 80% EtOH
 - 1 hour at room temperature in 60% EtOH
 - 1 hour at room temperature in 40% EtOH
 - 1 hour at room temperature in 20% EtOH
 - 1 hour at room temperature in dH₂O
6. Remove excess stain by leaving limbs in 1% trypsin in saturate sodium borate for 5-6 hours at room temperature
7. Wash 3x15mins in 1xPBS
8. Store in 4°C

Solution Composition:

Alcian Blue stain – 100ml:

20ml 99.7% acetic acid (Fisher Scientific, A38212)

80ml 95% EtOH

10mg Alcian Blue (Sigma, A3157)

1% Trypsin in saturated sodium borate – 30ml:

0.3g trypsin (Fisher Scientific, T6146)

30ml saturated sodium borate

Appendix A3: Preparing LB Broth and Agar Plates

LB Broth – 100ml:

2.5g LB (BD, 244620)

100ml dH₂O

Dissolve in flask, cover with foil, autoclave and store in 4°C once cool

Agar Plates (6):

6.25g LB

3.75g Agar (BD, 214530)

250ml dH₂O

1. Heat and stir in flask until dissolved. Cover the flask with foil and autoclave
2. Once cool, add 0.0025g ampicillin (Sigma, A6140)
3. Pour solution into petri plates and allow to solidify.
4. Once solidified, parafilm the plates and store upside down in 4°C

Appendix A4: Removing Plasmids from Filter Paper:

1. Using forceps and lab scissors (clean first with 70% EtOH and let dry) cut around the area on filter paper that contains the plasmid
2. Place the cut out piece of filter paper containing plasmid in a 1.5ml sterile Eppendorf tube
3. Add 100ul of TE buffer (pH8.0) to the tube
4. Let sit for 5mins at room temperature
5. Vortex, then centrifuge at 3000rpm for 1min
6. Let sit for 30mins at room temperature
7. Remove filter from tube using a pair of blunt forceps (clean first with 70% EtOH and let dry) and place in new sterile Eppendorf tube
8. Store both tubes in -20°C

Solution composition:

TE Buffer (pH8.0) – 50ml:

0.5ml 1M Tris-HCl

0.1ml 0.5M EDTA (Sigma, E5134)

40ml DepC H₂O

pH to 8.0 and top up to 50ml with DepC H₂O

Appendix A5: Cloning:

The day before cloning, chill plastic Nalgene tubes and pipette tips overnight.

DAY 1:

1. Remove competent *E.Coli* cells (Promega, L1011) from -80°C and place on ice until thawed
2. Using chilled pipette tips, gently mix cells and transfer $100\mu\text{L}$ into chilled Nalgene tubes
3. In experiment tubes, add $10\mu\text{L}$ of DNA from filter and into control tube, add $10\mu\text{L}$ of TE buffer
4. Put tubes on ice for 10-20mins
5. Heat shock tubes for 45secs in 42°C water bath
6. Place tubes on ice for 2min
7. To each tube, add $900\mu\text{L}$ of cold LB broth and incubate for 1hr at 37°C with shaking at 145-185rpm
8. Dispense $100\mu\text{L}$ /plate on to agar plates and spread by streaking
9. Incubate overnight at 37°C

DAY 2:

1. Flame the edge of flask containing LB broth as well as autoclaved glass tubes
2. Pour a small amount of LB broth into the glass tubes (use one tube per plate)
3. Using a autoclaved plastic pipette tip, scrape up an isolated colony

4. Throw tip into the tube and plug tube using a ball of sterile cotton
5. Incubate tubes overnight at 37°C with shaking at 145rpm

DAY 3 (mini-preparation):

1. Transfer 2ml of the overnight culture into a 2ml Eppendorf tube
2. Centrifuge at 13000rpm for 1min, repeat twice for increased pellet size
3. Discard the supernatant and add 250µL of cold buffer + 0.82µL of RNase A (Sigma, R4642)
4. Resuspend the pellet by dragging tubes over a rack, solution should be homogenous with no visible clumps
5. Add 250µL cold lysis solution, mix by inverting three times and place on ice for 5mins
6. Add 250µL cold KAc, mix by inverting three times and let settle on ice for 5mins
7. Centrifuge at 13000rpm for 5min
8. Pour supernatant into new Eppendorf tube and discard the white pellet
9. Add 200µL phenol-chloroform and shake for 30secs
10. Centrifuge 13000rpm for 5mins
11. Remove top layer with a pipette and dispense into a new tube, discard bottom layer
12. Add equal volumes of isopropanol, mix and let stand for 5mins at room temperature
13. Centrifuge at 13000rpm for 5mins

14. Discard the supernatant and add 200 μ L cold 95% EtOH, dislodge pellet and invert tube
15. Centrifuge at 13000rpm for 5mins
16. Discard supernatant and keep the pellet
17. Allow tube to completely bench dry
18. Re-suspend pellet in 50 μ L SuperQ H₂O

For long-term storage of remaining overnight culture, mix equal volumes of culture in 50% glycerol and store in -80°C

Solution composition:

Cold Buffer (pH8.0) – 1ml:

50 μ L 1M Tris-HCl (pH8.0)

10 μ L 1M EDTA

940 μ L dH₂O

Cold Lysis Buffer -1ml:

100 μ L 2M NaCl (Sigma, S9888)

100 μ L 10% SDS (Sigma, L4390)

800 μ L dH₂O

Potassium Acetate:

3.75ml 5M KAc (Sigma, P1191)

0.7ml glacial acetic acid

1.7ml dH₂O

95% EtOH – 1ml:

950µL 100% EtOH

50µL dH₂O

Appendix A6: Restriction Digestion and Clean-up of Plasmid:

Restriction Digestion:

1. In a sterile Eppendorf tube create a reaction mix as follow:

Component	Volume (μL)
Plasmid from miniprep	5
NCol restriction endonuclease	1.5
10x buffer (endonuclease SH)	5
DepC H ₂ O	38.5
Total	50

2. Incubate at 37°C overnight
3. Heat inactivate overnight digest in 65°C for 15mins

Clean-up of digest

High-Pure PCR product purification kit (Roche-11 732) was used to clean up the digest

1. To the 50 μL digest, add 50 μL of DepC H₂O
2. Add 500 μL of binding buffer to the digest and spin briefly to mix
3. Attach one filter tube to one collection tube and transfer digest into the Roche filter tube

4. Centrifuge at 13000 rpm for 1min, discard the flow through and reconnect the filter to the collection tube
5. Add 500 μ L of wash buffer to the filter and centrifuge at 13000 rpm for 1min
6. Discard the flow through, add 200 μ L of wash buffer to the filter and centrifuge at 13000 rpm for 1min
7. Discard the flow through, connect the filter to a sterile Eppendorf tube (elution 1 - E1) and add 30 μ L of warm elution buffer
8. Centrifuge at 13000rpm for 1min
9. Connect the filter to a sterile Eppendorf tube (elution 2 - E2) and add 30 μ L of warm elution buffer
10. Centrifuge at 13000 rpm for 1min
11. Store both E1 and E2 at -20°C

Appendix A7: Polymerase Chain Reaction:

1. In a sterile Eppendorf tube make a master mix as the following:

Component	Volume (μL)
5x reaction buffer	10
dNTP mix	1
M13 forward primer	2.81
M13 reverse primer	2.81
Taq Polymerase	0.25
DepC H ₂ O	32.63
Total	49.5

2. To the tube, add 0.5 μL of the template DNA
3. Spin briefly to mix and run in PCR machine under the following conditions:

Step	Temperature ($^{\circ}\text{C}$)	Time
Lid	95	∞
Pre-denaturation	95	30 secs
Denaturation	59	20 secs
Annealing	46.5	40 secs
Elongation	68	12 secs
Final Elongation	68	5 mins
Cooling and store	4	∞

35X {

4. Store tube at -20°C

PCR Product Clean-up

High-Pure PCR product purification kit (Roche-11 732) was used to clean up the digest

1. To the 50µL PCR product, add 50µL of DepC H₂O
2. Add 500µL of binding buffer to the PCR product and spin briefly to mix
3. Attach one filter tube to one collection tube and transfer PCR product into the filter tube
4. Centrifuge at 13000rpm for 1min, discard the flow through and reconnect the filter to the collection tube
5. Add 500µL of wash buffer to the filter and centrifuge at 13000rpm for 1min
6. Discard the flow through, add 200µL of wash buffer to the filter and centrifuge at 13000rpm for 1min
7. Discard the flow through, connect the filter to a sterile Eppendorf tube (elution 1 - E1) and add 30µL of warm elution buffer
8. Centrifuge at 13000rpm for 1min
9. Connect the filter to a sterile Eppendorf tube (elution 2 - E2) and add 30µL of warm elution buffer
10. Centrifuge at 13000rpm for 1min
11. Store both E1 and E2 at -20°C

Appendix A8: RNA Probe Synthesis:

Probes were constructed using DIG-RNA labelling kit (Roche -11 175 029 10)

1. Add 1µg of template DNA to a sterile RNase free Eppendorf tube
2. Add enough DepC H₂O to make a total volume of 13µL
3. To each of the tubes add the following:
 - 2µL 10x DIG labelling mix
 - 2µL 10x transcription buffer
 - 1µL protector RNase inhibitor
 - 2µL RNA polymerase T7 (for FGFR1c, 2b, 2c, 3b and 3c) or RNA polymerase Sp6 (for FGFR1b)
4. Mix gently and incubate for 2hrs at 37°C
5. Add 2µL of DNaseI recombinant RNase free to remove template DNA
6. Incubate for 15mins at 37°C
7. Stop the reaction by adding 2µL of 0.2M EDTA (pH8.0)
8. Store 1µL of the probe in a new 0.2ml Eppendorf tube (this will be used for Dot Blot)
9. Store both tubes in -20°

Appendix A9: DIG-High Prime Labelling and Detection Protocol (Dot Blot):

1. Using 1 μ L of the RNA probe and a control labelled RNA (provided in the DIG-RNA labelling kit) create a dilution series as follows:

Tube	RNA (μL)	From Tube (μL)	Dilution Buffer (μL)	Final RNA concentration
1	1	-	40.6	10ng/ μ L
2	2	1	18	1ng/ μ L
3	2	2	198	10pg/ μ L
4	15	3	35	3pg/ μ L
5	5	3	45	1pg/ μ L

2. Place a 1 μ L blot of RNA probe from each of tubes in the dilution series onto a nitrocellulose membrane (Roche-11 209 299 001)
3. Place the membrane in a sterile glass petri dish and bake for 30mins at 120°C to fix the nucleic acids onto the membrane
4. Transfer the membrane onto a sterile plastic petri plate with maleic acid buffer and incubate for 2mins at room temperature with shaking
5. Incubate for 20mins in fresh blocking solution at room temperature with shaking
6. Wash in 1x TBST for 5mins at room temperature with shaking
7. Incubate in 10ml antibody solution for 30mins at room temperature with shaking

8. Wash for 2x15mins in washing buffer at room temperature with shaking
9. Incubate in detection buffer for 5mins at room temperature with shaking
10. Add 10ml of fresh colour substrate solution and place in dark
11. Observe reaction every 30sec until the appearance of first dot and then every few mins for 30mins
12. Stop the reaction by placing membrane in TE buffer (pH8.0) for 5mins at room temperature with shaking
13. Remove membrane and store in a plastic bag

Solution Composition:

Dilution buffer – 1.5ml:

750 μ L DepC H₂O

450 μ L 20x SSC (Sigma, S6639)

300 μ L formaldehyde (Sigma, F8775)

Maleic acid buffer – 100ml:

1.607g maleic acid (Fisher Scientific, 03417)

0.8677g NaCl

60ml DepC H₂O

pH to 7.5 and top up to 100ml with DepC H₂O

Blocking solution – 10ml:

0.2ml sheep serum (Sigma, S3772)

0.3g milk powder

10ml 1xTBST

Antibody solution – 10ml:

2 μ L Anti-DIG-AP-FAB fragments (Roche-11 093 274 910)

10ml 1x TBST

Washing buffer – 100ml:

1.1607g maleic acid

0.8766g NaCl

60ml DepC H₂O

pH to 7.5 and top up to 100ml with DepC H₂O

0.3ml Tween 20 (Sigma, P9416)

Detection buffer – 100ml:

10ml 1M Tris-HCl

0.5844g NaCl

100ml DepC H₂O

Colour substrate solution – 10ml:

1 Sigma Fast BCIP/NBT tablet (Sigma B5655)

10ml dH₂O

TE buffer – 100ml:

1ml 1M Tris-HCl

0.2ml 0.5M EDTA (Sigma, E5134)

pH to 8.0 and top up to 100ml with DepC H₂O

Appendix A10: Whole Mount In Situ Hybridization Protocol:

Collection of embryos:

1. Fix embryo head overnight at desired stage at 4°C in 4% PFA made in 1x PBS
2. Next day, wash 2x10mins in 1x PBST at room temperature
3. Serially dehydrate the embryo heads into 100% MeOH at room temperature:
 - 15mins in 12.5%/87.5% MeOH/1x PBST
 - 20mins in 25%/75% MeOH/1x PBST
 - 20mins in 50%/50% MeOH/1x PBS
 - 30mins in 75%/25% MeOH/DepC H₂O
 - 30mins 85%/15% MeOH/DepC H₂O
 - 5mins in 100% MeOH
4. Store the embryo heads in 100% MeOH at -20°C until required. (Heads should be stored for at least one month before use to allow for better dissection)

Dissection of embryos prior to WMISH:

1. Bisect head using a fresh blade
2. Using fine curved forceps, remove the eyelids and nictitating membrane
3. Using fine dissection scissors, cut the back of the eye to give access to the vitreous humor
4. Remove the vitreous humor and the lens from inside the eye
5. Remove brain tissue around the eye

At this point, the embryos can either be used for WMISH-day 1 or stored in 100% MeOH at -20°C until required.

DAY 1:

1. Rehydration of embryos:

- 15mins (or until embryo sinks) in 85%/15% MeOH at room temperature with shaking
- 15mins (or until embryo sinks) in 75%/25% MeOH at room temperature with shaking
- 15mins (or until embryo sinks) in 50%/50% MeOH at room temperature with shaking
- 15mins (or until embryo sinks) in 25%/75% MeOH at room temperature with shaking
- 15mins (or until embryo sinks) in 12.5%/87.5% MeOH at room temperature with shaking

2. Wash 2x10mins in 1x PBST with shaking at room temperature

3. Bleach overnight in 10% H₂O₂ in 1x PBST at room temperature without shaking.

DAY 2:

1. Wash 2x10mins in 1x PBST at room temperature with shaking

2. 30mins in 10µg/ml ProK in 1x PBST at room temperature with shaking

3. 20mins in 4% DepC PFA/0.25% glutaraldehyde/1x PBS at room temperature with shaking
4. Wash 2x 10mins in 1x PBST at room temperature with shaking
5. 2hours in fresh pre-hybridization solution at 60°C with shaking
6. Place embryos in fresh pre-hybridization solution with 20-100ng/ml of desired probe and incubate overnight at 60°C with shaking

DAY 3:

1. Wash 3x20mins in washI at 60°C with shaking
 - during the last 10mins of wash1 heat inactivate sheep serum by placing it in 60°C for 30mins and make 20% sheep serum in 1x TBST
2. Wash 3x20mins in washII at 60°C with shaking
3. Wash 3x10mins in 1x TBST at room temperature with shaking
4. 2 hours in 20% sheep serum made in 1x TBST at 4°C with shaking
 - ~30mins prior to next step, pre-absorb Ab in the following way:
Take 1ml 20% sheep serum in 1x TBST in an RNase-free Eppendorf tube.
Add required amount of anti-DIG-AP-FAB fragments (Roche-11 093 274 910) and a small amount of chick powder. Shake vigorously and allow to settle for 30mins on ice.
 - At the end of 30mins, add this 1ml of pre-absorbed antibody to fresh 20% sheep serum in 1x TBST such that the final concentration of Ab is 1ul/10ml of solution.

5. Incubate embryos overnight in antibody solution at 4°C with shaking

DAY 4:

1. Wash 3x10mins in 1x TBST at 4°C with shaking
2. Wash in fresh 1x TBST + 2mM levamisole at 4°C with shaking

DAY 5-7:

Wash in fresh 1x TBST + 2mM levamisole at 4°C with shaking

DAY 8:

Earlier in the day, make colour detection solution by boiling PVA in 1x NTMT

1. Wash 3x10mins in 1x NTMT + 2mM levamisole at 4°C with shaking
 - add NBT and BCIP solutions to the colour detection solution
2. Place embryos in colour detection solution in dark at room temperature without shaking until colour has developed (usually takes 24hours, therefore best to leave overnight)

DAY9:

1. Wash in 1x PBST + 5mM EDTA at room temperature without shaking
2. Fix embryos in 4% PFA for 20mins at room temperature without shaking
3. Wash 2x10mins in 1x PBS at room temperature without shaking

- At this point, either further dissect the embryos and remove the retinal pigmented epithelium or store the embryos in 1x PBS in 4°C until ready to dissect.
4. If the developed colour is extremely dark or embryos have a high background, the colour can be leached in 90% MeOH at 4°C without shaking post dissection of retinal pigmented epithelium. Watch this step to prevent loss of desired staining
 5. Rinse briefly in dH₂O
 6. Store in 50% glycerol in dH₂O in 4°C

Solution Compositions:

0.01% DepC H₂O – 1L:

1L dH₂O

100µL diethyl pyrocarbonate (DepC) (Sigma, D5758)

Shake vigorously for 30mins, leave overnight in fumehood with lid cracked open to allow excess DepC to evaporate. Autoclave

4% Paraformaldehyde (PFA) – 500ml

20g PFA (Sigma, P6148)

Add 450mL 1x DepC PBS, add one NaOH pellet (Sigma, S5881) and dissolve over heated stir plate in fume hood

pH to 7.4 and top up to 500ml with 1x DepC PBS

Aliquot and store in -20°C

5M NaCl – 500ml:

146.1g NaCl

400ml DepC H₂O

Dissolve and top up to 500ml with DepC H₂O

4M KCl – 50ml:

14.912g KCl (MP Biochemicals, 191427)

40ml DepC H₂O

Dissolve and top up to 50ml with DepC H₂O

1M KH₂PO₄ – 50ml:

6.805g KH₂PO₄ (Sigma, P5655)

40ml DepC H₂O

Dissolve and top up to 50ml with DepC H₂O

1M Na₂HPO₄ – 50ml:

7.098g Na₂HPO₄ (EMD Millipore, SX0720)

40ml DepC H₂O

Dissolve and top up to 50ml with DepC H₂O

1M Tris-HCl (pH7.5) – 250ml:

30.275g Tris Base

200ml DepC H₂O

pH to 7.5 with HCl, top up to 250ml with DepC H₂O

1M Tris-HCl (pH9.5) – 50ml:

6.055g Tris Base

40ml DepC H₂O

pH to 9.5 with HCl, top up to 50ml with DepC H₂O

1M MgCl₂·6H₂O – 50ml:

10.165g MgCl₂·6H₂O (Fisher, BP214-500)

40ml DepC H₂O

Dissolve and top up to 50ml with DepC H₂O

10x PBS (pH7.4) – 500ml:

137ml 5M NaCl

3.37ml 4M KCl

21.5ml 1M Na₂HPO₄ (EMD, SX0720-1)

7ml 1M KH₂PO₄ (Sigma, P5655)

400ml DepC H₂O

pH to 7.4, top up to 500ml with DepC H₂O

1X PBS – 1L:

100ml 10x PBS

900ml DepC H₂O

1x PBST – 1L:

100ml 10x PBS

900ml DepC H₂O

1ml Tween 20 (Sigma, P9416)

10x TBS – 500ml:

140ml 5M NaCl

3.37ml 4M KCl

125ml 1M Tris-HCl pH7.5

Top up to 500ml with DepC H₂O

1x TBST – 1L:

100ml 10x TBS

900ml DepC H₂O

1ml Tween 20

12.5%/87.5% MeOH/1x DepC PBST – 500ml:

62.5ml MeOH

437.5ml 1x PBST

25%/75% MeOH/1x DepC PBST – 500ml:

125ml MeOH

375ml 1X PBST

50%/50% MeOH/1x DepC PBS – 500ml:

250ml MeOH

250ml 1x PBS

75%/25% MeOH/DepC H₂O – 500ml:

375ml MeOH

125ml DepC H₂O

85%/15% MeOH/DepC H₂O – 500ml:

425ml MeOH

75m DepC H₂O

10% H₂O₂ in 1x PBST – 45ml:

15ml 30% H₂O₂ (VWR, BOH3742-1)

30ml 1x PBST

10µg/ml ProK in 1xPBST – 50ml:

50µL Prok (10mg/ml stock) (Sigma, P2308)

50ml 1x PBST

4% DepC PFA + 0.25% glutaraldehyde/1x PBS – 50ml:

250µL glutaraldehyde (Sigma, G5882)

25ml 4% DepC PFA

25ml 1x PBS

Pre-hybridization solution – 50ml (make in order given):

5ml 10% SDS (Sigma, L4390; 0.5g in 5ml DepC H₂O)

7.5ml DepC H₂O

0.0025g yeast tRNA (Roche, 10 109 223 001)

0.0025g heparin (Sigma, H3393)

12.5ml 20x SSC

25ml deionized formamide

WashI – 50ml (make in order given):

2.5ml 20% SDS (0.5g in 2.5ml DepC H₂O)

12.5ml DepC H₂O

10ml 20x SSC (Sigma, S6639)

25ml deionized formamide (VWR, AC97062)

WashII – 50ml:

20ml DepC H₂O

5ml 20x SSC

25ml deionized formamide

20% sheep serum in 1x TBST – 50ml:

10ml heat inactivated sheep serum (Sigma, S2263)

40ml 1x TBST

Chick Powder:

1. Collect four 4-5 days old embryos in a small amount of 1x PBS
2. Add 4 volumes of cold acetone and homogenize the embryos
3. Incubate on ice for 30mins
4. Spin at 10,000rpm for 10mins and pour off supernatant
5. Place embryos onto a filter paper and crush/cut into a powder

6. Store in Eppendorf tube in -20°C

1xTBST + 2mM levamisole – 50ml:

0.0242g levamisole

50ml 1xTBST

1x NTMT – 50ml:

1ml 5M NaCl

5ml 1M Tris-HCl pH9.5

1.25ml 1M MgCl₂

0.25ml Tween 20

1x NTMT + 2mM levamisole – 50ml:

0.0242g levamisole (Sigma, L9756)

50ml 1x NTMT

Colour Detection Solution – 50ml:

1ml 5M NaCl

5ml 1M Tris-HCl pH9.5

0.25ml Tween 20

Top up to 35ml with DepC H₂O. Add 5g of poly vinyl alcohol and boil in water bath.

When cool, add:

1.25ml 1M MgCl₂

150μL NBT (75mg/ml stock)

115μL BCIP (50mg/ml stock)

NBT (75mg/ml stock) - 100μL:

0.0075g NBT (Sigma, N6876)

70μL N,N-dimethyl formamide

30μL DepC H₂O

Dissolve by repeated pipetting until clear yellow solution forms

BCIP (50mg/ml) - 100μL:

0.005g BCIP (Sigma, B6777)

100μL N,N-dimethyl formamide

1x PBST + 5mM EDTA – 50ml:

0.093g EDTA

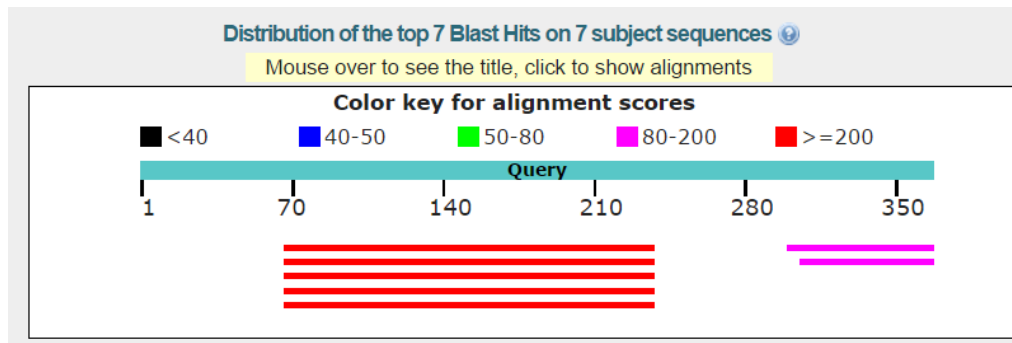
50ml 1x PBST

Appendix B: Blast Outcomes for Sequencing Data Using NCBI Blast:

FGFR 1b blast against *Gallus gallus* genome:

FGFR1b sequence; total 170bp:

gatcctgaagcactcgggaattaatagctctgatgcgagggtgctgaccctgtataatgtgacagaggcggagagcggggagtatgtttgtaaggttccaattatattggcgaggccaaccagt
 ctgcgtggctcactgtcaccagacctctggcaaaagctactgagc

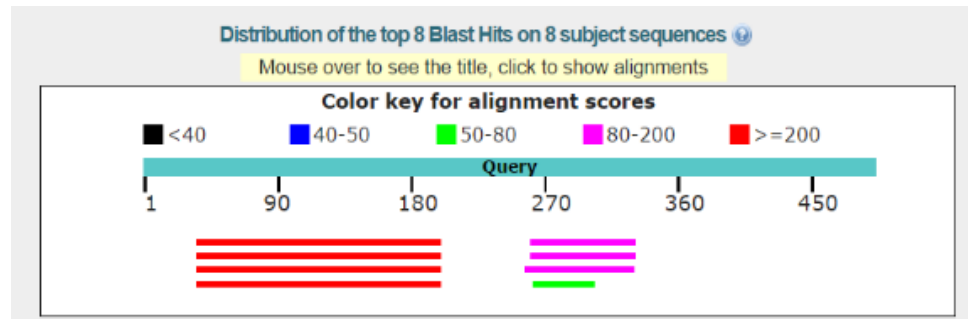


<input type="checkbox"/> PREDICTED: Gallus gallus fibroblast growth factor receptor 1 (FGFR1), transcript variant X5, mRNA	316	316	46%	6e-85	100%	XM_015297366.1
<input type="checkbox"/> PREDICTED: Gallus gallus fibroblast growth factor receptor 1 (FGFR1), transcript variant X4, mRNA	316	316	46%	6e-85	100%	XM_015297364.1
<input type="checkbox"/> PREDICTED: Gallus gallus fibroblast growth factor receptor 1 (FGFR1), transcript variant X3, mRNA	316	316	46%	6e-85	100%	XM_015297363.1
<input type="checkbox"/> PREDICTED: Gallus gallus fibroblast growth factor receptor 1 (FGFR1), transcript variant X1, mRNA	316	316	46%	6e-85	100%	XM_015297361.1
<input type="checkbox"/> Gallus gallus fibroblast growth factor receptor 1-IIIb (Fgfr1IIIb) mRNA, partial cds	316	316	46%	6e-85	100%	GU053725.1

FGFR1c blast against *Gallus gallus* genome:

FGFR1c sequence; total 165bp:

gatcctgaagacggctggcgtaacacgacagacaaagagatggaagtccttacttaaggaatgtctcattgaggatgctggggagatacatgtttggcgggtaattctattgggatctccc
atcactctgcatggttgacagttctcgaagctactgagca



<input type="checkbox"/> PREDICTED: Gallus gallus fibroblast growth factor receptor 1 (FGFR1), transcript variant X6, mRNA	305	305	33%	2e-81	100%	XM_015297367.1
<input type="checkbox"/> PREDICTED: Gallus gallus fibroblast growth factor receptor 1 (FGFR1), transcript variant X2, mRNA	305	305	33%	2e-81	100%	XM_015297362.1
<input type="checkbox"/> Gallus gallus fibroblast growth factor receptor 1 (FGFR1), mRNA	305	305	33%	2e-81	100%	NM_205510.1
<input type="checkbox"/> Gallus gallus fibroblast growth factor receptor 1-llc mRNA, partial cds	294	294	33%	4e-78	99%	GU065444.1

FGFR1b blast against FGFR1c:

Job title: Nucleotide Sequence (170 letters)

RID [M3PC481R114](#) (Expires on 06-16 08:49 am)

Query ID Icl|Query_134857
Description None
Molecule type nucleic acid
Query Length 170

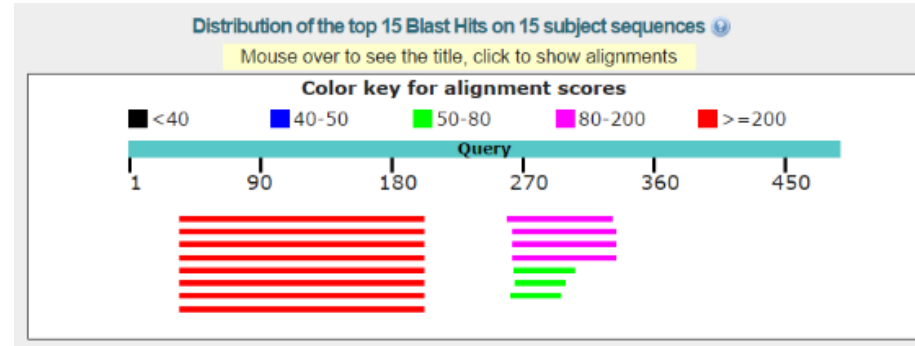
Subject ID Icl|Query_134859
Description None
Molecule type nucleic acid
Subject Length 165
Program BLASTN 2.6.1+ [▶ Citation](#)

 No significant similarity found. For reasons why, [click here](#)

FGFR2b blast against *Gallus gallus* genome:

FGFR2b sequence; total 170bp:

ggttttaagcattcggggataaatagttccaatgctgaagtgctgacactgtacaatgtgacagaggcggacgctggagaatatattgtaaggtctccaattatataggggaggccaaccagt
ctgcctggctctctgttctgccgagtttacaagctcctgaaaaag

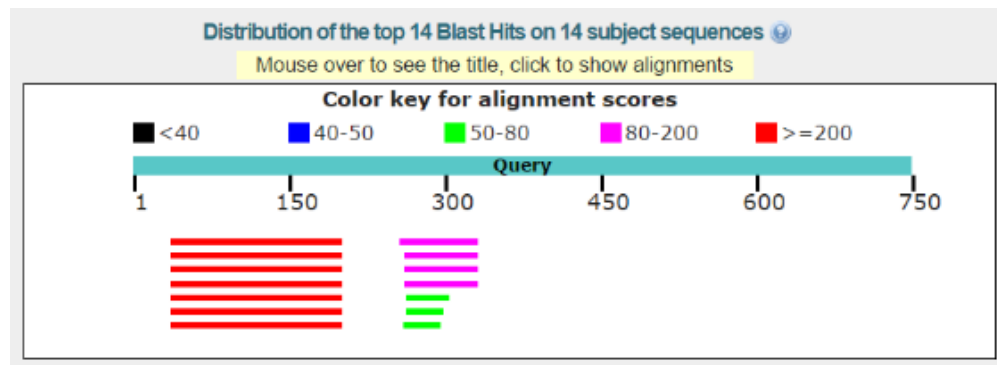


<input type="checkbox"/> PREDICTED: Gallus gallus fibroblast growth factor receptor 2 (FGFR2), transcript variant X10, mRNA	311	311	34%	4e-83	100%	XM_015288593.1
<input type="checkbox"/> PREDICTED: Gallus gallus fibroblast growth factor receptor 2 (FGFR2), transcript variant X8, mRNA	311	311	34%	4e-83	100%	XM_015288591.1
<input type="checkbox"/> PREDICTED: Gallus gallus fibroblast growth factor receptor 2 (FGFR2), transcript variant X6, mRNA	311	311	34%	4e-83	100%	XM_015288589.1
<input type="checkbox"/> PREDICTED: Gallus gallus fibroblast growth factor receptor 2 (FGFR2), transcript variant X5, mRNA	311	311	34%	4e-83	100%	XM_015288588.1
<input type="checkbox"/> PREDICTED: Gallus gallus fibroblast growth factor receptor 2 (FGFR2), transcript variant X3, mRNA	311	311	34%	4e-83	100%	XM_015288586.1
<input type="checkbox"/> PREDICTED: Gallus gallus fibroblast growth factor receptor 2 (FGFR2), transcript variant X2, mRNA	311	311	34%	4e-83	100%	XM_015288585.1
<input type="checkbox"/> PREDICTED: Gallus gallus fibroblast growth factor receptor 2 (FGFR2), transcript variant X1, mRNA	311	311	34%	4e-83	100%	XM_015288584.1
<input type="checkbox"/> G.gallus mRNA bek for receptor tyrosine kinase	311	311	34%	4e-83	100%	X61992.1

FGFR2c blast against *Gallus gallus* genome:

FGFR2c sequence; total 165bp:

ggttttaaaggctgccggtgtaacactacggacaaagaattgaggttctctatatacggaatgtaactttgaggatgctggggagtatacatgcttggcgggtaatyctattgggatatccttt
cacactgcatggttgacagttctgccagctcctgaaaa



<input type="checkbox"/> PREDICTED: Gallus gallus fibroblast growth factor receptor 2 (FGFR2), transcript variant X11, mRNA	302	302	22%	4e-80	99%	XM_015288594.1
<input type="checkbox"/> PREDICTED: Gallus gallus fibroblast growth factor receptor 2 (FGFR2), transcript variant X9, mRNA	302	302	22%	4e-80	99%	XM_015288592.1
<input type="checkbox"/> PREDICTED: Gallus gallus fibroblast growth factor receptor 2 (FGFR2), transcript variant X7, mRNA	302	302	22%	4e-80	99%	XM_015288590.1
<input type="checkbox"/> PREDICTED: Gallus gallus fibroblast growth factor receptor 2 (FGFR2), transcript variant X4, mRNA	302	302	22%	4e-80	99%	XM_015288587.1
<input type="checkbox"/> Gallus gallus fibroblast growth factor receptor 2 (FGFR2), mRNA	302	302	22%	4e-80	99%	NM_205319.2
<input type="checkbox"/> Gallus gallus finished cDNA, clone ChEST75721	302	302	22%	4e-80	99%	CR523637.1
<input type="checkbox"/> Chicken tyrosine kinase (cek3) mRNA, complete cds	302	302	22%	4e-80	99%	M35196.1

FGFR2b blast against FGFR2c:

Job title: Nucleotide Sequence (170 letters)

RID [M3PJ1KGN114](#) (Expires on 06-16 08:52 am)

Query ID Icl|Query_66441
Description None
Molecule type nucleic acid
Query Length 170

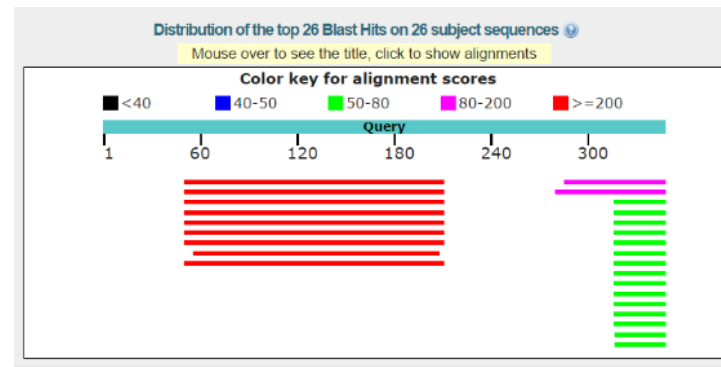
Subject ID Icl|Query_66443
Description None
Molecule type nucleic acid
Subject Length 165
Program BLASTN 2.6.1+ [▶ Citation](#)

 No significant similarity found. For reasons why, [click here](#)

FGFR3b blast against *Gallus gallus* genome:

FGFR3b sequence; total 161bp:

gctcctctgcttttggttgcgaaatgtggagccaaaatggctttcggctatgcctacgaaattgttgctctacacagatattctctcatctgttctgtcacattgaacagattaggttagcatc
ggcttcagcgttttactgatccaagacgctc

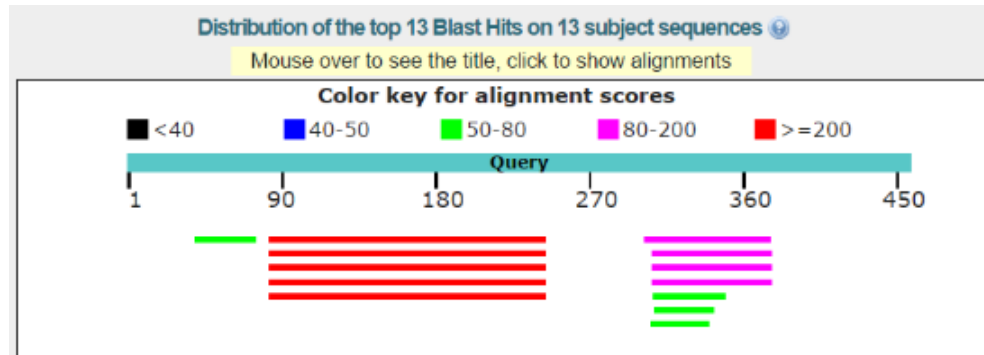


<input type="checkbox"/>	PREDICTED: Gallus gallus fibroblast growth factor receptor 3 (FGFR3), transcript variant X9, mRNA	278	278	46%	3e-73	98%	XM_015285884.1
<input type="checkbox"/>	PREDICTED: Gallus gallus fibroblast growth factor receptor 3 (FGFR3), transcript variant X8, mRNA	278	278	46%	3e-73	98%	XM_015285883.1
<input type="checkbox"/>	PREDICTED: Gallus gallus fibroblast growth factor receptor 3 (FGFR3), transcript variant X5, mRNA	278	278	46%	3e-73	98%	XM_015285879.1
<input type="checkbox"/>	PREDICTED: Gallus gallus fibroblast growth factor receptor 3 (FGFR3), transcript variant X4, mRNA	278	278	46%	3e-73	98%	XM_015285878.1
<input type="checkbox"/>	PREDICTED: Gallus gallus fibroblast growth factor receptor 3 (FGFR3), transcript variant X3, mRNA	278	278	46%	3e-73	98%	XM_015285877.1
<input type="checkbox"/>	PREDICTED: Gallus gallus fibroblast growth factor receptor 3 (FGFR3), transcript variant X2, mRNA	278	278	46%	3e-73	98%	XM_015285876.1
<input type="checkbox"/>	PREDICTED: Gallus gallus fibroblast growth factor receptor 3 (FGFR3), transcript variant X1, mRNA	278	278	46%	3e-73	98%	XM_015285875.1

FGFR3c blast against *Gallus gallus* genome:

FGFR3c sequence; total 162bp:

```
gctcctctgctgtagcaccgtcagccaagcagagtgatgtgagaaccaatagaattccctgcgagacaagtatattccccagcatcctcaaaagtaacatttcgcaagtacagaatctctagc  
tccttatccgttggttaaacacctgccgtcttcagca
```



<input type="checkbox"/> PREDICTED: Gallus gallus fibroblast growth factor receptor 3 (FGFR3), transcript variant X7, mRNA	300	300	35%	6e-80	100%	XM_015285882.1
<input type="checkbox"/> PREDICTED: Gallus gallus fibroblast growth factor receptor 3 (FGFR3), transcript variant X6, mRNA	300	300	35%	6e-80	100%	XM_015285881.1
<input type="checkbox"/> Gallus gallus fibroblast growth factor receptor 3-IIIc mRNA, partial cds	300	300	35%	6e-80	100%	GU065445.1
<input type="checkbox"/> Gallus gallus fibroblast growth factor receptor 3 (FGFR3), mRNA	300	300	35%	6e-80	100%	NM_205509.2
<input type="checkbox"/> Chicken tyrosine kinase (cek2) mRNA, complete cds	300	300	35%	6e-80	100%	M35195.1

FGFR3b blast against FGFR3c:

Job title: Nucleotide Sequence (161 letters)

RID [M3PSD5SJ114](#) (Expires on 06-16 08:55 am)

Query ID Icl|Query_141755
Description None
Molecule type nucleic acid
Query Length 161

Subject ID Icl|Query_141757
Description None
Molecule type nucleic acid
Subject Length 162
Program BLASTN 2.6.1+ [▶ Citation](#)

 No significant similarity found. For reasons why, [click here](#)

Appendix C: Supplementary Figures

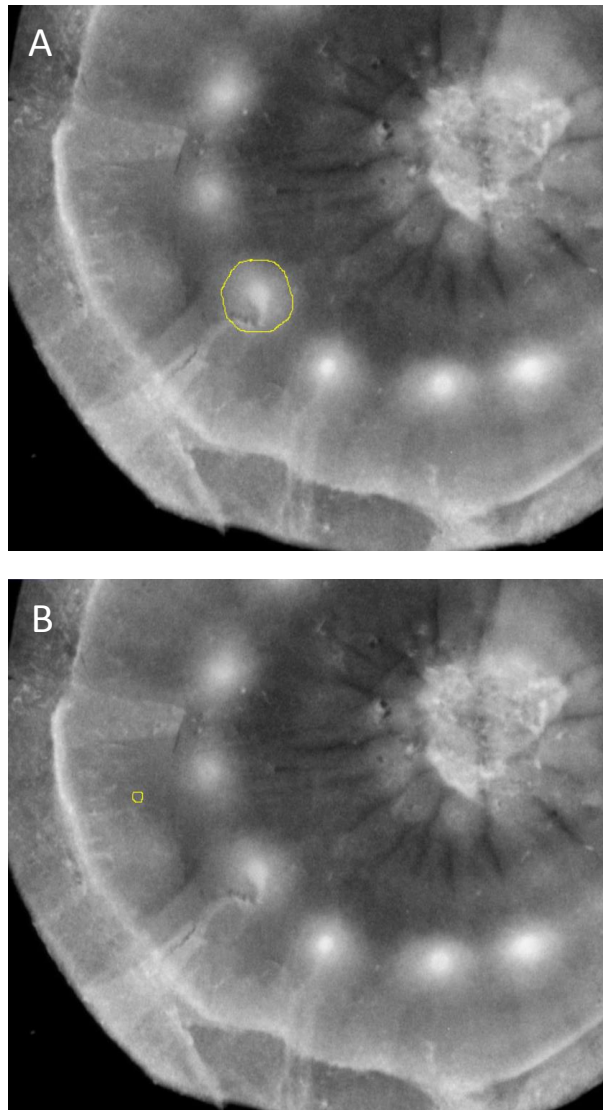


Figure C1. Methodology for ImageJ analysis of expression intensity at papilla #12. (A) Intensity was measured in an area which included the papilla as well as a small area of its CR. (B) Intensity was measured in area of no expression (background).

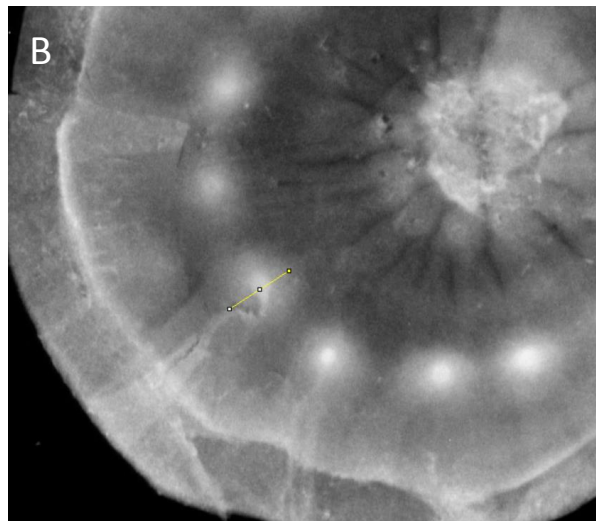


Figure C2. Methodology for ImageJ analysis of field of expression at papilla #12. (A) Measurement of maximum diameter 'a'; (B) Measurement of maximum diameter 'b' (at 90° to a).

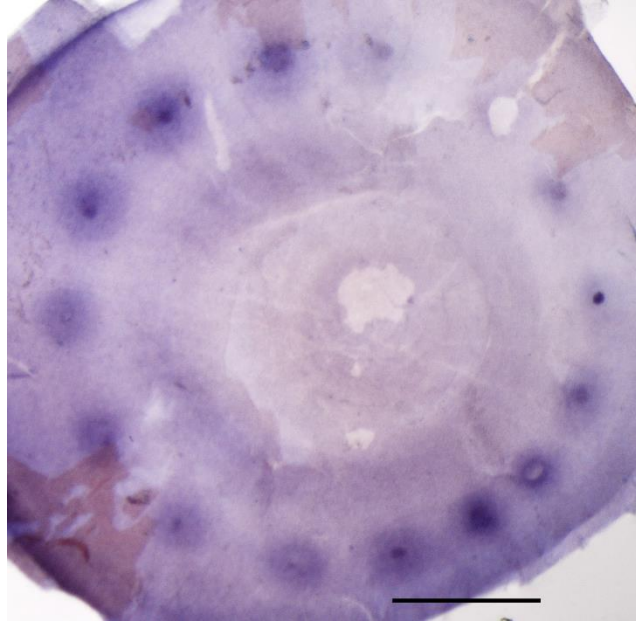


Figure C3. The whole mount in situ hybridization of *BMP2* at HH35. Scale bar represents 1mm.

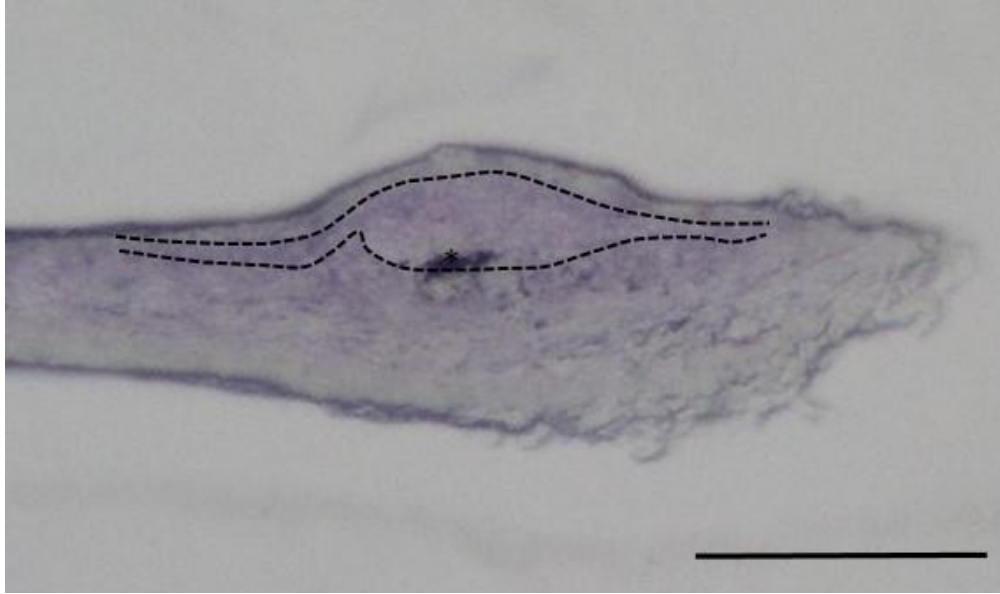


Figure C4. Cryosection of *FGFR2c* in situ hybridization in nasal group papilla. Section at HH34 showing expression in the papilla (indicated by dashed lines) but absence of expression in the apical region of the papillae. Expression is also observed in the superficial mesenchyme. No expression in the deep mesenchyme. Asterisk indicates an artifact. Scale bars represents 100 μ m.


- = strong expression
- = low expression
- = faint expression
-  = ciliary artery
- = strong expression in zone around papilla
- = low expression in zone around papilla
- = faint expression in zone around papilla

Figure C5. Key for the schematics of *FGFR* ISH expressions in Figure 4.1, 4.2 and 4.4 as well as Figure C6 to C11.

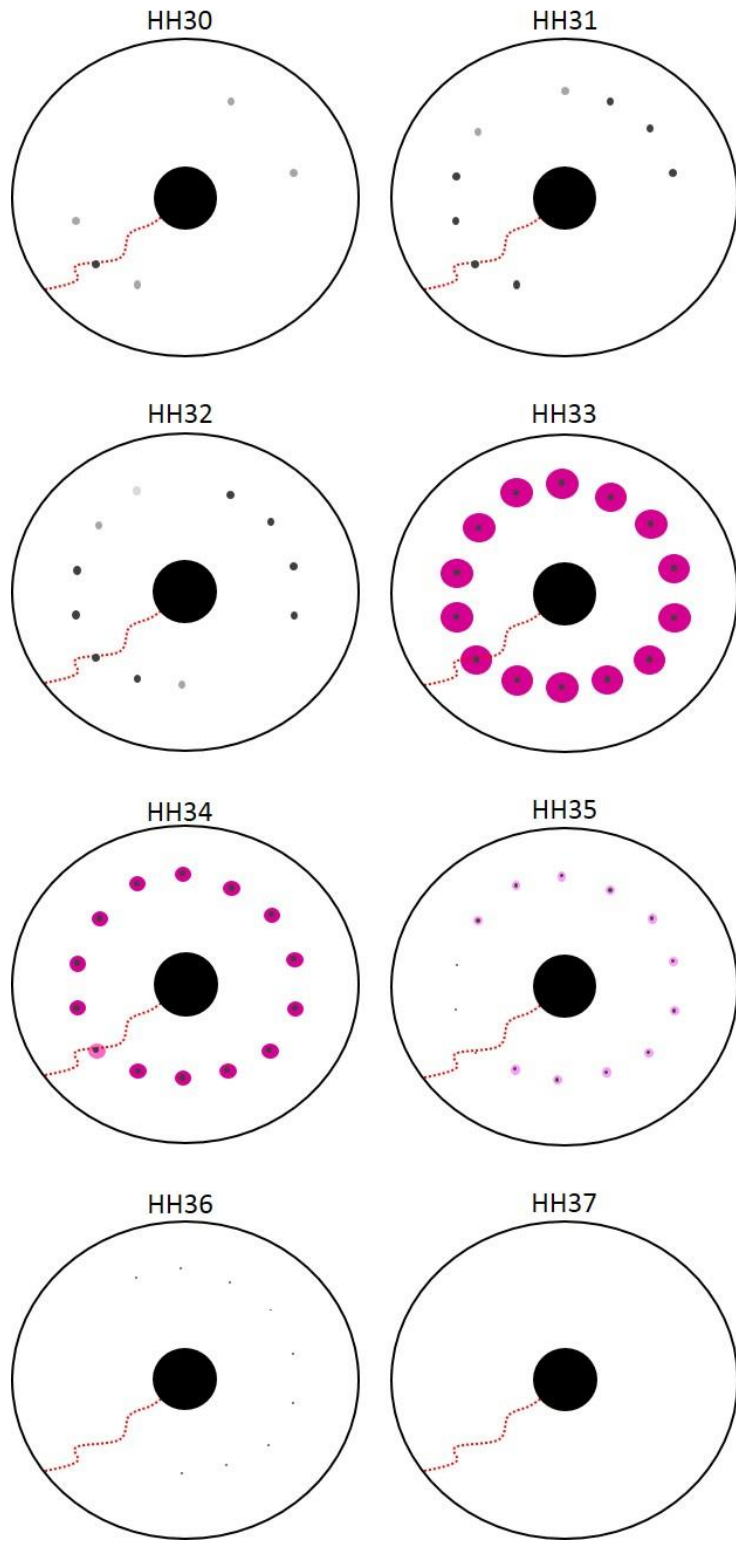


Figure C6. Schematic of *FGFR1b* ISH.

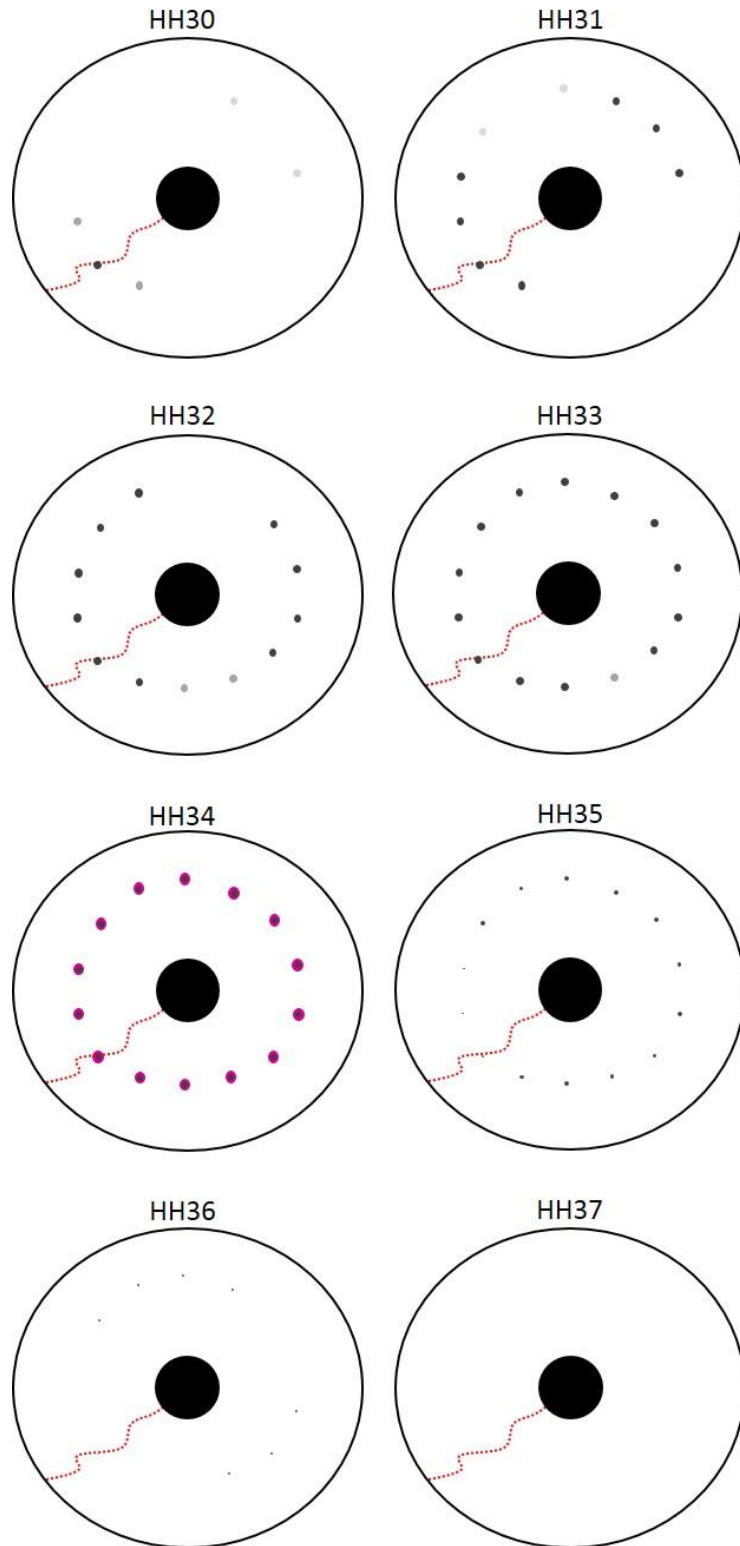


Figure C7. Schematic of *FGFR1c* ISH.

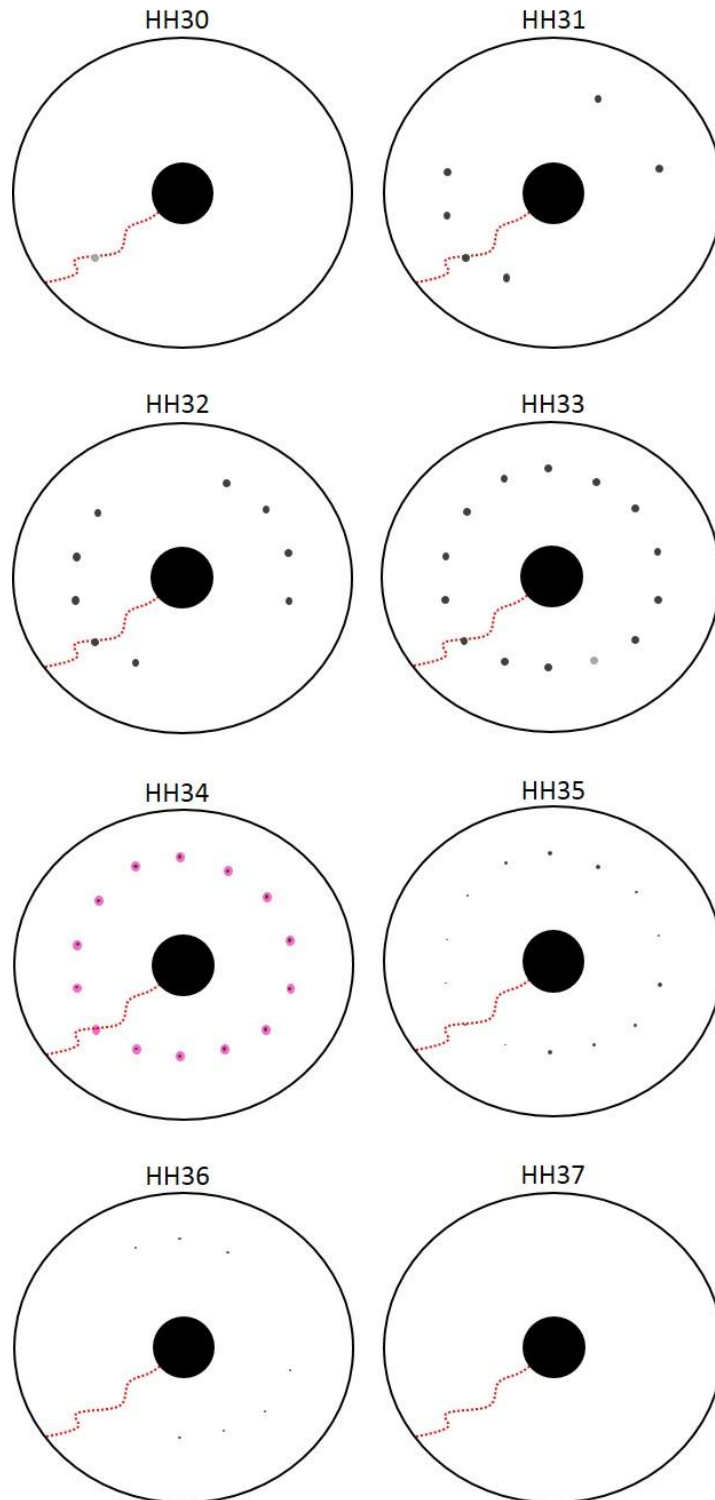


Figure C8. Schematic of *FGFR2b* ISH.

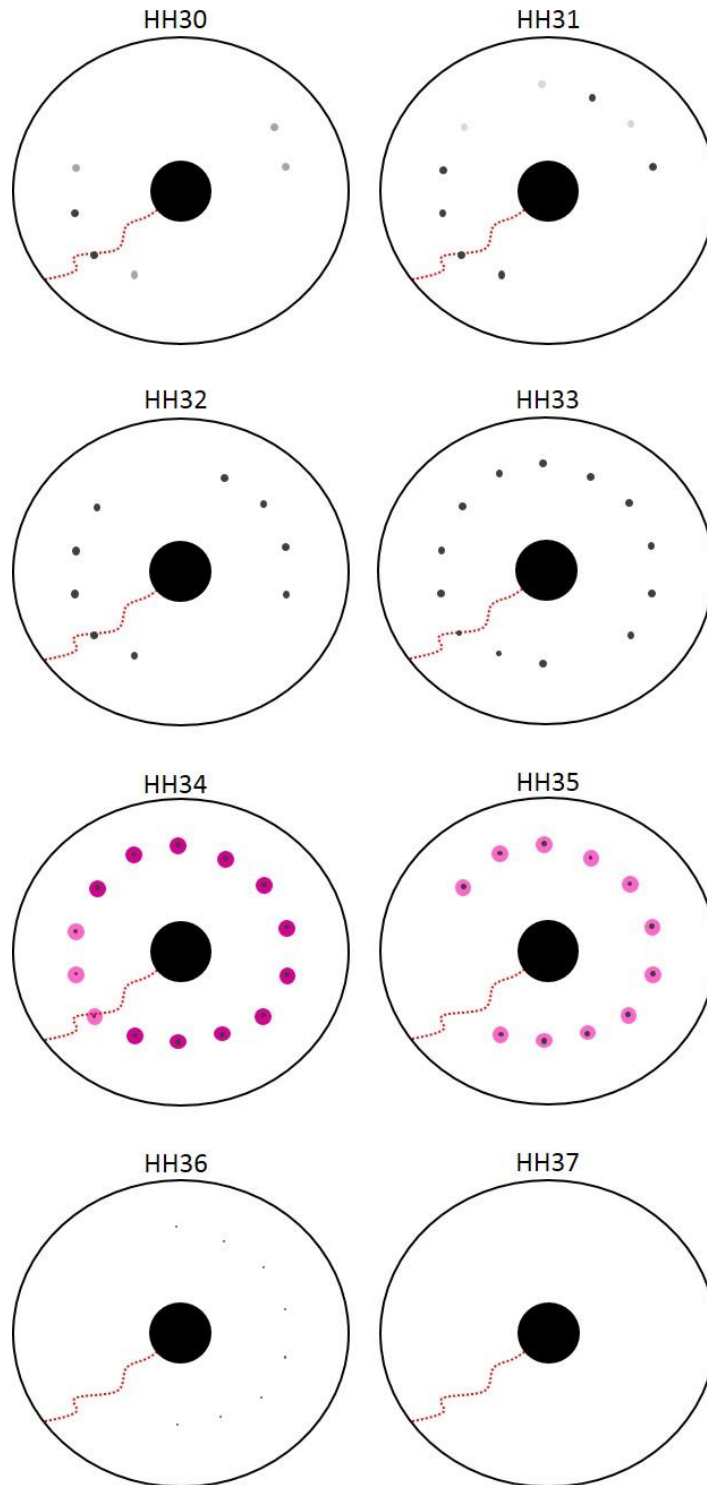


Figure C9. Schematic of *FGFR2c* ISH.

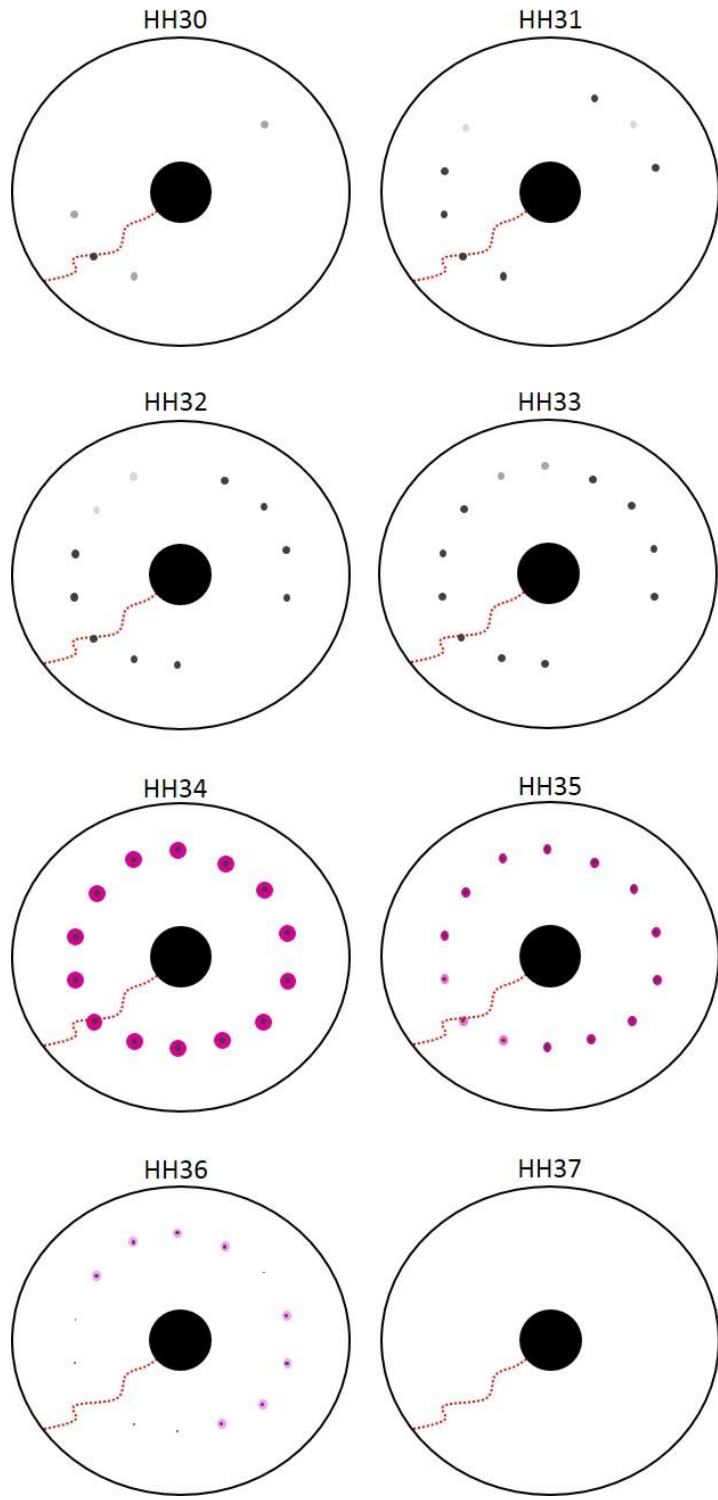


Figure C10. Schematic of *FGFR3b* ISH.

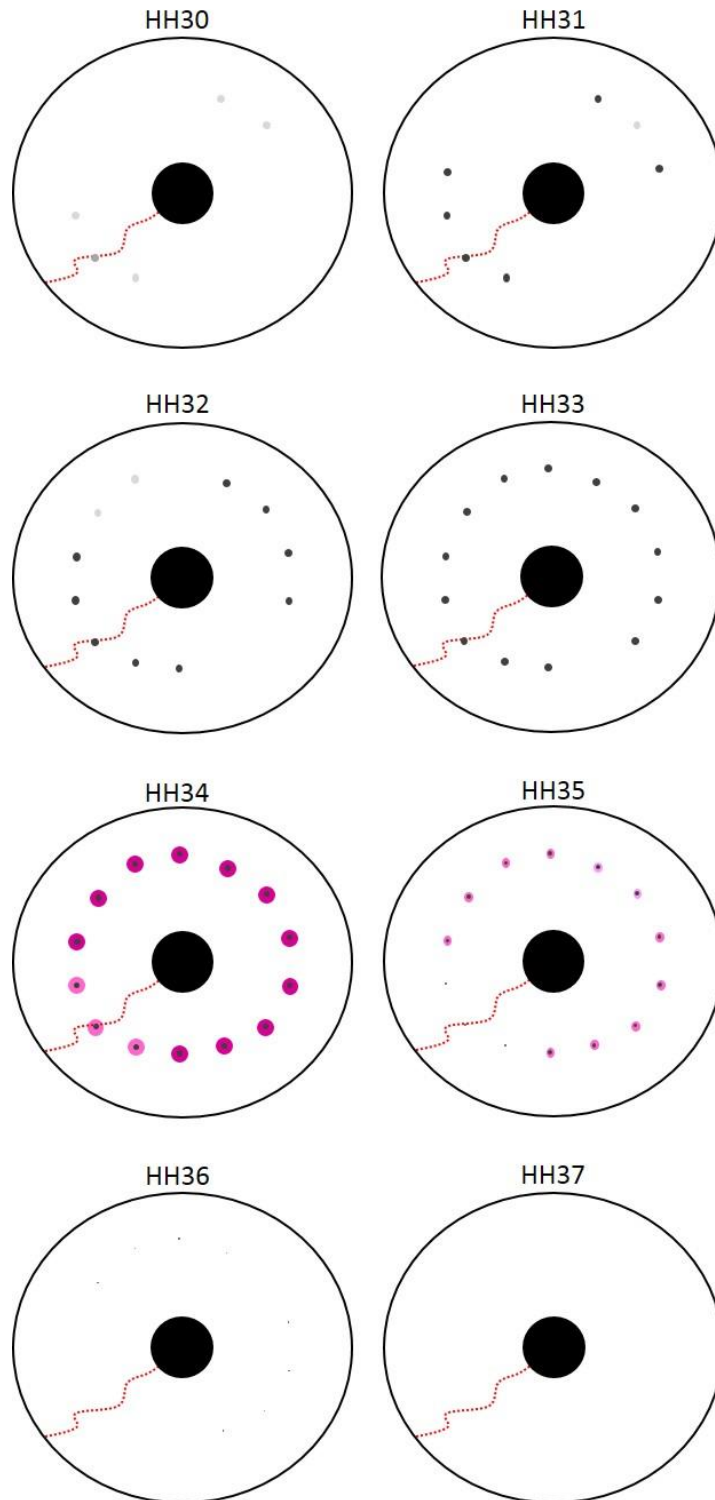


Figure C11. Schematic of *FGFR3c* ISH.

Appendix D: Supplementary Tables:

Table D1. Measurements of wing cartilages at HH29/30 after affigel bead implantation at HH20/21.

	Left Unimplanted Wing (mm)			Right Implanted Wing (mm)		
	Radius	Ulna	Humerus	Radius	Ulna	Humerus
3mg/ml-SU5402	1.1	0.9	1.25	1.05	0.85	1.25
	1.1	0.85	1.1	1.25	0.85	1.15
	1.15	0.8	1.25	1.2	0.9	1.3
Average	1.23	0.85	1.20	1.16	0.87	1.23
Standard Deviation	0.03	0.05	0.09	0.10	0.03	0.08

Table D2. Number of papillae in left and right eye of control non-injected embryos. Data from Hammer (2016).

	Left Eye	Right Eye
	14	14
	14	14
	14	14
	14	14
	14	14
	15	14
	15	14
	15	14
	14	15
	15	15
	15	15
Average	14.45455	14.27273
Standard deviation	0.49793	0.445362

Table D3. Raw ImageJ data for quantitative analysis of expression intensity of papilla #12 and its contiguous region. Method used to obtain this data is shown in Appendix C, Figure C1.

Gene	Stage	Mean Area	Mean Grey Value	Mean Integrated Density	Mean Grey Value of Background	Corrected Intensity
<i>FGFR1b</i>	HH30	389.67	211.52	82421	162.26	46182
	HH31	705	237.98	167373	86.43	106441.03
	HH32	1393.67	187.73	259606.33	60.3	175567.3
	HH33	2146	213.62	457220	165.32	102443.61
	HH34	1508.33	200.42	302122	124.19	114803.61
	HH35	1106	157.59	174057	111.77	50437.17
	HH36	721.33	172.6	124283.67	131.73	29264.11
	HH37	18	131.44	24466	110.04	3961.88
<i>FGFR1c</i>	HH30	218.33	187.3	40853.67	86.48	21972.35
	HH31	436.67	228.45	99603.33	91.48	59655.61
	HH32	2842.33	171.48	487190.3	125.78	129678.8
	HH33	2964.67	190.12	563582.3	151.54	114331.6
	HH34	2641.33	214.01	564671.3	177.58	95625.12
	HH35	440.67	174.44	76819.67	114.58	26327.93
	HH36	186	122.8	22818.67	111.1	2153.39
	HH37	Intensity could not be determined				
<i>FGFR2b</i>	HH30	542	165.54	98826	71.88	51611.69
	HH31	687	230.4	158304	120.11	75787.51
	HH32	1396	189.22	262857.7	77.3	154942.2
	HH33	1629	173.05	281841.3	98.12	121999
	HH34	1261	161.67	203700	112.84	61412.12
	HH35	276.67	147.98	40924	104.81	11926.2
	HH36	169	184.16	31052	130.1	9065.38
	HH37	157.67	120.01	18714	87.02	4993.16

Table D3 (Continued)

Gene	Stage	Mean Area	Mean Grey Value	Mean Integrated Density	Mean Grey Value of Background	Corrected Intensity
<i>FGFR2c</i>	HH30	339.67	181.38	61608.67	124.14	19442.33
	HH31	945	185.73	176706	104.78	76744.29
	HH32	851	245.53	209087.7	151.85	79766.06
	HH33	2592	141.02	364711.7	104.64	80536.88
	HH34	2595.67	118.4	307015	51.58	173133.1
	HH35	334.67	161.3	53854	96.71	21487.16
	HH36			Intensity could not be determined		
	HH37			Intensity could not be determined		
<i>FGFR3b</i>	HH30	975.33	157.48	153325.7	54.12	100541.9
	HH31	1471.67	152.63	224242	69.82	11493.7
	HH32	1110.67	109.63	121545.3	46.82	69541.33
	HH33	847	218.41	184949.3	129.35	75356.5
	HH34	2112	141.85	299137.7	102.38	82911.81
	HH35	475.33	178.99	84967.7	132.01	22216.85
	HH36	272.33	165.52	44854	130.92	9199.76
	HH37			Intensity could not be determined		
<i>FGFR3c</i>	HH30	249.33	138.96	34532.67	88.71	12514.55
	HH31	730	208.65	152261.7	120.65	64185.22
	HH32	2299.33	181.71	417879.3	117.25	148277.9
	HH33	2485.33	176.04	436825.3	93.8	203696.1
	HH34	2557.67	179.94	4590577	117.3	154047.6
	HH35	1710	168.57	288051.3	119.56	83611.14
	HH36	188.07	154.46	24433.67	107.53	7371.87
	HH37			Intensity could not be determined		

Corrected Intensity = Integrated Density - (Mean Area x Mean Grey Value of Background)

Table D4. Raw ImageJ data for field of FGFR expression in papilla #12 and its contiguous region. All values are in mm. Method used to obtain this data is shown in Appendix C, Figure C2.

Gene	Average max. diameter 'a'	Standard deviation	Average max. diameter 'b'	Standard deviation
<i>FGFR1b</i>	0.32	0.02	0.26	0.01
<i>FGFR1c</i>	0.28	0.002	0.29	0.01
<i>FGFR2b</i>	0.2	0.01	0.23	0.01
<i>FGFR2c</i>	0.21	0.01	0.24	0.01
<i>FGFR3b</i>	0.3	0.01	0.25	0.01
<i>FGFR3c</i>	0.27	0.002	0.25	0.003

Appendix E: Statistical Calculations

Appendix E1: Calculations for Dixon's Q-test for outliers

Dixon's Q-test was performed for both DMSO controls and SU5402 in both left and right eye at 95% confidence interval.

Two outliers were found in the left eye of SU5402 microinjections. Total number of ossicles were arranged in ascending order:

7, 10, 13, 13, 14, 14, 14, 14, 14, 14, 14

The following equation was used for Dixon's Q-test:

$$Q_{exp} = \frac{x_3 - x_1}{x_{n-1} - x_1}$$

x_3 = 3rd smallest value

x_1 = smallest value

x_{n-1} = value before x_n

The value is considered an outlier if the Q_{exp} is greater than $Q_{critical}$

$$Q = \frac{13 - 7}{14 - 7} = 0.857$$

The $Q_{critical}$ for n=11 at 95% confidence interval is 0.708

$$0.857 > 0.708$$

Therefore, the eye with 7 ossicles was considered an outlier

$$Q = \frac{13 - 10}{14 - 10} = 0.75$$

The $Q_{critical}$ for $n=11$ at 95% confidence interval is 0.708

$$0.75 > 0.708$$

Therefore, the eye with 10 ossicles was considered an outlier

Appendix E2: Fisher's Exact test SPSS outputs:

Fisher's Exact test of frequency of defects between right eyes of DMSO and SU5402 microinjections

Case Processing Summary

	Valid		Cases Missing		Total	
	N	Percent	N	Percent	N	Percent
treatment * defects	15	100.0%	0	0.0%	15	100.0%

treatment * defects Crosstabulation

Count		defects			Total
		mild	normal	severe	
treatment	DMSO	1	2	1	4
	SU5402	4	7	0	11
Total		5	9	1	15

Chi-Square Tests

	Value	df	Asymptotic Significance (2-sided)	Exact Sig. (2-sided)
Pearson Chi-Square	2.955 ^a	2	.228	.429
Likelihood Ratio	2.859	2	.239	.429
Fisher's Exact Test	2.541			.429
N of Valid Cases	15			

p= 0.429

Fisher's Exact test of frequency of defects between left eyes of DMSO and SU5402 microinjections

Case Processing Summary

	Valid		Cases Missing		Total	
	N	Percent	N	Percent	N	Percent
treatment * defects	13	100.0%	0	0.0%	13	100.0%

treatment * defects Crosstabulation

Count		defects				Total
		mild	moderate	normal	severe	
treatment	DMSO	1	0	2	1	4
	SU5402	1	2	6	0	9
Total		2	2	8	1	13

Chi-Square Tests

	Value	df	Asymptotic Significance (2-sided)	Exact Sig. (2-sided)
Pearson Chi-Square	3.611 ^a	3	.307	.530
Likelihood Ratio	4.278	3	.233	.530
Fisher's Exact Test	3.319			.432
N of Valid Cases	13			

p=0.432

Appendix E3: Independent Two-tailed T-tests MiniTab outputs:

Two-tailed T-test between DMSO treated AG1X2 beads in left and right limbs

Two-Sample T-Test and CI

	N	Mean	StDev	SE Mean
DMSO.L.Limb	5	2.998	0.620	0.28
DMSO.R.Limb	5	3.096	0.300	0.13

Difference = μ (1) - μ (2)
Estimate for difference: -0.098
95% CI for difference: (-0.890, 0.694)
T-Test of difference = 0 (vs not =): T-Value = -0.32 P-Value = 0.763 DF = 5

Two-tailed T-test between DMSO and SU5402 treated AG1X2 beads in left limbs

Two-Sample T-Test and CI

	N	Mean	StDev	SE Mean
DMSO.L.Limb	5	2.998	0.620	0.28
SU5402.L.Limb	5	3.420	0.240	0.11

Difference = μ (1) - μ (2)
Estimate for difference: -0.422
95% CI for difference: (-1.186, 0.342)
T-Test of difference = 0 (vs not =): T-Value = -1.42 P-Value = 0.215 DF = 5

Two-tailed T-test between DMSO microinjections left and right eyes

Two-Sample T-Test and CI

	N	Mean	StDev	SE Mean
DMSO.L.E	4	13.25	2.20	1.1
DMSO.R.E	4	13.50	1.00	0.50

Difference = μ (1) - μ (2)
Estimate for difference: -0.25
95% CI for difference: (-3.21, 2.71)
T-Test of difference = 0 (vs ≠): T-Value = -0.21 P-Value = 0.843 DF = 6

Two-tailed T-test between SU5402 microinjections left and right eyes

Two-Sample T-Test and CI

	N	Mean	StDev	SE Mean
SU5402 L.E	9	13.78	1.20	0.40
SU5402 R.E	11	14.180	0.390	0.12

Difference = μ (1) - μ (2)

Estimate for difference: -0.400

95% CI for difference: (-1.343, 0.543)

T-Test of difference = 0 (vs \neq): T-Value = -0.96 P-Value = 0.362 DF = 9

Two-tailed T-test between DMSO and SU5402 microinjection left eyes

Two-Sample T-Test and CI

	N	Mean	StDev	SE Mean
DMSO L.E	4	13.25	1.92	0.96
SU5402 L.E	9	13.78	1.20	0.40

Difference = μ (1) - μ (2)

Estimate for difference: -0.53

95% CI for difference: (-3.42, 2.36)

T-Test of difference = 0 (vs \neq): T-Value = -0.51 P-Value = 0.637 DF = 4

Two-tailed T-test between DMSO and SU5402 microinjection right eyes

Two-Sample T-Test and CI

	N	Mean	StDev	SE Mean
DMSO.R.E	4	13.50	1.00	0.50
SU5402.R.E	11	14.200	0.400	0.12

Difference = μ (1) - μ (2)

Estimate for difference: -0.700

95% CI for difference: (-1.450, 0.050)

T-Test of difference = 0 (vs \neq): T-Value = -2.02 P-Value = 0.065 DF = 13

Two-tailed T-test between CNI and DMSO microinjection left eyes

Two-Sample T-Test and CI

	N	Mean	StDev	SE Mean
CNI.L.E	11	14.500	0.500	0.15
DMSO.L.E	4	13.30	2.20	1.1

Difference = μ (1) - μ (2)

Estimate for difference: 1.200

95% CI for difference: (-0.243, 2.643)

T-Test of difference = 0 (vs \neq): T-Value = 1.80 P-Value = 0.096 DF = 13

Two-tailed T-test between CNI and DMSO microinjection right eyes

Two-Sample T-Test and CI

	N	Mean	StDev	SE Mean
CNI.R.E	11	14.300	0.500	0.15
DMSO.R.E	4	13.50	1.00	0.50

Difference = μ (1) - μ (2)

Estimate for difference: 0.800

95% CI for difference: (-0.020, 1.620)

T-Test of difference = 0 (vs \neq): T-Value = 2.11 P-Value = 0.055 DF = 13

Appendix E4: Calculations for one way ANOVA

Summary of data:

i	Treatment	Measures	Number of samples	Mean number of ossicles	\hat{A}_i
1	CNI	14,14, 14, 14, 14, 14, 14, 14, 15, 15, 15	11	14.2727	0.1527
2	DMSO	12, 14, 14, 14,	4	13.5	-0.62
3	SU5402	14, 14, 14, 15, 14, 15, 14, 14, 14, 14, 14,	11	14.1818	0.0618

$$\hat{A}_i = \text{Mean}_{\text{group}} - \hat{\mu}$$

$$\text{Where, } \hat{\mu} = \frac{\sum \text{all measures}}{\text{total number of samples}}$$

$$\hat{\mu} = \frac{\sum 14 + 14 + 14 + \dots 12 + 14 + 14 + \dots 14 + 14 + 15 \dots + 14}{25}$$

$$\hat{A}_1 = 14.2727 - 14.12 = 0.1527$$

$$\hat{A}_2 = 13.5 - 14.12 = -0.62$$

$$\hat{A}_3 = 14.1818 - 14.12 = 0.0618$$

ANOVA table:

Cause of variation	Degrees of freedom (df)	Sum of Squares (SS)	Mean Square (MS)
Treatment	2	1.8357	0.9178
Residual	23	6.8182	0.2964
Total	25	8.6539	

$$df_{treatment} = \text{total number of groups} - 1$$

$$df_{treatment} = 3 - 1 = 2$$

$$df_{total} = \text{total number of samples} - 1$$

$$df_{total} = 26 - 1 = 25$$

$$df_{residual} = df_{total} - df_{treatment}$$

$$df_{residual} = 25 - 2 = 23$$

$$SS_{treatment} = \sum (\hat{A}_1^2) \times \text{number of samples}$$

$$SS_{treatment} = (0.1527)^2 \times 11 + (-0.62)^2 \times 4 + (0.0618)^2 \times 11 = 1.8357$$

$$SS_{residual} = \sum_i \sum_j (y_{ij} - y_i)^2 = \sum_i SS_{row_i}$$

$$SS_{residual} = [(14 - 14.27)^2 + (14 - 14.27)^2 + \dots + (15 - 14.27)^2] + [3] + [1.6364] \\ = 6.8182$$

$$SS_{total} = SS_{treatment} + SS_{residual}$$

$$SS_{total} = 1.8357 + 6.8182 = 8.6539$$

$$MS_{treatment} = \frac{SS_{treatment}}{df_{treatment}}$$

$$MS_{treatment} = \frac{1.8357}{2} = 0.9178$$

$$MS_{residual} = \frac{SS_{residual}}{df_{residual}}$$

$$MS_{treatment} = \frac{6.8182}{23} = 0.2964$$

F -value is given by:

$$F = \frac{MS_{treatment}}{MS_{residual}}$$

$$F = \frac{0.9178}{0.2964} = 3.096$$

The $F_{critical}$ value for $df_{2,23} = 3.42$. My F -value is less than the critical value signifying that there is no statistical difference between the three treatment groups.